UNIVERSITÀ' DEGLI STUDI DI BOLOGNA

PhD Program in Biochemistry
XXIII Cycle

Scientific Area Code BIO/15

Preclinical neuroblastoma models for a pharmacological study of a new *MYCN* oncogene inhibitor

PhD Candidate
Dott. Erika CANTELLI

Supervisor
Prof. Andrea PESSION

PhD Program Coordinator
Prof. Giorgio LENAZ

Final Exam – Bologna, June 2011

1

Introduction

1.1 Neuroblastoma

1.1.1 Epidemiology

Neuroblastoma (NB) is the most common extracranial solid tumor in childhood and it is responsible for 8 to 10% of pediatric cancers. The incidence is 10.4 / million /for year in Caucasians children and 8.3 / million /for year in black children under 15 years [1]. The tumor is slightly more common in males (M: F = 1.1:1) [2].

The most common site of event depends on the age of the patient, it is often in the chest in children under one year (33%), the site is the abdominal region in older infants (55-75%). The first description of a case of neuroblastoma dates back to 1864 by Virchow, but the name was coined by Homer Wright in 1910.

The average age at diagnosis is 22 months after birth, 97% of cases are diagnosed in childhood, only 10% of cases exceeds the age of 5 years old, 1.5% aged over 14 years old [3]. The 60% of patients are diagnozed at an advanced stage of disease: this means that in about 2/3 of cases, the tumor is inoperable or disseminated and prognostically unfavorable [4].

1.1.2 Etiopathogenesis and inheritance

Although some studies have shown that maternal age (under 20 years) and high blood pressure of mother could be considered prenatal risk factors [5], the etiology of NB is still poorly understood. Usually NB occurs sporadically, but 5% of patients have a genetic predisposition to develop the disease [6]. The familiar NB is inherited in a Mendelian autosomal dominant pattern with incomplete penetrance.

Approximately 22% of NB is caused by a germline mutation [7] and this fits the theory proposed by Knudson for the origin of pediatric tumors [8], where two mutations in a post-zygotic single cell define a non-hereditary NB. Hereditary NB show instead a germline mutation which is followed to a somatic mutation. Other studies confirm this ipothesis underlined the role of ALK and PHOX2B genes in the progression of hereditary NB [9] [10].

Neuroblastoma arises from neuroepithelial primitive cells of the neural crest and it is localized mainly in the adrenal gland (50%), in retroperitoneal region (25%), in chest area (15%), in pelvis and in pre and para-vertebral sympathetic ganglia (5%). These tumors show a spontaneous or induced differentiation in ganglioneuroblastoma but the differentiating factors are not known. An important system seems to be the homologous family of neurotrophins (NGF, BDNF, NT3, NT4/5) and their receptors (TrkA, TrkB and TrkC): activation of TrkA leads to inhibition of growth, inhibition of angiogenesis, increased chemotherapeutic sensitivity and induction to differentiation. In contrast, activation of TrkB promotes the proliferation, invasiveness and chemotherapeutic resistance [11].

Chromogranin A and neuropeptide Y are two other markers of neuronal differentiation and sometimes they are associated to NB differentiation.

Chromogranin A is an acidic protein, and it is a component of granules of neurosecretion of cells, of tissues and of neuroendocrine tumors, and its expression is regulated during development [12] [13] [14]. This protein is present in NB patients' serum and it can be useful as a sensitive and specific marker of the disease activity and of the response to treatment [15] [16].

Neuropeptide Y is a neurosecretory protein whose expression is regulated in the development and related to the nervous system [17] [18]. These two proteins may be useful to characterize the NB in terms of their state of differentiation or to monitor patients [19] [20] [21].

The vasoactive intestinal peptide (VIP) and somatostatin are other peptide hormones associated with the neuroblastoma. The expression of somatostatin receptors in NB cell is correlated with higher histological differentiation, a more low-stage disease and a favorable outcome [22] [23] [24]. The expression of VIP is associated with differentiated tumors, and it can induce *in vitro* neuronal differentiation in NB cells [25] [26]. The role of these two proteins in regulating growth and differentiation of sympathetic neurons during normal development is not yet clear.

1.1.3 Histopathology

The histopathological classification highlights four classic histologic types that have varying degrees of maturation and differentiation [2]:

- neuroblastoma is the most malignant histological type, it is characterized by small, uniform cells called 'small round blue cells'. These cells present dense and hyperchromatic nuclei and scant cytoplasm. The presence of neuritic processes, or neuropil, is a characteristic feature especially of primitive NB. 15-50% of cases present the Homer-Wright pseudorosette, it is a ring of neuroblasts surrounding areas of eosinophilc neuropil;

- ganglioneuroma is the benign and fully differentiated counterpart of neuroblastoma. It is composed primarily of mature ganglion cells, neuropil and Schwann cells;

- ganglioneuroblastoma defines a heterogeneous group of tumors with histopathologic features spanning the extremes from a predominance of neuroblastic elements with rare maturing cells to neoplasms comprised almost exclusively of ganglioneuroma and containing occasional rest of neuroblasts;

- nodular ganglioneuroblastoma is composed by rich or poor in stroma cells and by neuroblasts to variable differentiation.

1.1.4 Staging

Different staging systems were developed in the last forty years: the clinical-instrumental classical method, proposed by Evans in 1971 [27], the system used by St. Jude Children's Research Hospital and by the Pediatric Oncology Group (POG) [28] [29] and TNM

classification [30] [31]: they allow to distinguish between low-stage patients with good prognosis and those patients at high stage with poor prognosis. Especially for patients at intermediate stages, there are substantial differences between the various staging systems. For this reason the International Neuroblastoma Staging System (INSS) has been created which incorporates the main points of Evans, the POG, in light of the different criteria for assessing the therapeutic response [32] [33] [34].

International Neuroblastoma Staging System Stages

Stage 1: localized tumor with complete gross excision, with or without microscopic residual disease; representative ipsilateral lymph nodes negative for tumor microscopically (nodes attached to and removed with the primary tumor may be positive).

Stage 2A: localized tumor with incomplete gross excision; representative ipsilateral nonadherent lymph nodes negative for tumor microscopically.

Stage2B: localized tumor with or without complete gross excision, with ipsilateral nonadherent lymph nodes positive for tumor. Enlarged contralateral lymph nodes must be negative microscopically.

Stage 3: unresectable unilateral tumor infiltrating across the midline, with or without regional lymph node involvement; or localized unilateral tumor with contralateral regional lymph node involvement; or midline tumor with bilateral extension by infiltration (unresectable) or by lymph node involvement. The midline is defined as the vertebral column. Tumors originating on one side and crossing the midline must infiltrate to or beyond the opposite side of the vertebral column.

Stage 4: any primary tumor with dissemination to distant lymph nodes, bone, bone marrow, liver, skin, and/or other organs (except as defined for stage 4S).

Stage 4S: localized primary tumor (as defined for stage 1, 2A, or 2B), with dissemination limited to skin, liver, and/or bone marrow (limited to infants less than 1 year of age). Marrow involvement should be minimal (i.e., <10% of total nucleated cells identified as malignant by bone biopsy or by bone marrow aspirate). More extensive bone marrow involvement would be considered to be stage IV disease. The results of the meta-

iodobenzylguandine (MIBG) scan (if performed) should be negative for disease in the bone marrow.

1.1.5 Genetics of neuroblastoma

The identification and staging of neuroblastoma are not based only on clinical and structural prediction models, like INSS; in fact the alterations at the genomic level play a crucial role in the prognosis of this malignancy.

All the neuroblast tumors can therefore be divided into two main subgroups based on the degree of ploidy and related chromosomal changes associated with tumor cells (Fig. 1) (http://atlasgeneticsoncology.org/Tumors/neurob5002.html).

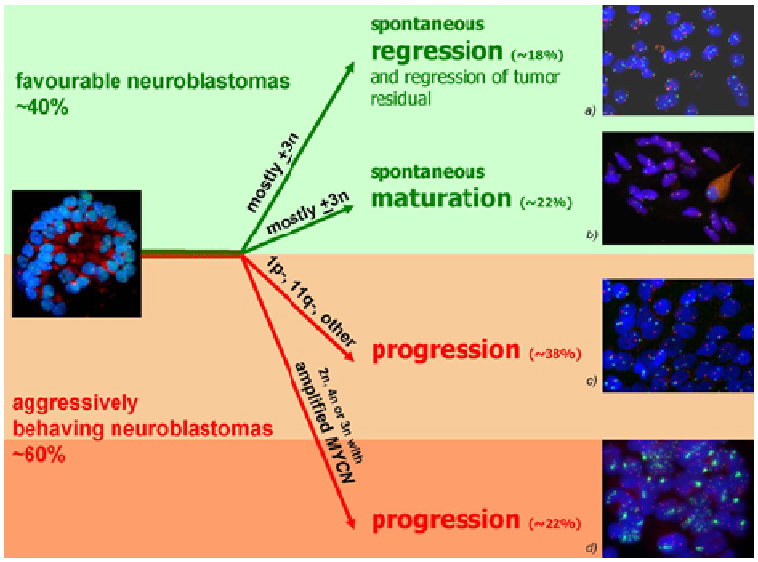

Fig.1 Genetic characteristics and biological pathway in neuroblast tumors. Neuroblastoma tumors can be subdivided into two biological/clinical groups: 'benignly' behaving neuroblastomas are indicated by a green background, aggressive neuroblastomas are marked by a orange or red background. The 'beningly' behaving neuroblastomas virtually always show a near-triploid, near-pentaploid or near-hexaploid DNA Index, without any structural aberrations: in a) nuclei with a typical I-FISH picture with 3 spots each for D1Z2 at 1p36 and D1Z1 for the para centromeric region of chromosome 1 shown. Spontaneously maturing tumours show two types of cells, but only a small fraction of the cells are tumour cells. In b) one aneuploid ganglionic cell with reddish cytoplasm is shown beside a majority of cells showing 2 signals with all used FISH probes representing non neoplastic Schwann cells. Neuroblastomas with aggressive clinical behavior can further be subdivided in those without MYCN amplification but with segmental aberrations like del1p, del11q, add17q (shown in c): tumor cells with only 1 sub-telomeric I-FISH signal in red and 2 paracentromeric I-FISH spots in green) and those with MYCN amplification (an example is given in d): tumour cells displaying both types of amplification, DMs and HSRs in green, while the reference probe is given in red).

The importance of the cellular content of DNA is demonstrated by flow cytometry in children. In fact, children with tumors that have a hyperdiploid content of DNA (DNA index > 1) have generally low stages of the disease and they respond to initial therapy, while NB tumors with a diploid DNA content (DI = 1) usually have advanced stages of disease and do not respond to certain combinations of chemotherapy [35] [36].

Near triploid (-penta, hexaploid) neuroblastomas (±3N) represent about 45% of neuroblastomas, with a survival of approximately 100% and they can be compared to stages 1, 2, 4S of the INSS. Genetic alterations include a gain of genetic material on chromosomes 2, 7, 9, 12, 17 and a loss for chromosomes 3, 4, 6, 11, 14 [37] [38] [39]. In particular, specific gains in chromosome 7 (7p11.2p22) are associated with a higher probability of survival in patients with neuroblastoma in recovery [39].

The tumor may undertake a spontaneous maturation in 22% of cases. This subset of patients, however, shows a distinct diploid genotype, due to a large number of non-cancerous cells, mainly Schwann cells, involved in maturation. The component with triploid DNA borders 1% and it is mostly made up of ganglion cells.

Di-tetraploid neuroblastoma (2N/4N) constitute the remaining 55% of cases, they are identified by a poor prognosis and are characterized by specific genetic alterations (deletions, translocations) (INSS Stage 4).

22% of these tumors show amplification of the MYCN gene, alterations at the genomic level, association with advanced disease, rapid tumor progression and poor prognosis [40] [41]. The amplification of MYCN in human neuroblastoma was discovered for the first time by Schwab in 1983 [43]. Following studies have confirmed that amplification of the MYCN gene greater than 10 copies for haploid genome, it's an unfavorable prognostic indicator, independent of the anatomical state, age, and other biological parameters.

In the cytogenetic analysis the manifestation of the MYCN gene amplification are the extra chromosomal chromatin bodies, called double-minutes chromatin bodies (DMs) and the chromosomal regions that do not undergo banding, called homogenously staining regions (HRSs) [42]. The genetic material from chromosome region 2p24 is in fact transported through the DMs during the amplification process and these are then integrated into a random chromosomal region as HSRs. The DMs predominate in primary tumors and HSRs in the cell

lines [40]. The HSRs are generally located on different chromosomes, not in the resident site 2p24 of MY CN [43] [44]. The values of amplification in neuroblastoma can change between 5 and more than 500 copies, but usually the number of copies seen in cancers values are approximately 50-100 copies.

The deletion of the short arm of chromosome 1 (1p,36) seems to play a key role in the progression of these tumors and prognosis [45]: it is in fact the common alteration presents in the most aggressive NB. The 1p region can contain one or more tumor repressor genes important in neoplastic transformation or progression of neuroblastoma [46]. The deletion at 1p is associated with MYCN amplified neuroblastomas and poor prognosis, however, rare cases of MYCN not amplified neuroblastoma show a deletion of a smaller number of bases in chromosome 1p and a similar outcome [37].

Another important aberration is the gain in chromosome 17. The 17q gain is more common in children over one year of age, with tumors at an advanced stage, showing the absence of 1p, MYCN amplification and diploid - tetraploid DNA content. The gain in position 17q is the result of a translocation between chromosomes 17 and 1.

The remaining 38% of tumors presents deletions in chromosomes 1, 3, 4, 11, 14, as well as gains on chromosome 17 [37] [39] and no MYCN amplification. Experimental studies have demonstrated that the gain on the q arm of chromosome 17 is significantly associated with tumor progression [25] even among patients without MYCN amplification or 1p deletion [47] [48]. Each translocation of material in 17q is associated with events of deletion in "partner" chromosomes (1p, 11q). In this case, this subclass of diploid neuroblast tumors shows a translocation between chromosome 17 and 11.

Rearrangements of 11q were observed in many patients, which is a deletion of 11q23-qter, balanced translocations involving 11q21 and 11q22, and an inversion of 11q21-q23 [49]. The role of these alterations is not clear, but it has been assumed that the rupture of one or more genes on 11q may predispose to the development of neuroblastoma. Small deletions of 11q usually occur in no MYCN amplified neuroblastomas [37] [50]. The loss of 11q is significantly associated with adverse clinical parameters, such as older than 1 year, 4-stage disease and unfavorable histology [51].

Recent studies seem to confirm the hypothesis that the chromosomal alterations

described above are essential in identifying the different stages of neuroblastoma, but other genetic alterations included in the same chromosome regions possess the same predictive power against the disease.

The high proportion of translocations in 17q and the combination with a low survival rate, leading to think that in the additional region of 17q are found genes important for tumor progression. The survivin gene is one of the possible candidates: the survivin is an anti apoptotic protein that maps in the 17q25; it's expressed in many cancers (stomach, lung, pancreas) and its expression is indicative of a high degree of malignancy, poor prognosis and probability of relapse [52] [53].

Array CGH studies have also highlighted a possible role of retinoic acid receptor α (17q21), the receptor for nerve growth factor NGF (17q21.22) and NM23 gene (17q21.3) as possible tumor markers: in particular the last of these is over expressed and amplified in MYCN *amplified* neuroblastomas [54].

Another gene noteworthy is CAMTA1 (Calmodulin-binding trascriptors Activators). This cistron unit belongs to the family of calmodulin-binding transcription factors and it lies in the short arm of chromosome 1 that it is deleted in neuroblastoma stage IV and this gene is poorly expressed in MYCN amplified neuroblastomas. Moreover the low levels of expression of CAMTA1 define a poor prognosis even in the absence of 1p deletions [55].

1.1.6 Genetic model of neuroblastoma development

The genetics and genomics research suggest there are at least two subsets of neuroblastomas that are highly correlated with clinical behavior. One classification takes into account the assessment of DNA content; MYCN copy number; abnormalities of 1p, 3p, 11q, and other changes; the expression of TrkA or TrkB. Genomic data analysis of the different mutations have allowed to construct an evolutionary model that explains how, starting from a common ancestor cell, other tumor histo types have been developed [2].

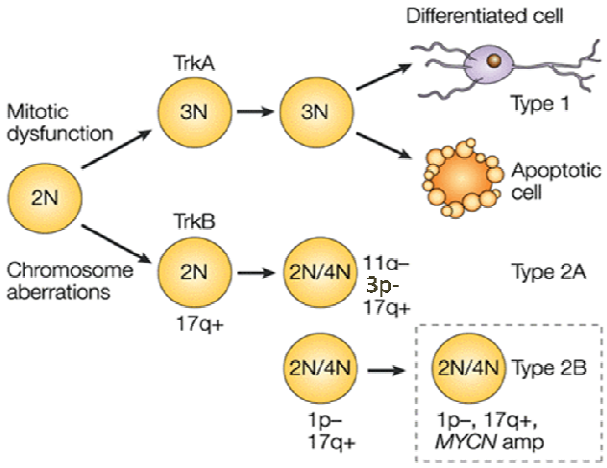

Fig.2 Genetic model of neuroblastoma development. 2N = diploid karyotype; 3N = triploid karyotype; 2N/4N = di-tetraploid karyotype.

It is possible that all neuroblastomas have a common ancestor diploid cell, but a commitment is made fairly early to develop into one of two major subtypes:

Type 1. This subtype is characterized by mitotic dysfuction leading to a hyperdiploid or near-triploid modal karyotype with low chromosome rearrangements, no amplification of MYCN, deletions in 1p and gain in 17q, high expression of TrkA receptor. These tumors are prone to differentiation or undergo programmed cell death, depending on the presence or absence of NGF in the microenvironment. These genetic representation belong to patients with 1, 2 and 4S stages of the disease.

Type 2. It represents the most aggressive neuroblastomas with di-tetraploid karyotype with high expression of the receptor TrkB. Within this type, two subsets can be distinguished:

Type 2A is characterized by alterations in 3, 11 and 17 chromosomes; lack of MYCN amplification and 1p deletion. Representative patients show 3 and 4 stages of the disease and they are older.

Type 2B is characterized by alterations in 1 and 17 chromosomes and amplification of MYCN. Representative patients belong to 3 and 4 stages of disease and they are usually between 1 and 5 years of age with rapidly progressive disease that is frequently fatal.

This model is similar to that proposed by Sven Bilke and co-workers, as the result of an analysis conducted on different patients at different stages of the disease (1, 4, 4S) [56]. The model proposed by Bilke shows that more aggressive stages of the disease (with or without MYCN amplification) have evolved separately and have developed different mutations than less aggressive stages (1, 4S). Such genetic diversity reflects perfectly those at the clinical level; according to the INSS in fact the patients with 4 stage, with or without MYCN amplification, are the major causes of a poor prognosis [56].

1.1.7 Diagnosis and treatment

Neuroblastomas generally arise in the adrenal medulla or along the sympathetic chain. To confirm this diagnosis, it is required an histological evidence on primary tumor biopsy to confirm the neural origin, accompanied by measure of increase level in urinary catecholamine metabolites. Because the bone marrow is frequently involved, children older than 2 years with metastatic disease may not require a biopsy but NB can be diagnosed based on the presence of neuroblastic cells involving the bone marrow. On bioptic or bone marrow materials MYCN, ploidy and histology studies are evaluated, because tumor specific genetic markers and histo pathological evaluation are critical determinants of treatment planning [2]. For tumor staging, meta-iodobenzylguanidine (MIBG) scintigraphy (or a technetium-99 bone scan in case of negative MIBG), computed tomography or nuclear magnetic resonance, and bilateral bone marrow aspirates and trephine biopsies are valuable methods.

According to risk group assignment, there are the following treatment modalities: surgery, standard chemotherapy, intensive multiagent chemotherapy, myeloablative chemotherapy, followed by autologous stem cell transplantation, external radiation therapy, 13-cis retinoic acid, anti-GD2 monoclonal antibody adjuvant therapy, MIBG-therapy .

For patients with low risk NB that belong to stage 1, 2 and 4s, chemotherapy and radiation are usually avoid; for patient with intermediate-risk NB that belong to stage 3, chemotherapy and radiation are used cautiously and individualized as needed; for patient with high risk NB that belong to stage 4 metastatic NB diagnosed after 18 months of age or that presents MYCN amplification, a multimodal approach is needed. These treatments are conducted in phases: chemotherapy, surgery, radiation, immunotherapy.

Chemotherapy is certainly the predominant modes of treatment NB patients and metastatic forms of localized un-resectable neuroblastoma at diagnosis. The chemotherapy is also used in patients at lower risk with important symptoms. Several international groups have developed a model of stratification.

Among the various protocols used, the European protocol currently used for high-risk neuroblastoma see a rapid treatment that give cisplatin [C], vincristine [O], carboplatin [J], etoposide [E] and cyclophosphamide [C] known as COJEC [57] (Fig. 3).

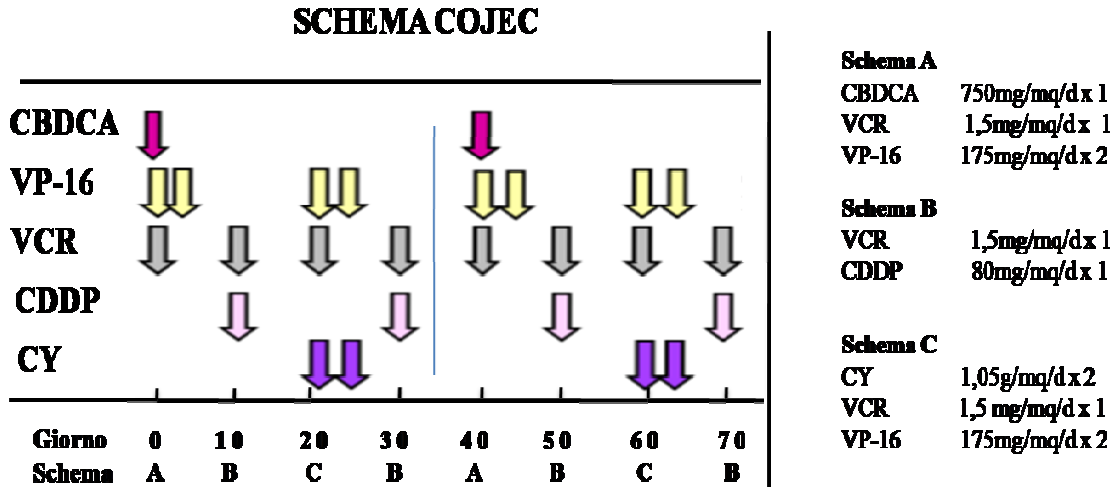

Fig. 3: Treatment schedule of Neuroblastoma-1 high-risk according to the Society of Paediatric European Oncology Group Neuroblastoma (HR-NBL1/SIOPEN). COJEC schedule include different drugs and different way to administer the drugs: carboplatin CBDCA 750 mg/m^2, rapid infusion; etoposide VP-16 175 mg/m^2, infusion for 4 hours; vincristine VCR 1.5 mg/m^2 IV bolus; cisplatin CDDP 80 mg/m^2 24 hours of continuous perfusion; cyclophosphamide CY 1.050 mg/m^2 rapid infusion. Each arrow indicates a single dose of medication according to the amount set out in schedules A, B, C.

The goals of primary surgery are to establish the diagnosis, to provide tissue for biologic studies, to stage the tumor surgically, to attempt to excise the tumor without injury to vital structures, and during second look surgery the goals are to determine response to therapy and to remove residual disease.

The radiation therapy has been used for local control of primary tumor and refractory metastatic site in patient with high risk disease, for neonates who develop respiratory distress

secondary to hepato megaly and when the treatment is ineffective.

Stem cell transplantation is used to destroy the patient's neuroblastoma-infected bone marrow and replace it with stem cells that are relatively free of neuroblastoma.

Immunotherapy is used after tumors have been surgically removed, when the patient has only minimal disease left. This treatment is designed to train the body's own immune system to detect and destroy neuroblastoma cells that have survived chemotherapy or radiation therapy.

1.2 *MYCN* Gene

1.2.1 MYC gene family

The family of proto-oncogenes MYC is composed of a group of transcription factors belonging to the class *basic-helix-loop-helix-zipper* (bHLHZ). The Myc proteins family is involved in the regulation of proliferation and cell cycle [58], in the processes that lead to differentiation and to apoptosis, in genomic instability and neoplastic transformation [59]. MYC genes are among those most frequently involved in human cancers [60]. Most studies on gene MYC is focused on three members (c-MYC, MYCN and L-MYC), which, when activated, appear to be important in the development of various human cancers [61]. c-MYC was the first of the three to be discovered through its homology with v-MYC, the transforming gene of the MC29 virus of avian myelocytic [62]. MYCN and L-MYC were subsequently identified through their homology with v-MYC amplicons in the cells, respectively, of neuroblastoma [63] and small cell lung cancer [64]. To this family it belongs to at least three other genes: S-MYC, B-MYC and P-MYC. The proteins encoded by the first two appear to suppress the neoplastic transformation as opposed to c-MYC, MYCN and L-MYC [65] [66] [67]. P-MYC is instead a pseudogene derived from a region of L-MYC [68]. The MYC genes can be activated through different mechanisms such as gene amplification [69], the chromosomal translocation [70], proviral insertion [71], retroviral transduction [72] and other processes not yet known. The members of this family play a key role in activating and control of gene expression: in fact they have the same structural motifs present in many transcriptional factors. Such as those present in the oncoproteins v-Fos and v-Jun, leucine-zipper motifs are set in the C-terminus of the protein where, due to their α-helices, they are able to wrap the DNA [73]. Immediately before there is a *helix-loop-helix* domain [74],

already identified in several transcription factors, such as proteins E12 and E47 [75]. Myc proteins also contain a stretch of basic amino acids upstream of helix-loop-helix motif. This pattern, called "basic region", was previously identified in the myogenic transcription factor MyoD, which is the region involved in sequence-specific DNA binding [76]. Considering all these structures Myc gene family contain a motif of bZIP-bHLH able to interact with DNA in which the bZIP and bHLH domains lie in adjacent positions separated by only a basic domain "b ". Unlike normal bHLH domains, it allows fusion of that structure to hang the DNA through the basic regions of bHLH motif, while any dimerization (Myc-Max) of protein monomers are guaranteed by the bZIP motif [77] (Fig. 4).

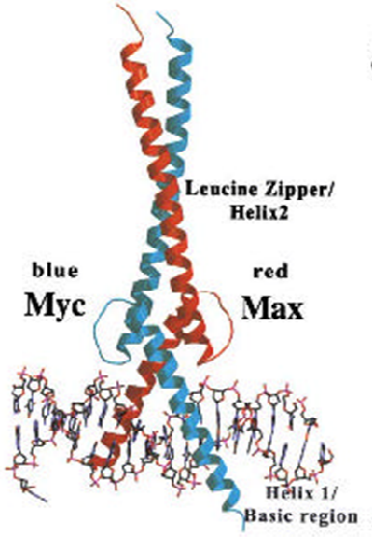

Fig. 4 Structure of a bZIP-bHLH motif: we can see Myc-Max heterodimer and the binding with DNA.

1.2.2 From *MYCN* gene to N-myc protein

The MYCN oncogene was identified in 1983 due to its partial homology with the proto-oncogene c-MYC in neuroblastoma cell lines with DMs (double minute chromatin bodies) and / or HSRs (homogeneously staining regions) [63] [78]. In situ hybridization allowed us to locate on the short arm of human MYCN distal chromosome 2, region 2p23 -24 [79]. Only the second and third exons of the gene are translated and they lead to the formation of the protein.

The post-transcriptional regulation of MYCN is influenced by a signal of ribosomal internalization located at 5'-UTR of the mRNA of the gene, which amplifies the translation initiation and it determines the redistribution in the cytoplasm [80]. The N-myc degradation in

neuroblastoma is ATP dependent and it is mediated by the 26S proteasome in the nucleus; degradation can however be done by the employee via calpain [81].

MYCN acts as a classic dominant oncogene. The forced expression of MYCN can transform normal cells, usually it happen in cooperation with the RAS oncogene [82] [83] [84]. The over-expression of MYCN can release the embryonic fibroblasts from the senescence [85], the addition of a RNA antisense MYCN in cell lines of neuroblastoma that over-express MYCN can reduce the proliferation or induce differentiation and / or its apoptosis [86] [87]. In addition, the over-expression of human MYCN in the neuroectoderm of the transgenic TH-MYCN mouse produces, in a dose-dependent way, neuroblastoma tumors resembling [88].

N-myc protein is a nuclear phosphoprotein with a short half-life (30-50 min) [89] and it shows regions of high homology (overall 38% amino acid identity) with c-myc [90]. Like all the MYC family proteins, N-myc has three specific amino acid sequences [91]:

- a globular domain of transactivation in N-terminus, containing the Myc Boxes I (MBI) and II (MBII): they contain regions rich in glutamine and proline, and an acid region essential for all known biological activities of N-myc protein. The transactivator domain is involved in the balance between apoptotic and proliferative signals [92] and it is also the binding site of proteins that regulate the activity of N-myc;
- an unstructured intermediate region
- a C-terminus domain containing a basic region (BR), which is involved in the recognition and specific binding to DNA [93], a pattern *helix-loop-helix/leucine zipper* (bHLH-LZ), responsible for DNA binding and for the activation of other proteins bHLH-LZ like Max (Fig.5)

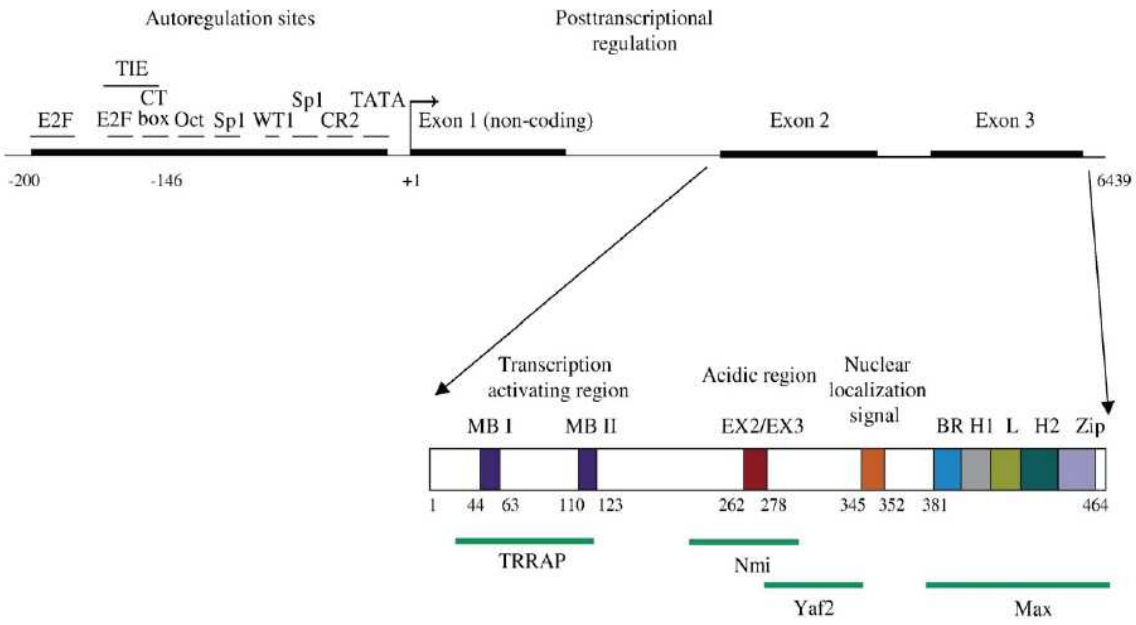

Fig. 5 Structure of N-Myc protein. We can see an N-terminus with Myc Boxes I (MBI) and II (MBII), an acid region, a NLS, a C-terminus domain containing a basic region (BR), a pattern *helix-loop-helix/leucine zipper* H1-L-H2-Zip.

Some studies showed that the protein Myc may form complexes with DNA only at very high concentrations, indicating that these interactions may not be physiologically significant [94]. So it was supposed that Myc required interaction with a second protein to play its role as a transcription factor. It's subsequently identified a small protein called Max [95].

Max is a ubiquitous nuclear protein with a long half-life, similar to Myc because it also contains helix-loop-helix and leucine-zipper basic motif, and it was therefore considered a possible dimerization partners. By *in vitro* assays we have seen that Max is able to form dimeric complexes with each members of Myc family, at a concentration lower than the concentration required for homodimerization of Myc.

During G_0 phase of cell cycle, the expression of Max is high and it favors the formation of homodimers Max/Max, this complex are able to repress transcription. Heterodimerization of N-myc and Max usually corresponds to an increased production of N-myc. This complex binds DNA specifically to a palindromic nucleotide sequence CACGTG, called E-box [96]; another binding site between N-myc and DNA is constituted by asymmetric sequence CATGTG. These two sequences are not exclusive of Myc protein, as they are also recognized

by transcription factors such USF, TFE3 and TFEB. This leads to an great series of transcriptional activation of genes that promote cell growth [97].

Myc is also able to suppress the activity of other specific genes, although the molecular mechanisms underlying these processes are not yet known.

The repression mechanism does not appear to involve direct interaction with DNA; Myc, in fact, raised to the level of promoters through protein-protein interactions with positive transcription factors, such as TFII-I, NF-Y and Miz-1, or actively recruiting co-repressive protein [98].

Despite the structural and functional homology, the expression of c-MYC and N-myc are very different [99]: c-myc is ubiquitous expressed in proliferating cells, while N-myc has a pattern of expression quite restricted [100]. The development of mouse shows that N-myc is mainly expressed during the early stages of differentiation: at the birth it still express in brain, kidney, intestines, heart and lungs, but it is subsequently down-regulated and in the adult mouse its expression occurs mainly in the early development of B lymphocytes [100].

In 1997 Wakamatsu and co-workers [101] found that, during the development of the neural crest of chicken embryos, N-myc is initially expressed in the entire cell population. This expression is turned off during the colonization of the ganglia and of the spinal cord, except for cells to undergo neuronal differentiation. The high expression of N-myc results in a massive migration of the population of ventral neural crest and subsequently these cells migrate into the ganglia subjected to neuronal differentiation. Then N-myc is involved in regulating the fate of neural crest in two aspects: the ventral migration and neuronal differentiation.

The transcript of N-myc is rather complex: it begins in different sites that can be grouped under the control of two promoters; the multiplicity of sites to start combines with alternative splicing to generate two forms of mRNA. The mRNAs have different 5' leader sequences but identical structure. Both forms of mRNA are unstable with a half-life of 15 min. They encode the two N-myc proteins of 65 and 67 kD [102]. However, the first alternative exons contain open reading frames distinct, which can diversify the coding potential of the gene, and this reflects the complexity of the control of gene expression. Both proteins are phosphorylated by casein kinase II (CK-II) [103] and they are localized in the

nucleus linked to single-or double-stranded DNA [89].

1.2.3 Role of *MYCN* in neuroblastoma

Approximately 25-30% of primary untreated NB shows the amplification of MYCN, which is associated with advanced disease, rapid progression and poor prognosis [91]. The reason of this association is still uncertain. There is also a direct correlation between the levels of N-myc protein and the aggressiveness of this tumor [104].

MYCN amplification in human neuroblastoma was discovered in 1983 by Schwab and colleagues [63]. Following studies have confirmed that the presence of more than 10 copies of MYCN gene per haploid genome is an unfavorable prognostic marker, independent from other parameters.

The MYCN amplification was identified as a single genetic factor which adds a prognostic significant information to clinical variables such as age and stage [105], in fact, currently the status of MYCN is the only genetic variable of cancer used as a criterion for stratification of treatment in clinical trials of NB.

In 1997 Weiss W.A. and his group showed that MYCN contributes to the genesis of neuroblastoma with the creation of a transgenic mice that over-express MYCN in neuro-ectodermal cells and for this develop neuroblastoma [88].

Amplified copies of MYCN gene can be present either as extra chromosomal DMs, that as intra chromosomal HSRs. The DMs predominate in primary tumors and the HSRs are present in cell lines [79]. The HSRs are generally located on different chromosomes, not in the 2p24 MYCN site [79] [106]. The values of amplification in neuroblastoma can vary between 5 and more than 500 copies, but usually in tumors there are values around 50-100 copies. MYCN can be duplicated in the 2p24 site, as shown in FISH data [107]. It is not clear whether the duplication represents a prelude to amplification or an alternative pathway for the activation of the oncogenic potential of MYCN. The number of copies of MYCN is usually present in a tumor in different moment during the development and this suggests that amplification of MYCN in positive tumors is usually present at diagnosis [103].

Usually there is a positive correlation between the number of copies of MYCN gene and N-myc expression [38],but in TH-MYCN transgenic murine tumors this relation does not

exist [109]. For *in vitro* analysis, there are few cell lines that express high levels of mRNA or N-myc protein, without gene amplification [41] and this is due to alterations in the pathway of protein degradation or loss of self-regulation of gene transcription [40] [41].

The molecular mechanism of MYCN amplification remains enigmatic. According to one of the most accredited models, the amplification mechanism involves a extraordinary replication of DNA, a recombination and the formation of a extra-chromosomal circular DNA (DM), followed by the integration into a chromosome and subsequent amplification in situ (HSR) [110].

MYCN is centrally located in the DNA amplified and its coding region has never been affected by recombination. The length of amplified DNA comprising MYCN can range from 100 kb to more than 1 Mb [110]. These large dimensions raised the possibility that other genes are co-amplified. Various studies found that the single gene consistently amplified is MYCN, although in approximately 50-70% of cases of NB positive to MYCN, DDX1 gene is co-amplified [111] [112]. It has also been shown that neuroblastoma amplified genes (NAG) are co-amplified in 70% of NB with MYCN amplified [113] but never we have seen amplification of DDX1 or NAG without the amplification of MYCN. This suggests that MYCN is functionally responsible for the maintenance of DNA amplification in 2p24.

The amplification of MYCN is associated with the development of several pediatric tumors, as well as NB: glioblastoma (< 5%), medulloblastoma (5-15%), melanoma of neuroectoderm tumor, astrocytoma, small cell lung cancer (10%) and retinoblastoma (10-20%).

1.2.4 p53 and MYCN in neuroblastoma

p53 is a nuclear phosphoprotein, that function as a transcription factor. The human gene is located on chromosome 17 and mouse gene on chromosome 11, it encodes a tetrameric polypeptide of 393 amino acids. p53 is composed of several functional domains [114]:

• an amino-terminal region whose function is to interact with various components of the transcription complex;

• a proline rich domain, important for p53 activity as tumor suppressor;

• a central domain, responsible for binding to specific DNA sequence;

• a c-teminal region that regulates its oligomerization and localization inside the cell and that contains several sites of non-specific DNA binding

p53 binds a consensus sequences on the DNA and it activates or represses the transcription of several genes (Fig. 6).

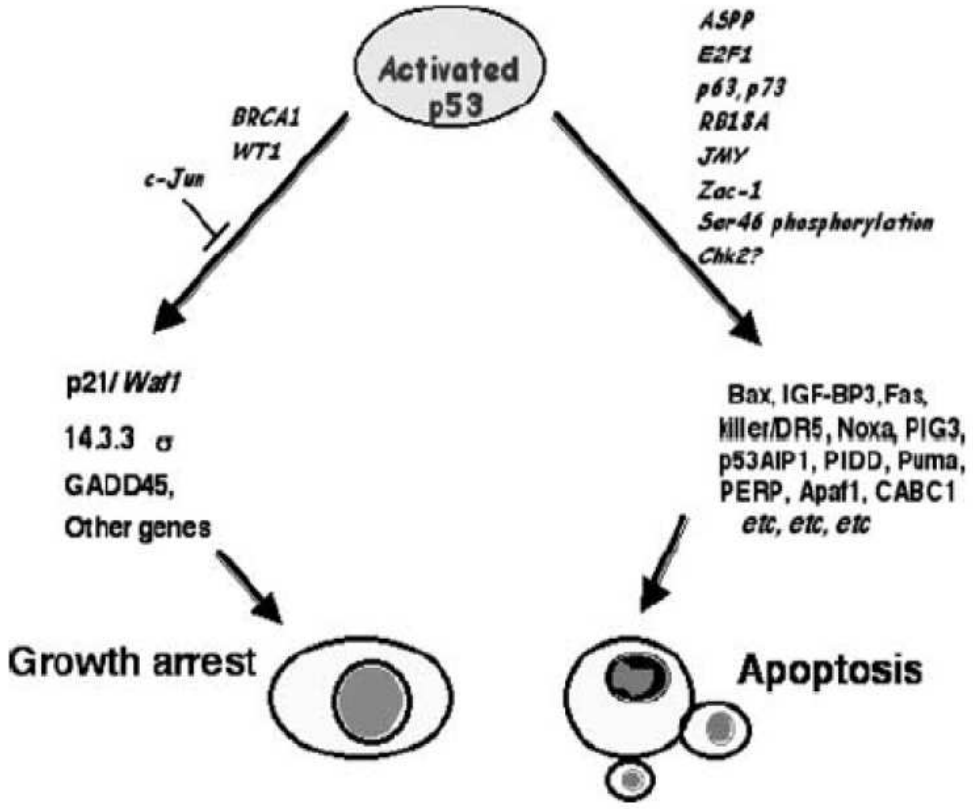

Fig. 6 Some genes involved in p53 pathway.

Depending on what type of genes p53 activates, that it can stimulate apoptosis or inhibit cell cycle progression or promote DNA repair or induce differentiation [115] [116]. Normally p53 intracellular levels are low because the protein is rapidly degraded by ubiquitin-dependent proteolysis induced by Mdm2 factor. Following stress signals p53 can be activated with a consequent increase of intracellular levels. This increase is mainly due to an increase of the stability of the protein, but we can not exclude the presence of a transcriptional or translational control. The stress signals that activate p53 are represented by DNA damage, chromosomal aberrations, oncogenes activities, hypoxia, shortening of telomere, lack of

growth factors [114] [115] [116].

Mutations in p53 or alterations in the p53 pathway are frequent in human tumors [116]. p53 is involved in both hereditary and sporadic tumors. Li-Fraumeni syndrome is a rare hereditary disease transmitted as an autosomal dominant character. In this ereditary tumor p53 mutation is present in the germ line. Individuals with this disease develop various types of primary tumor in different organs and tissues in young age. In rare cases the Li-Fraumeni syndrome with p53 germline mutation developed neuroblastoma [117] [118]. Mutations in p53 are found in 50% of sporadic human cancers [119]. These mutations affect mainly exons 5, 6, 7, 8 [119] [120].

Neuroblastoma at diagnosis presents a low frequency of p53 mutation (< 2%) [121]. It appears that p53 can present mutations more commonly in cell lines derived from relapsed patients. In some indifferentiated neuroblastoma, the sequestration of p53 in the cytoplasm alters the normal G1 checkpoint after DNA damage [122] [123]. Although many studies have shown that in some neuroblastomas p53 is sequestered in the cytoplasm, recently it is shown that cytoplasmic localization and iper ubiquitination of p53 is the result of reduced interaction of p53 with HAUSP [124]. Many studies have demonstrated an important role of p53 in chemotherapy response in neuroblastoma. *In vitro* studies using p53 wild type NB cell lines and p53 mutated NB cell lines show that the cell lines with p53 inactivated are less responsive to chemotherapic drugs [125][126]. *In vivo* studies using a MYCN transgenic mouse model and a transgenic p53 aploinsufficient mouse model show that the p53 mouse model is more resistant to treatment with cyclophosphamide and show in this model reduced levels of apoptosis and PUMA, BIM, and BAX genes [127].

1.3 Peptide Nucleic Acid

1.3.1 Structure and properties

The PNAs are synthetic analogs of nucleic acids, in which the normal phosphodiester backbone is replaced by a pseudo-peptide chain composed of monomers of N-(2-aminoethyl) glycine. The nucleobases are covalently linked to this structure through a polyamide-carbonyl methylene bridge [128].

Despite these changes with respect to natural nucleic acids, the PNA bind sequence-specific DNA and RNA according to the rules of Watson-Crick pairing [129]. The PNA can hybridize with complementary sequences of DNA or RNA, according to two schemes:

- PNA containing the four natural nucleobases, hybridize with complementary nucleic acids according to the rules of base pairing Watson-Crick. Result of the pairing is a *duplex* PNA / DNA or PNA / RNA that resembles the shape of B DNA [130] [132];

- PNA containing only pyrimidines (T or C) can hybridize with complementary sequences of DNA double strand. In this case, the PNA invades the double helix of DNA and hybridizes with the target sequence, while the second strand of DNA is removed and forms a "D" loop [128]. So a triplex is formed PNA / DNA / PNA, in which a portion of the PNA binds to the *target* sequence according to the rules of standard Watson-Crick pairing, while the other portion of the PNA forms the third strand of the *triplex* with a Hoogstein pairing [129] [132].

The PNA are achiral and non-ionic molecules, and the lack of electrostatic repulsion between the filaments makes the hybrid duplex PNA / DNA and PNA / RNA more stable than the natural homo-and hetero-duplex [133]; they are not substrates of hydrolytic enzymes as proteases and nucleases, so they are not degraded in cells and are extremely stable in biological fluids [133].

Since the PNA and DNA have no functional groups in common with the exception of nitrogen bases, their chemical properties differ significantly from those of DNA.

The compounds are neutral and therefore have a low solubility in water compared to DNA. The neutral PNA molecules have a tendency to form aggregates in the nucleotide sequence-dependent manner. The solubility of PNA is also linked to the length of the oligomer and the purine relationship: pyrimidine [134]. Some modifications, including the incorporation of positively charged lysine residues, showed an improvement in solubility. To increase the solubility in water, can also be introduced negative charges, especially in the PNA-DNA chimeras.

The extinction coefficients of the PNA monomers are not well characterized as those of DNA and RNA. It is expected that the PNA oligomers have extinction coefficients different from their counterparts DNA and RNA, because the peptide skeleton would otherwise disrupt

the π system of nucleobases. For this reason, for all practical purposes the concentration of a PNA oligomer is determined by measuring the absorbance at 260 nm at 80°C [135]. At this temperature, the nitrogen bases are considered completely detached and the disruption of π system by the peptide skeleton takes less important.

The proteins that recognize DNA do not interact with the PNA of the same nucleotide sequence, probably due to the lack of electrostatic interactions with the skeleton [136].

The hybridization PNA-nucleic acid is very sensitive to mismatch, in fact it is seen that the PNA bind preferentially to the complementary sequences; more weakly to those containing a mismatch and will not be displayed to those containing two mismatches [137] .

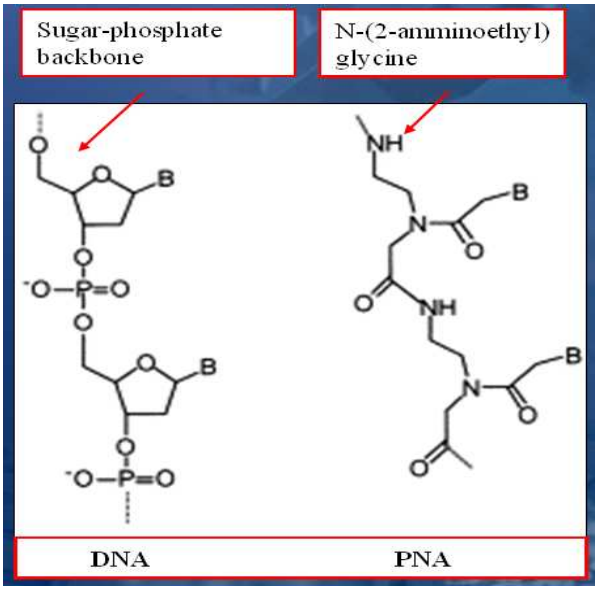

Fig.6 DNA and peptide nucleic acid: comparison between the two different structures.

1.3.2 PNA anti-gene

The PNA is able to block gene expression through two mechanisms:

- inhibition of transcription by binding to DNA (anti-gene strategy)
- inhibition of translation by binding to mRNA (anti-sense strategy)

The PNA antigen can stop the transcription process through their ability to invade the double helix of DNA and form a complex or a stable triplex structure. The PNA can bind to DNA to inhibit the initiation and elongation of RNA polymerase [138] [139] [140]. They can

also be designed to bind the binding sites for transcription factors within the internal promoter, thus inhibiting the binding and action of corresponding transcription factors [141]. The PNA against the promoter region can form a stable PNA-DNA complex that reduces the access to the DNA polymerase. The PNA-DNA complexes located far downstream of the promoter, can also efficiently block progression of polymerase and transcription elongation and so produce truncated mRNA. The triplex PNA2/DNA stop transcription *in vitro* and are able to act as an anti-gene agent [142].

In physiological saline conditions, the binding of PNA to super-coiled plasmid DNA is faster than the linear DNA [143]. This result is based on the fact that usually the transcriptional active chromosomal DNA is negatively super-coiled, and it can act as a better target for the binding of PNA *in vivo*. In addition it was shown that the binding of PNA to double-stranded DNA increases as the DNA is transcribed.

The anti-gene strategy has the advantage, compared with antisense, to block the gene of interest even before it is transcribed: the PNA anti-gene can then be used at lower concentrations and shows a stronger inhibitory effect and prolonged over time compared to antisense [91].

1.3.3 Uptake of PNA *in vitro* and *in vivo*

The poor cellular uptake of PNA is considered the biggest obstacle in the potential of using the PNA as therapeutic agents.

Using phospho-lipid vesicles (liposomes) as a model of cell membranes, Wittung and colleagues have demonstrated that the PNA has a speed of efflux from liposomes very slow (t ½ of 5.5 and 11 days for two PNA of 10 nucleotides) [144]. From these experiments it is concluded that the entry of PNA into cells, by passive diffusion, is very slow. In other studies, has been shown that the PNA's entry in some cells and cell lines is too slow or even undetectable.

In contrast, several groups have found that some cells are subjected to the entry of PNA, suggesting specific transport mechanisms for these molecules [139]. It has been reported, in studies both *in vitro* and *in vivo*, that the PNA enter in mouse neuronal cells. In cultured mouse neurons, not only the PNA are absorbed by cells, but also show an inhibiting of the

expression of target genes, depending on the time and dose [145]. The uptake by neurons is also been shown in vivo. When injected into mouse brain, the PNA are able to decrease the expression of target gene activity, showing an antisense activity [146]. In addition, several groups have shown that, injected intravenously or intra peritoneum, the PNA can cross the blood-brain barrier and enter neurons, causing an antisense reply [139] [145].

So the uptake of PNA appears to depend on cell type. In fact, it is seen after using high concentrations of PNA and long incubation times, it is possible to induce the uptake of PNA even by myoblasts, fibroblasts, lymphocytes and other cell types [142] [147].

To facilitate the uptake of PNA in eukaryotic cells have been proposed several methods:

- permeabilization of the cell membrane with lisolectina [140] or detergents like Tween [148];
- temporary permeabilization with streptolysin O [149];
- PNA modification of hydrophobic motif [150];
- use of transport vesicles such as liposomes;
- PNA conjugation to receptor ligands or antibodies that induce endocytosis receptor-mediated of their respective conjugates [151];
- conjugation with peptides that promote translocation across the cell membrane [152] and targeting specific compartments [153]. The class of Cell Penetratine Peptides, CPP, is growing rapidly. Different studies have shown that penetratine [154] [152] are able of carrying the PNA through the cytoplasmatic membrane in eukaryotic cells. In addition constructs PNA-NLS (nuclear localization signal) increase cellular uptake of PNA and facilitate their transport from cytoplasm to nucleus [153]. The anti-gene PNA conjugated with the NLS peptide, designed for selective inhibition of MYCN gene in human neuroblastoma cells (GI-LI-N and IMR-32: MYCN amplified and over-expressed, SJ-N-KP and NB-100: MYCN not amplified and low expressed), bring inhibition of transcription, inhibition of protein expression, inhibition of cell growth: the cells are stopped in G1, and they should then undergo apoptosis. Its inhibitory effect against the MYCN gene transcription, is highly specific and selective [155].
- binding of PNA to a DNA sequence in a linear oligonucleotide chain and conjugation of

PNA/ DNA chimera with cationic lipids [156];

- micro-injection [138], electroporation.

1.3.4 Therapeutic applications of PNA anti-gene

The high stability at the cellular level, due to their structure and their lack of charge, and the ability to define are fairly stable with DNA, provide to the peptide nucleic acids a significant therapeutic role in treating several tumors. PNA directed against the early-genes E6-E7 of human papilloma virus, responsible for about 100% of cervical tumors, restore the normal function of genes such as p53 and pRB (normal targets of the virus) and attach a normal phenotype to HeLas cells [157].

Further therapeutic evidence has been reported in prostate carcinoma cells where PNA directed to the c-MYC gene inhibit the transcription and translation at 24, 48 and 72 hours in addition to defining a decrease in cell growth [158].

And more selective inhibition of Eμ enhancer regions responsible of the over-expression of c-MYC in Burkitt lymphoma lines (BL) defined cellular cycle arrest in G1 phase, and blocking the expression of that gene [159].

The effectiveness of PNA anti-gene was also tested in different cell lines of neuroblastoma. Sun and colleagues have shown that these third-generation antisense conjugated to somatostatin analogs (SSA), are able to penetrate the nuclear area, to selectively inhibit the expression of MYCN in IMR-32 lines and stopping the growth [160].

Recent studies have also shown that PNA conjugated to specific nuclear localization sequences (NLS) define the most evident effects in MYCN amplified neuroblastoma cell lines compared to not-amplified. The cell cycle arrest in G1 phase is in fact more pronounced in lines such as IMR-32 and GI-LI-N (80-90%) compared with lines containing fewer copies of target gene (50-60% for SJ -N-KP and NB-100).

This ratio is also reflected in the decrease of the expression of MYCN to 24, 48 and 72 hours and the concomitant entry into apoptosis [155].

The evident therapeutic results obtained from *in vitro* studies have laid the foundations for subsequent testing *in vivo*.

Pharmacokinetic studies have shown no toxicity of this molecule in the long and short-term in mouse model of Burkitt's lymphoma; the molecule also remains in the tissues, especially in the tumor for at least 600 minutes *in vitro* at concentrations that inhibit BL [161].

1.4 Chemotherapic compounds

The chemotherapy drugs identify all those drugs whose chemical structure and physical properties are useful in the treatment against the majority of tumors present.

These substances may be synthetic or produced by strains of microorganisms, possess selective toxicity and infectious agents to cancer cells and absence (or reduced) toxicity to normal cells of the human organism.

The chemotherapeutic agents act causing death cell in several ways. Some of these drugs are naturally occurring compounds, identified in several plants, and some are synthetic chemicals. Anti-neoplastic agents are divided into specific categories based on their mechanism of action.

In the following paragraphs we will analyze three classes in particular: alkylating agents, inhibitors of the mitotic spindle (SPs/MIS) and inhibitors of topoisomerase II.

Recent studies have demonstrated the high efficacy of these drugs toward more or less aggressive forms of neuroblastoma. In particular, *in vitro* studies have shown as the apoptosis induced by these drugs and alterations in cell cycle are directly related to levels of MYCN amplification [163] [164].

1.4.1 Alkylating agents

The term alkylating agents comprise compounds that have the ability to become strong electrophiles, thus interacting with nucleophilic groups (phosphate groups, amino, sulfhydryl, hydroxyl, carboxyl, imidazole) alkylating proteins and nucleic acids. Crucial importance has the cytotoxic effect related to the association of these drugs with DNA. The reaction that leads to the formation of stable drug-DNA complex (and / or protein) is schematically divided into two phases:

- activation
- nucleophilic attack

During activation, the alkylating agent is activated by cellular metabolic processes to form an interim net positive charge. Once activated, the compound is able to interact with a number of groups which have a high electron density (phase nucleophilic attack).

The main target of the alkylating agent is DNA; the chemical structure determines the degree of alkylation of various nucleophilic groups found in the nucleic acid molecule. In addition, both the structure and the charge of alkylating agents affect the specificity sequence of alkylation.

The alkylation of DNA bases leads to various physiological changes such as base-pairing errors and subsequent mutations during replication; chemical injury and subsequent excision of bases, formation of covalent bonds within a filament and / or between filaments of DNA matched, stable ties with the associated proteins. In addition to altering the functions of nucleic acids, the chemical alteration of cellular proteins leads to changes in different enzymatic functions, including those responsible for DNA repair.

These agents do not distinguish between cells in the middle of the cell cycle and in quiescent cells (Go phase), however, they are more toxic to rapidly proliferating cells. They are used to treat, in combination with other compounds, a wide variety of solid tumors and lymph [165] [166]

Cyclophosphamide

It is an anti-neoplastic agent belonging to the group of nitrogen mustards, containing a cyclophosphamidic group, is used in the treatment of many forms of cancer, largely as an immunosuppressant (Fig. 7)

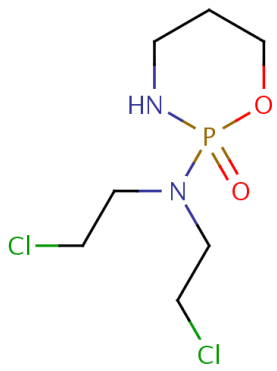

Fig.7 Cyclophosphamide structure.

Its activation involves enzymatic reactions by cytochrome P450, which define the active form (idrossi-cyclo-phosphamide) ionizing the chlorine. However, the intermediate more reactive is mustard phosphoramidates with a capacity to alkylate nitrogen N7 DNA of the guanine causing:

- Alterations in the genetic code: the altered structure of guanine causes abnormal GT pairs
- Broken imidazole ring of guanine
- Depurination DNA for release of a guanine residue and subsequent collapse of the propellers of the desossinucleic acid
- Cross-link of a pair of molecules of guanine

Recent studies have placed the emphasis on the immunomodulatory effects of cyclophosphamide. This drug imposes alterations in lymphocyte populations of T-type determining the decline. These properties of cyclophosphamide, a potent immunomodulator therapies often used prior to bone marrow transplantation.

Cyclophosphamide is also widely used in the treatment of lupus heritematosus, various lymphomas, in care of gromerulonefriti in combination with glucocorticoids and azatriopina [165] [166] [167].

Cisplatin and carboplatin

Compounds of the class of alkylating similar, in fact, have the same function of normal alkylating agents does even not possessing alkyl groups.

Cisplatin has a structure consisting of two labile ligands, two chlorides, and two inert binders, two amines; both in cis position. Carboplatin has instead a motif CBDC (bidentate cyclobutane dicarboxylate), which gives more stability to the compound (Fig.8)

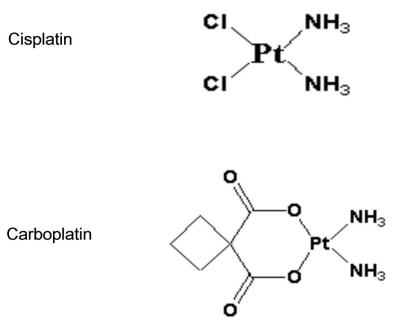

Fig.8 Structure of cisplatin and carboplatin.

The diversity at the structural level between the two molecules is evident in the processes that define the training compounds chemically active.

Once entered into the cell due to a lowering of the concentration of chloride (20 mM), cisplatin undergoes strong hydration in fact, becomes net positive charge and must be made to interact with nucleophiles.

Carboplatin instead once entered in a cellular compartment can generate the reactive intermediate through hydration process (such as cisplatin) or by activation by a nucleophile.

The main target is the DNA: both compounds may in fact contact two nucleotides of the same strand (intrastrand crosslink) or different strands (interstrand); in addition it can define DNA-protein crosslink. The most frequently cited is the intrastrand crosslink between two adjacent guanine [154]. Cisplatin and carboplatin in fact contacted the N group in position 7 by defining a two-purine intrastrand crosslink 1.2 (GGA) or 1.3 (GAG). Other interactions, however, have to be taken into consideration: mitochondrial DNA, actin (shift in composition), phospholipids and phosphatidylserine (Jameson and Lippard 1999). The crosslink format involves a folding of the DNA, with exposure of the minor groove to the hooking of different proteins [165] [166] [168] [169].

Both compounds are broad spectrum in the treatment of ovarian tumor, metastatic testicular cancer in combination with bleomycin vinblastine, and ovarian cancer in combination with cyclophosphamide.

Cito-toxicity

The alkylating compounds are cell cycle non-specific drug, thus causing damage to cell cycle phase-regardless, in particular the cross-links formed are mostly in G1 and G2 phases of the cell cycle. Alterations in DNA structure result in the block of the cell cycle through specific checkpoints in G1/ S and G2/M: in fact the cell tries to remove such alterations by specific repair mechanisms before to entry into S and M phase. The arrest in G1/S and G2/M is the result of a number of factors that recognize the damage (ATM/ATR), define the onset of specific pathways (CHK1, CHK2) and culminate in the activation of p53 and the inhibition of complex CDK /cyclin-specific [170].

At this point, the cell attempts to repair the damage through various mechanisms such as:

- BER (Base Excision Repair),
- NER (Nuclear Excision Repair),
- MMR (Mis Match Repair),
- HMG (High Mobility Group proteins).

Where such errors persist in the genome sequence the apoptosis is triggered. In the case of cisplatin it has been shown that the alleged intrachain 1,2-d (GpG) is removed by excision repair mechanism [169]. This adduct formed in smaller quantities, it is removed more easily while it is uncertain whether the alleged interchain also be removed from this system. However, the initiation of the apoptotic cascade sees as fundamental responsible the class of HMG proteins. This fact suggests that adducts formed by cisplatin are intercepted by these proteins which, when linked to, prevent a shelter by the NER Mechanisms. This leads to a prolonged cell cycle arrest and subsequent cell death.

1.4.2 Mitotic spindle inhibitor

Vincristine

Anticancer drug is derived from the *Catharanthus roseus* plant, also known as common "*vinca rosea*". *Vinca* alkaloids are defined as drugs in this class work by blocking the formation of a structure essential for cell division, the mitotic spindle [161].

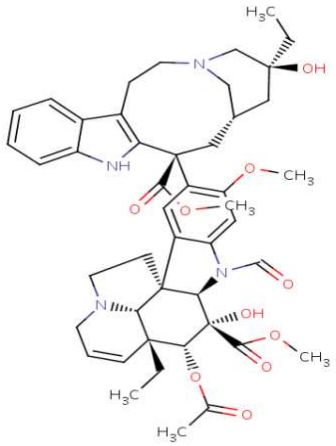

Fig.9 Vincristine structure.

Belonging to the class of inhibitors of the mitotic spindle (SPs/MIS) vincristine is considered a cell cycle specific drug: its action involves in fact the molecules of tubulin (α and β) deputies to the formation of the mitotic spindle useful for the migration of chromosomes during mitosis [165] [166]. In particular, the drug has the peculiarity of intercalation between the α and β tubulin dimers during the formation of microtubules by defining reversible bonds with a frequency of 2 molecules per heterodimer formed vincristine [171]. It has been shown that high concentrations of drug has the appearance of micro tubular crystals [171]. The cytotoxic action of vincristine in the first instance involves a failure to block the metaphase mitotic spindle formation and missed snapping kinetochores, with subsequent initiation of checkpoint the mitotic spindle.

Checkpoint determines the block in anaphase with selective inhibition of the promoting complex of the anaphase (Anaphase Promoting Complex APC) by Mad2 [171]. The block in anaphase leads to events of mitotic death (through the apoptotic cascade) or events of mitotic death after they see the formation of cells from the altered genomic content (polyploidy), intended to succumb [171]. Although some studies have shown high levels of caspase-3 after the block of cells in anaphase the mechanism that connects this block to a subsequent triggering of the apoptotic cascade is still unknown. Vincristine is currently used in treatment in non-Hodgkin's lymphomas, acute lymphoblastic leukemia in the treatment of Wilm's tumors, and occasionally as an immunosuppressant in cases of thrombocytopenia.

1.4.3 Topoisomerasi IIα inhibitor

Etoposide (VP-16)

Etoposide is a semisynthetic derivate of the vegetal alkaloid podophyllotoxin responsible for inhibition of an essential enzyme for structural maintaining of DNA: mouse isomerase II α (α Topo2). It induces the formation of a ternary complex DNA-drug Top2-α disrupting the normal role of this enzyme on nucleic acid [172].

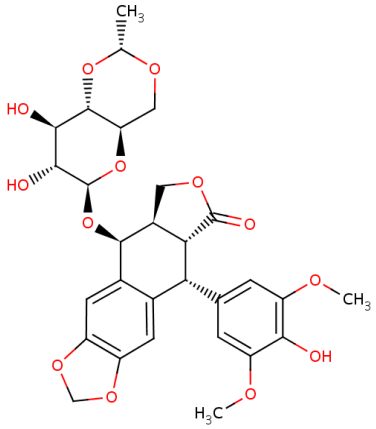

Fig. 10 Etoposide structure.

Topoisomerase II defines in fact a break in both strands of DNA and, through its tyrosine residues that contact covalently the residues at the 5' of DNA [173], is responsible for supercoiling desossimucleic acid. Plays a direct role in S/G2 phase of cell cycle since it leads to condensation and segregation of chromosomal structures [173].

The drug (Fig. 10) involves the inhibition of the enzyme through steric hindrance (direct entry to the cleavage site that the enzyme has created), triggering the following apoptotic cascade. The VP-16 is sterically tolerated in the cleavage site and its activity is directly proportional to the concentration of ATP present. Apoptosis is triggered by the persistence of a DSB [172]. The formation of an irreversible complex that become so after cutting the loop formed by the enzyme-VP-16 by nucleases, triggers a process of apoptosis *via* the extrinsic Fas-FasL [174]. It's also reported that interactions of Top2 α with the Rb protein are altered as a result of the use of inhibitors of the enzyme itself [173].

Etoposide also involves inhibition of Topoisomerase I by an indirect mechanism: the drug, binding to Top2 α, triggers the apoptotic cascade through deregulation of BCL-2, an important anti-apoptotic factor, hence activation of effector caspases (9-3), alteration of mitochondrial potential and the formation of toxic oxygen reactive inducing the block of Topoisomerase I. The blockade of this enzyme only requires further trigger the apoptotic cascade that amplifies the cytotoxic effect of the etoposide [172].

The drug is used as a chemotherapeutic agent in various forms of cancer: Ewing's

sarcoma, lung cancer, testicular cancer, lymphoma, non-lymphocytic leukemia and glioblastoma multiform, and of course neuroblastoma. It is also administered to patients before bone marrow and stem cells transplants.

1.5 Gene targeting by single-stranded DNA oligonucleotides

Gene targeting by single stranded oligodeoxyribonucleotides (ssODNs) is a new technique that gives the possibility to introduce a site-specific sequence alterations in the genome. This tecnique was created in the group of Prof. Hein te Riele at the Netherlands Cancer Institute and permits to generate subtle mutations in the genome of mouse embrionic stem cells, and also use this cells to create a mouse mutant [174].

Strategies based on homologous recombination require the design and costruction of a targeting vector and multiple round of selection and clonal purification of modified cells. Oligo targeting strategy is an alternative approach to introduce subtle gene modifications into mouse genome without affect the genomic organization of the target locus. This tecnique makes use of short single stranded DNA oligonucleotides that are identical to the target gene except for the codon to be modified.

DNA mismatch repair (MMR) system suppress the efficiency of gene targeting single stranded DNA nucleotides in mouse embryonic stem (ES) cell but inactivation of the MMR system also if improved the targeting frequency several fold, it could not be used due to the mutator phenotype associated with constitutive MMR deficiency [175]. In te Riele group they have seen that transient down regulation of the MMR gene Msh2 allowed effective substitution of four adjacent nucleotides in wild-type ES cells. It is not possible introduce single mutation with Msh2 gene transient inactivation because single substitution were still suppressed by 10% of residual MSH2 activity. Instead transient suppression of MLH1, a downstream MMR gene, made cells permissive for all nucleotide substitutions ranging from one to four nucleotides. Although MLH1 knockdown resulted in some what higher mutation frequencies than MSH2 knockdown, the ssODN-modified ES cells retained pluripotency and could contribute to the mouse germ line [176]. The basal mechanism of ssODN-mediated gene targeting is not yet fully understood but the proposed model sees ssODN annealing to its chromosomal complement within the context of a replication fork. The single stranded DNA

regions present during DNA synthesis may enhance ssODN annealing. The possibility to site specifically alter endogenous genes may make ssODN-mediated gene targeting a possible tool for therapeutic applications.

1.6 Murine models of neuroblastoma

An obligatory step in the process of drug discovery regards animal testing. The models described here identify what is the next step after an *in vitro* testing and the analysis of a molecule in a biological system more complex than cellular, more human-like: here we are talking about *in vivo* study. The use of animal models in preclinical studies appears to be the approach best suited not only for drug discovery but also for the identification and study of potential targets at the base of the tumor of interest.

A good preclinical model must:

- Give a faithful reproduction of the main biological characteristics of human cancer of interest
- Allow an estimate of the molecular and cellular events associated with tumor growth and metastasis
- Adequately replicate the difficulties associated with the location of primary tumors and metastasis
- Allow objective and quantitative estimate of the endpoint associated with therapeutic response
- Must be reliable, accessible, reproducible, easy to administer

All mouse models have most of these characteristics, but they show also some limits [177]. For this reason it is necessary to use different models.

1.6.1 Transgenic models

The term transgenic was coined in 1981 by Gordon and Ruddle [178] to describe an animal whose genome is introduced into an exogenous gene; in the 80s the term was extended to the experiments of “gene-targeting ", a method used to insert genes into specific points of

the genome and production of chimeric and knockout mice, in which one or more genes are selectively removed from the genome. Today transgenic animals are called the animals that have undergone any type of genetic specific modification [179].

To be able to insert a gene "exogenous" in an animal, so that it also will be expressed in its progeny, it is necessary to place as early as possible, and that is when the individual is made up of a few cells or even from oocyte just been fertilized. Five different protocols are currently known to produce transgenic animals:

1) the integration of retroviral vectors in the embryo at a very early stage;

2) microinjection of DNA into the male pronucleus of a newly fertilized oocyte *in vitro* or *in vivo;*

3) incorporation in the embryo at a very early stage of embryonic totipotent cells (ES), genetically modified;

4) sperm-mediated gene transfer;

5) transfer of genetically modified nuclei in denucleated oocytes.

After the change in embryo or gamete, the resulting embryos are matured in a pseudo-pregnant female.

The use of transgenic mice to study specific genes that cause the onset of determinate cancers is the best approach in spite of the use of xenograft animals in which human cancer cells are injected under the skin or in the site of origin of the human tumor. This choice depends by several reasons: the similarity of the histological tumor; the tumor is not usually immunogenic, but it develops in a immunocompetent mouse; the tumor develops spontaneous, and also it can present metastasis; it is possible to study a wide range of cancers [180].

The use of recombinant DNA technology and transgenic models has provided much information about the genetic and molecular bases of human disease, in my field of interest the TH-MYCN transgenic model represents the best model to study neuroblastoma. This model has been created in 1997 by WA Weiss and his staff to demonstrate for the first time that over-expression of the MYCN proto-oncogene contributes to transformation of neuroblasts *in vivo*, and thus also participate in the genesis of neuroblastoma [88]. In human

the proto-oncogene MYCN is amplified in approximately one third of patients with neuroblastoma, and it is correlated with advanced disease [83] [155] [156]. There are several experimental demonstrations of its oncogenic potential, and its role in modulating cell proliferation. The over-expression of MYCN combined with H-RAS mutated gene activation can transform rat embryo cells [83]; transgenic mice with over-expression of MYCN under the control of the enhancer of the immunoglobulin heavy chain develop lymphoid tumors [179] [180].

The importance of TH-MYCN transgenic mouse model resides in the tissue specific expression of MYCN transgene: using Western blot analysis it is proven that the N-myc protein is present at high levels in the adrenal glands, derived from the neural crest, from which originates the NB. There is also a marginal expression in brain, heart, testis and spleen [88]. To achieve this result has been used the pTH-MYCN plasmid (Fig. 11), consisting of a fragment of 4.8 Kb of the rat Tyrosine Hydroxylase promoter, follow by the intron of the rabbit beta globin, the human MYCN cDNA and the sequence of the Thymidine Kinase gene of Herpes Simplex Virus.

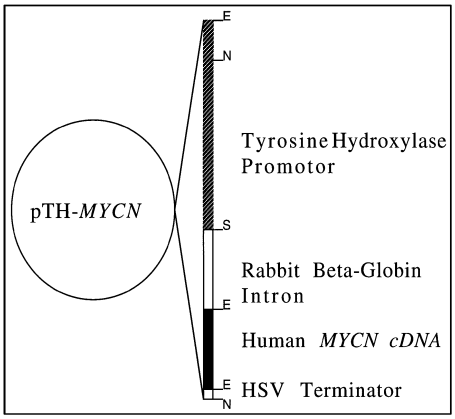

Fig.11 Plasmid inserted into the TH-MYCN transgenic mouse

The tyrosine hydroxylase promoter is responsible for tissue specific expression, as it is active in neural crest migrating cells, early in the development [183], it is also related to the direct state of the chloramphenicol-acetyl-transferase in sympathetic ganglia and adrenal glands, from which neuroblastoma is often derived [183].

The Beta Globin intron has the function of enhancer of the expression, while the Thymidine Kinase gene serves to terminate transcription, because it contains a polyA sequence [88].

The first TH-MYCN mice were created using the technique of the transgene injection in eggs of C57BL/6J and BALB/c strains. The generation so obtained, containing 4 copies of the transgene, was serially crossed to the parental strain C57BL/6J for 7 generations. The F7 females were then mated with *castaneus* males, as females castaneus rarely take care of their children [184]. Several lines of transgenic mice were then created.

The clinical outcome varies from animal to animal and the tumor is localized in the chest or in abdomen. Mice with chest para spinal tumor appear emaciated, dispneic and bent; mice with abdominal tumor usually appear normal but the tumor may envelop other organs like adrenal gland, kidney, intestines. Sometimes there is a paralysis of the lower extremities, and the tumor, as well as in the thoracic and abdominal positions, takes position along the peripheral nerve and also infiltrated into the spinal cord. Some animals show large metastases in liver, lungs and ovaries and other microscopic metastases to the lymph nodes, kidney, testes, brain and muscle.

In histology, the mouse tumors were similar to human tumor, and they show various degrees of neuronal differentiation: there are small round blue primitive cells, neuropil and ganglion cells; the tumors are positive for staining with the neuronal markers synaptophysin and neuron specific enolase NSE. The electron microscope also reveals the formation of synapses and neuro secretory granules.

The Western Blot analysis shows that N-myc protein levels, although varies from tumor to another, are equivalent to those found in human Kelly NB cell line, which has high levels of MYCN gene amplification [63] [88].

The transgene dosage is directly associated with tumor incidence, number of individuals affected by the disease in a determinate period and tumor latency: in 100% of homozygous mice the tumor occurs in 4-7 weeks, while in 27-33% of hemizygous mice at 13-15 weeks [185] [186] [187]. The penetrance, the probability of a specific gene to be expressed, varies instead with the type of strain used for mating: crossing serially with the C57BL/6J strain penetrance decreases, and crossing with the strain 129Sv1 / J penetrance increases[184] [88].

Different studies on this transgenic model, have shown that there is no correlation between expression and dosage of MYCN transgene in murine tumors: Western Blot analysis reveals that some of the most high levels of N-myc protein expression are found in hemizygous mice tumors rather than in homozygous mice. Also there are not significant differences in the transgene dosage in homozygous and hemizygous mice tumors [173]. There is no correlation even between the expression and tumor latency: some of the most high levels of expression of the protein N-myc are in mice that develop cancer after a very large latency period (> = 13 weeks) [186].

It was also shown that the process of gene amplification is specific for the transgene, in fact there are substantial differences in the dosage of murine MYCN between normal and tumor tissues [186].

The chromosome analysis on murine tumors has shown that many of the most frequent genetic aberrations in human NB, are also present in TH-MYCN mouse model, suggesting that this model could be useful in the future to discover genetic abnormalities in mice, and identify parallel genes important in human disease [188]. Thanks to Comparative Genomic Hybridization (CGH) were identified gains on chromosomes 1 and 3, orthologous with the human region 1q, gains on chromosomes 11, 14, 17 and 18, and losses on chromosomes 5, 9, 16, orthologous with regions 3p, 4p, 11q in human chromosomes and loss on X chromosome [88] [183] [187]. For example, the ortholog of human chromosome 17 is contained entirely in the mouse chromosome 11, in which we note a gain in 30% of murine tumors .

1.6.2 Tumor xenograft models

The term xeno-trasplantation derives from greek word ‘xeno’ that means "external" and provides the transplantation of cells, tissues or organs between different species of living beings. This technique differs from allo-transplantation, where donor and recipient belong to the same species. Few are the applications in the clinical field since there are many variables related to graft rejection by the immune system of the recipient, the size of tissues and organs and the average life of two different organisms.

The xenograft however is more useful in research: since the mid-60's in fact the development of animal models useful for the study of various forms of cancer has been

extensively studied with xenograft models. The development of tumor cell lines and primary human tumor cell lines in the last 25 years has paved the way towards the study of human cancer in other species as addressing the rejection of mass inoculated because of immune response. The used animals in fact have deficits in the immune system and mainly in the lymphoid component. The most commonly used strain are the nude mouse and the Severe Combined Immunodeficiency SCID mouse. Nude mouse does not present thymus and for this reason is immunodeficiency in T-lymphoid cell and presents total loss of hair; the SCID mice present genetic alterations, these are reflected in lack of lymphoid B cells, T cells and natural killer cells (NK).

The xenograft models are divided into:

- Ectotopic xenograft models
- Orthotopic xenograft models

The main difference between two models is the point where the tumor is inoculated: the ectotopic model refers to a transplant under the skin, instead the term orthotopic defines a transplantation in the same anatomical location where usually the tumor arises.

This spatial difference shows then substantial discrepancies in enforcement. Ectotopic xenograft models used to validate the therapeutic activity of several drugs in preclinical phase were considered poorly predictive for poor results in the clinical phase [189]. The causes of these differences in healing are largely associated with the different location of the tumor mass formed as well as any differences related to the size of the mass in relation to different stages of tumor present in the clinic phase [189]. The orthotopic model from this point of view is more predictive in that the mass is formed in the animal is in the same position respect to human cancer. This allows to perform studies that are closest to those observed in a clinical, vastly reducing false positives associated with an experimental drug.

1.6.3 Orthotopic xenograft neuroblastoma model

The high occurrence of neuroblastoma in specific areas, 50% adrenal, 25% retroperitoneum, together with the need to obtain pre-clinical prototypes that faithfully reproduce the cancer has led to develop an orthotopic xenograft model in immunodeficient animals within those anatomic compartments.

The current neuroblastoma orthotopic mouse model sees the injection of tumor cells obtained from biopsies of human primary tumors in retroperitoneal area or within the left adrenal gland. In both cases the animal is anesthetized, the first layer of the skin and secondarily the abdominal wall are cut. Approximately 2-2.5 x 10^6 cells are inoculated in the retroperitoneal area or in the adrenal gland [190] [191] [192].

Reports show an incidence of 100%, a latency of 14-20 days approximately and metastasis formation in liver, spleen and kidney after 4 weeks in both sites of injection [190] [192].

The difference between locations reflects differences with regard to development of the tumor mass, the adherent junctions with the surrounding tissues and the localization of metastases. Recent studies have confirmed this difference [190]. Neuroblastoma NB69 cell line injection in SCID mice within the left adrenal gland and in its proximity has established the formation of a nodular tumor with size, latency and morphology identical for the two methods. However, the inoculation in the retroperitoneal area has defined:

a) formation of a tumor adherent to the muscle tone of the animal;

b) skin lesions similar to infections in 50% of the specimens at the site of incision;

c) tumor nodules along the most abdominal wall.

The usefulness of these models has been found not only in studies of tumor progression, angiogenesis, metastasis and invasive capacity [191] [192] [193] but also to test the activity of several drugs [192].

In fact orthotopic xenograft models have been used to validate the action of anti-angiogenic drugs such as *Bevacizumab* or *Bortezomib* in neuroblastoma treatment [195] [196]. Such drugs like *Bevacizumab* reduct intratumoral vascularity powering the effect of traditional chemotherapeutic drugs [195].

Further studies highlight the usefully of the model for association studies between chemotherapy drugs: drugs such as vinblastine and rafamicina in combination would led a reduction in tumor vascularization, cell cycle arrest in G2-M phase and trigger the apoptotic cascade [194].

1.6.4 Transgenic model versus orthotopic model

The transgenic and orthotopic models described above are the best alternatives present today for *in vivo* testing, but it is necessary analyze the similarities and the differences between models to see which is more reliable and predictive for subsequent studies to the stage *in vitro*.

From a management perspective, orthotopic xenograft models show a greater simplicity compared with transgenic models and allow to obtain a large number of items representing the disease relatively quickly, compared to transgenic models characterized by redundant and highly useful analysis required to identify the correct genotype of the animals. This underlines the utility of orthotopic models in validation studies of drugs. It must also be considered the high invasiveness of the orthotopic model compared to the second model, the inoculation of cell lines in the body of the animal is a invasive surgery, this weakens the subject and the risk of infection is very high because of the host immune deficiencies.

Both models define the formation of tumor mass, however, the transgenic model is more predictive, tumor formed represents perfectly the human tumor, with the same cellular and genetic heterogeneity; which makes possible a more complete analysis of interactions between tumor cells and host cells: studies of angiogenesis and interaction with the matrix cells are the evidence [197]. Orthotopic models instead use a specific human cell line whose profile is only isolated oncogenomic combinations of a wide range of genetic and epigenetic mutations that define a case report [197]. The presence of genetic alterations from the embryonic state in transgenic animal models makes them useful for studying the early events leading to the development of the disease, for the design of potential therapies and prevention studies for target validation.

The removal of oncogene of interest or the inclusion of specific mutations help understanding which genes are the real culprits of tumor growth [197]. Should be emphasized, however, important limitations of the transgenic models related to differences between human and mouse genome, thus limiting their use in drug discovery processes [197]. The difference in chromosomal distribution of genes crucial for a study drug as p53, in conjunction with

differences in telomere makes transgenic models do not fully appropriate for studies of this magnitude. In contrast to orthotopic xenograft models, however, they are highly predictive for the immune system, pharmacokinetics, dosage and toxicology [197].

Despite substantial differences still are unable to distinguish which of the two models is better able to represent a clinical picture, in real they are complementary in some important aspects, such as the various applications in the process of drug discovery, as target validation and drug validation and the use of human cell lines or anatomical mouse compartments leads not to exclude either of them during pre-clinical experiments.

1.7 Molecular imaging

The investigation of the molecular alterations present in many diseases is pursued through genetic testing, blood specific tests and histopathologic analysis. In addition, many diagnoses are made only after the onset of first symptoms and in such cases the disease state is just advanced.

Therefore are needed new non-invasive methods for obtaining morphological and biochemical information for functional characterization of early molecular changes: for this reasons Molecular Imaging techniques are needed.

The term Molecular Imaging, coined in 1990, defines the visual representation, characterization and quantification of biological processes at cellular and subcellular level within living organisms "intact".

Imaging systems more used are the X-ray computed tomography (CT), magnetic resonance imaging (MRI), magnetic resonance spectroscopy (MRS), positron emission tomography (PET), optical molecular imaging, which includes fluorescence and bioluminescence (BLI).

1.7.1 Micro Positron Emission Tomography

Positron Emission Tomography (PET) is a non invasive technique of Nuclear Medicine that allows reconstruction of the distribution of radiotracers from the interior of a living subject. A radiotracer is a radioisotope associated with specific active molecules.

PET was developed in 1970 [198][199], the physical process behind the production of images with PET is the emission of a positron and a neutrino; the positron having mass equal and opposite charge compared to an electron, crosses the biological matter and then combines with an electron, before annihilating. The mass of the positron and of the electron is converted into two photons (radiation γ) emitted simultaneously along the same direction but in the opposite direction, and their direction of flight is measured using a set of detectors in time coincidence, placed around the subject [200]. Then the signal is amplified by photomultiplier tubes, which transmit it to a computer, which will build a three-dimensional image.

The advantage of these labeled molecules is that the isotope does not change the physiological behavior of the molecule so it does not alter the structure of its biochemistry. Most of the radioisotopes are generated inside the cyclotrons. A cyclotron is a particle accelerator, which includes a pair of metal electrodes positioned between the poles of a large electromagnet; a source of ions in the cyclotron generates charged particles, usually protons, which are accelerated and, when reached a level of sufficient energy, are directed on a target, causing a nuclear reaction that eventually transforms the substance of the target in the aspected isotope. The radioisotope products are automatically transferred to the target in radiochemistry modules in which are produced the radiopharmaceutical compounds.

Most of the radiotracers has a short half-life and must be produced near the point of use, so the use of these isotopes is limited only to centers that have their own cyclotron. So that a radioisotope can be used as a PET radiotracer must meet strict criteria: the isotope should not be easily dissociated from the molecule to which it binds, and this link should not alter the biological properties of the molecule itself as transportation or disposal; the tracer must be quickly eliminated from the blood and no target molecules, so that there is an high contrast between tumor tissue and adjacent materials.

The radioisotopes are typically administered intravenously and the dose of radiation received is higher than that of a normal radiograph. The PET is emerging as a technique of molecular imaging for the superior specificity and accurancy in spite of common techniques of diagnostic imaging (TAC, MR), and the main application areas are oncology, neurology and cardiology.

For many years researchers have used small experimental animals as models for human disease, following the disease development with radiotracers and autoradiography. However,

these techniques have two main disadvantages: the *post-mortem* data collection, which fails to provide a real representation of the processes *in vivo* and the inability to manage longitudinal studies on the same subject. The use of Micro-PET allows studies of this magnitude.

The creation of micro-PET scanners that could be relied upon as the classic PET scanners for human use, has been a long and arduous process, involving different practical issues, related mainly to the differences between man and animal laboratory.

The mouse, for example, is little more human than 3 orders of magnitude, weighing 20-30 grams against 70 kg of an average man. Because of this difference in Micro-PET must have a very high spatial resolution and sensitivity as to achieve the same level of accuracy achievable with PET [201].

The small size of the animal also limits the amount of tracer used, whereas it should not affect the process being studied, for example, in Micro-PET revealed that the ligand-receptor binding within cells, this parameter is satisfied when the tracer does not occupy more than 1% of free receptors [202].

In almost all molecular imaging technologies, the subject must remain fixed throughout the acquisition of the image, to produce a correct image to define the proper uptake of the radiopharmaceutical compounds. Radiotracers such as ^{18}F-FDG, for example, are also highly detected non-tumor areas with high glucose metabolism, such as the heart and muscles, increasing the chance of having false positives. As regards micro-PET studies is not possible that the animal remains motionless so voluntarily are used various forms of anesthesia [203] [204] [205] also to reduce the stress caused to the PET. It is important to understand the effects of anesthetics, in order to minimize them, as many studies have shown that the administration of anesthesia can compromise systems neuroreceptor.

1.7.2 MicroPET applications

The Micro-PET is used in various fields:

- images of gene expression: as the use of GFP as reporter gene in molecular biology, in PET it is used the PRG (PET reporter gene) expressing a PET reporter probe, which can tie a radiotracer [206]: the gene of interest, put under the control of the promoter of the PRG will always be expressed with the reporter gene, the quantity of the emitted signal will be directly

proportional to the amount of protein expressed by the gene of interest. In basic research that allows to study non-invasively the expression levels of genes in transgenic models *in vivo*, and monitoring the effectiveness of any gene therapy studies in pre-clinical setting [207].

- oncology: this is due to the large number of animal models available (transgenic models, xenograft, knock-out.) [201]. There are many radiotracers used: ^{18}F-FDG, FLT 3'-deoxy-3' -[^{18}F] fluorotimidina [208], labeled antibodies and fragments of antibodies [209].

- applications are still being investigated regarding the auto-immunity, tumor immunology, activation of T lymphocytes [201], longitudinal studies are carried out on glucose metabolism in the heart and brain of rats [210], studies on the cerebral dopaminergic system [211], studies on epilepsy [212] and rheumatoid arthritis [213].

In this study two radiotracers are analyzed: ^{18}F-FDG and ^{18}F-DOPA.

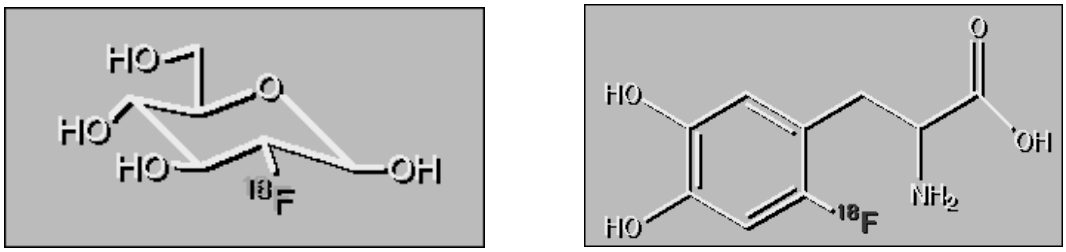

A **B**

Fig.12 The radiopharmaceutical compounds ^{18}F-FDG (A) and ^{18}F-DOPA (B).

Fluorine-18 (^{18}F) is an unstable isotope of fluorine, one of the most widely used tracer for conducting PET, CT-PET and SPECT scans. It presents a rather long half-life (t ½ = 109.6 minutes) and chemical properties similar to hydrogen, it is usually replaced to hydrogen atoms in many natural molecules such as amino acids, carbohydrates, lipids, and a large amount of drugs.

The ^{18}F is used primarily in the formation of ^{18}F-FDG (2-[^{18}F] fluorine-2deoxy-D-glucose) a precursor of glucose that follows its process of metabolism: after being injected into the blood it is transported within cells by glucose transporter and converted by the enzyme hexokinase to FDG-6-phosphate [214]. Unlike glucose, FDG has not the hydroxyl group in position 2 and its metabolite, FDG-6-phosphate can not be further metabolized, and

then remains trapped inside the cell, proportional to the rate of glycolysis. Its accumulation is then associated with the use of glucose, which is index of high cell metabolism [199]. These properties identify the ^{18}F-FDG as a molecule useful in the monitoring of various forms of cancer. The tumor cells in fact have a high metabolic activity.

The ^{18}F-FDG was used for the first time in the 80s in the study of tumors by Di Chiro and other [215] it was proved that the degree of malignancy of brain tumors was related to the uptake of ^{18}F-FDG. The first application of PET with ^{18}F-FDG which is not the neuro-oncology was instead in the study of lung cancer [216] [217]. PET with ^{18}F-FDG is the first molecular imaging technique to be applied on a large scale to imaging study of brain, heart and tumor [218]. ^{18}F-FDG, however, can not be used for some neoplastic diseases (particularly those with high differentiation and low growth rate) since burdened by too high share of false negatives. Moreover, it is no highly selective for tumor cells. Studies of this tracer have consistently revealed a high uptake for macrophages [219] [218] [220].

L-^{18}F-DOPA is used in neurology to study metabolism, neurotransmission and cell processes. L-DOPA is the precursor for the neurotransmitter dopamine and radiolabeled L-DOPA is taken up by dopaminergic terminals and becomes incorporated into the neurotransmitter. L-^{18}F-DOPA can be used to examine the presynaptic distribution of stored neurotransmitter and it used to diagnosis and follow up of neuroblastoma and other Neuro Endocrine Tumors characterized by increased activity of DOPA decarboxylase. It also has been used clinically in the study of Parkinson's disease [221].

1.7.3 Bioluminescent imaging

The bioluminescence imaging is a reporter system based on an enzymatic reaction catalyzed by the luciferase protein, the enzyme that generates light thanks to oxidation of its substrate, D-luciferin, in oxiluciferin, in living systems [222].

In nature there are different bioluminescent systems characterized by a specific enzyme system. The most used bioluminescent system in scientific research is the North American firefly luciferase (*Photinus pyralis*; FLuc), but several clones of luciferase were identified from jellyfish (*Aequorea*), from the sea pansy (*Renilla*), from corals (*Tenille*) and from various bacteria as *Vibrio fischeri* and *V. harveyi*.

Luciferase is an excellent marker for gene expression because it lacks post-translational modifications and has a half-life ($t_{1/2}$) *in vivo* of about 3 hours.

The firefly luciferase produces photons through the following reaction:

$$\text{ATP} + \text{D-luciferin} + O_2 \xrightarrow[\text{luciferasi}]{\text{Mg}^{++}} \text{Oxyluciferin} + \text{AMP} + \text{PPi} + CO_2 + \text{LUCE}$$

The spectrum of light is between 530 and 640 nm with an emission peak at 562 nm. This emission spectrum, coupled to the optical properties of tissue, allows light to penetrate through several centimeters of tissue. In this way it is possible detect light emitted from the internal organs of small mammals that express the luciferase as reporter gene. The photons are detected by a special Charge Coupled Device (CCD) camera that convert photons into electrons. The CCD camera spatially encoding the intensity of the incident photons into electrical charge patterns to generate an image. This camera is controlled by a computer for image acquisition and analysis.

The catalyzed luciferase reaction is a complex interaction between ATP, luciferin and oxygen, the exogenous substrate. The reaction occurs only in metabolically active cells, which contain the luciferase, because the reaction requires the presence of ATP. The light signal intensity depends on various factors such as the level of expression of luciferase, the substrate concentration, the wave length of light generated, the sensitivity of the detector and the localization system of labeled cells inside the body. In general, the signal strength decreases 10 times for each centimeter of tissue through [223].

The BLI is widely used in cancer research for identifying metastasis and to measure the proliferation of tumor cells that express luciferase. Some studies done using HeLa luminescent cells injected into the tail vein of immunodeficient mice have demonstrated the utility of BLI in the early detection of lung metastases. Similarly, other studies have shown that bioluminescence is a powerful methodology for understanding the pathogenesis of the

disease *in vivo*. It has been shown that the detection of tumor cells in internal organs by BLI has a sensitivity at least equal to that of positron emission tomography (PET), also with respect to PET, which requires toxic and radioactive tracers, the BLI requires only administration of D-luciferin, non-toxic even in newborn pups [224].

In conclusion, the BLI may be regarded as a powerful method of investigation and pre-clinical diagnosis, however, quantitative analysis must be done with caution and require validation of each specific application.

1.7.4 Transfection of cell lines throughout retroviral vectors

The stable expression of heterologous genes in the mammalian cells can be reached by the use of recombined retroviruses.

The most commonly studied and utilized retroviruses are those belonging to the Retroviriade subclass. This retrovirus typology is modified and it has lost its replicative capacity because it do not present some genes express within the wild type strain. They allow the stable integration of transgenes within the eukaryotic cells genome [225].

Retroviruses are defined as viruses whose genome is constituted by a singular RNA filament of around 10 Kb of size and by a region ψ for the packaging. It includes three essential genes, gal, pol, envelope. They codify respectively the core proteins, the inverse transcriptase and the capside.

Long Terminal Repeats (LTR) are placed to each edges and these sequences are implied in the integration phase. LTRs are divided in three regions: U3, R and U5. The 5’ R is defined as the initial signal sequence for the transcription phase in the 5' LTR, whereas the U3 region contains both the promoter and the enhancer element. Moreover, the U3 region contains the signal of poliadenilation. During the retrotranscription, the U3 region at the 3' LTR and the U5 region at the 5' LTR of the viral RNA are duplicated (Fig.13). Once the cell is infected, the RNA is retrotranscribed in a double DNA filament that entries in the nucleus and it is integrated in the genome of the host cell, expressing in this way the viral proteins. Simple retroviruses such as MLV are unable to cross the nuclear membrane and the infection is restricted to cells in mitosis, therefore when the nuclear membrane is dissolving.

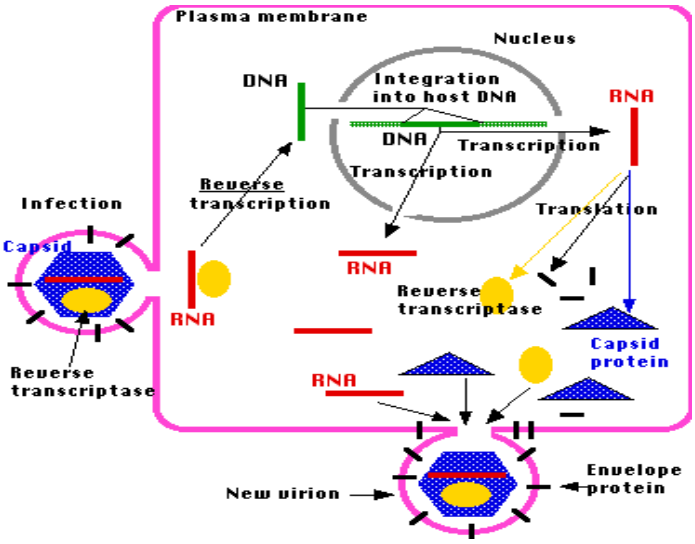

Fig.13 Life cycle of retrovirus.

The most common retroviral vectors are derived by MLV (Moloney Murine Leukaemia Virus), that is an amphotropic virus able to infect both human and murine cells.

In these vectors, viral genes are replaced by the transgene of interest, which is inserted between the LTRS downstream packaging signal and the promoter. They can also be added marker genes (such as neomycin) and alternative promoters of viral origin.

The gag, pol and env coding regions are separated into distinct transcriptional units in order to decrease the risk of production of wild-type virus through recombination, and added with stable integration in cell lines that are called packaging cells. The packaging cells are able to generate a complete virion, but empty because they do not contain the sequence ψ and can not package the viral genome in the virion. The viral vector instead contains the transgene downstream of ψ, and thus, if inserted into a packaging line, it produces a viral progeny which virion is provided by the packaging line and the genome is the recombinant viral vector containing the transgene .

The range of cells that can be infected by recombinant retroviruses thus produced, depends on the type of envelope protein in the virion. We can distinguish ectotropics retrovirus, which can only infect cells of rodents and anfotropics retrovirus, which infects almost all mammalian cells.

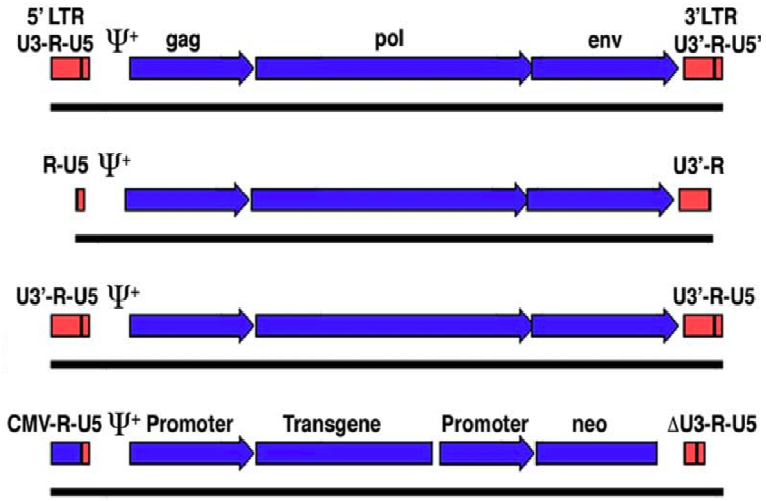

Fig.14 Schematic representation of the genome of retroviruses and retroviral vector.

The choice of vector system is highly dependent on target cells. Generally, vectors derived from MLV are easier to produce and, to date, are available in a wide range of packaging cells. However, infection by these viruses is extremely low in quiescent cells or low growth rate and therefore should be used only in cells with high growth rates such as tumor cells.

1.7.5 MicroPET versus bioluminescent imaging

The main difference between micro PET and bioluminescence lies in the portion of the electromagnetic radiation spectrum used, which affects the performance of each methodology. In fact, the high penetrating power of γ-rays created by the phenomena of annihilation in the microPET coupled with the limited thickness of the body of rodents allows more precise

quantification of the signal at the level of the deeper anatomical structures than the bioluminescence. However, both techniques have high sensitivity coupled with excellent spatial and temporal resolution.

Another difference consists in the type of molecular probe used. MicroPET uses radiolabelled probes: probes that consistently produce the signal through the decay of radioisotopes; while the bioluminescence uses active probes: probes that emit a signal only after interaction with their target.

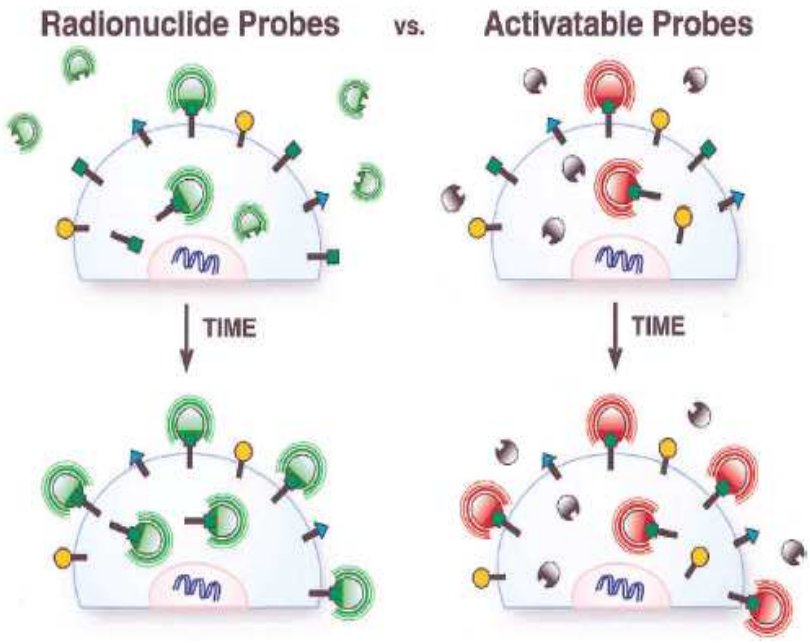

Fig.15 Comparison between the two different probes: a radionuclide probe for microPET experiment and a activable probe for bioluminescent analysis.

All probes must have some basic characteristics: biocompatibility, ability to cross biological barriers, the possibility of signal amplification *in vivo.* They must consider some important pharmacokinetic properties such as metabolism, excretion / reabsorption, urine excretion, cytotoxicity. The probes should be stable and especially should not be able to elicit the immune response.

Regardless of the differences inherent in each method, the investigator should consider the potential use and the limits of each one.

The specificity of the micro PET comes from the ability to mark a particular radioisotope molecule without perturbing its biological function for the small steric hindrance. However, because of their short half-life, it require to have a cyclotron on site or nearby. In addition, the radioactivity of the tracer could have effect on the patient, limiting its use. The sensitivity of micro PET is equivalent to 10-100 times the SPECT, CT and MRI and thisresults from the use of coincidence of counts of photon collimators and the ability to correct the resulting loss of signal due to attenuation of the photons. However you need a large number of crystal detectors.

The microPET allows to obtain sections of images and it is a translational method in fact, using the same technology in clinical practice, the transition between the preclinical and clinical applications is faster, reducing the time needed to transfer information in an other type of analysis.

One of the most important application of microPET is the oncology. With micro PET It is possible to monitor tumor progression during time and in the same subject characterizing the level of metabolism, hypoxia, perfusion, cell proliferation in tumor.

Micro PET does not give anatomic information and some radiotracers are aspecific. For example,^{18}F-FDG accumulates not only in cancer cells but also in sites of chronic inflammation or in high metabolic active organs like heart, also its uptake is not related to the tumor increase speed and for this reason the data must be interpret by expert investigator. Micro PET allows pharmacokinetic and pharmacodynamic studies for drug development also if it is a expensive technology.

Unlike the micro PET, bioluminescence has low running cost, there is not the problem of penetration of the beam of excitation in the tissues and there is no source of intrinsic autofluorescence so there are not false positive signals. The use of luciferase as a marker represent an advantage because it lacks post-translational modifications and it has a half-life *in vivo* of about 3 hours. Thanks to the short acquisition times it is possible to monitor different animals in the same analysis and also monitor biologic process during the time. The instruments analyze all the body of the animal given a complete view of all tissues and organs.

The disadvantages of this technique derive from two fundamental properties of light in tissues that depend on the wavelength: the diffusion and absorption. These affect the resolution. For example, high vascularized organs like spleen and liver show low levels of

light transmission because of the oxy hemoglobin and deoxy hemoglobin absorption [228]. *In vitro* it has been estimated that the reduction of bioluminescence signal is approximately 10 times for each centimeter of tissue analyzed. Moreover the reaction of luciferase requires the interaction with a variety of molecules including oxygen, ATP and luciferin, if any of these elements are not enough present in the tissue, the emission of light can not represent the real activities of luciferase [226]. The correlation and the application of the results are difficult because there is no equivalent in clinical practice.

Although micro PET and bioluminescent imaging present limits, they can be considered complementary and they provide a multimodal approach to research in order to cover the different experimental needs.

2

Materials and methods

2.1 Chemicals

The PNA was designed as homologous to a unique sequence of the noncoding (antisense) strand in exon 2 of MYCN (bp 1,650-1,665: 5'-ATGCCGGGCATGATCT-3'; Genbank accession no. M13241). This PNA antigene (PNAs), which is complementary to a unique sequence in the DNA strand, was designed to directly inhibit mRNA synthesis. To test the specificity of the activity of this PNAs, a mismatched PNA (PNAmt) was also designed containing a 3-base substitution (5'-**G**TGCCG**A**GCATG**G**TCT-3'). Specificity was verified using the BLAST homology program. All the PNA molecules were covalently linked to their COOH terminus with a nuclear localization signal (NLS) peptide (PKKKRKV) to mediate transfer across the nuclear membrane [229]. Synthesis, purification and characterization of the PNAs and PNAmt was made by our laboratory as described [155].

Vincristine, etoposide, carboplatin, cysplatin and isoflurane (Aerrane) were purchased from Baxter Health Care Pty Ltd (Lessines, Belgio).

The pSUPER vector (Sigma–Aldrich, Zwijndrecht, Netherlands) contains a puromycin resistancegene and pSUPER-MLH1 plasmid was constructed to obtain a transient inactivation

of MLH1 gene, involved in mismatch repair system (kindly provided from H. Te Riele, NKI, Amsterdam, The Netherlands).

Unmodified 35-mer single-stranded OligoDeoxyriboNucleotides (ssODNs) were designed to introduce a single base mutation in mouse MYCN sequence, in this way the human target sequence of PNAs would be also present in the mouse MYCN DNA sequence. Sequence sense ssODN (5'-GCGTCCACCATGCCGGG**C**ATGATCTGCAAGAACCC-3') is complementary to the transcribed strand except a single mutation in the centre (C versus G) of the oligonucleotide flanked by 17 matching nucleotides on each sides.

Anti-sense ssODN (5'-GGGTTCTTGCAGATCAT**G**CCCGGCATGGTGGACGC-3') has opposite polarity and it is complementary to the non transcribed strand but it introduces identical base change. Both ssODNs were ordered at Sigma–Aldrich (Zwijndrecht, Netherlands).

2.2 Cell lines

For *in vitro* proliferation assay, chemotherapeutic treatment and orthotopic mouse models I used the following adherent neuroblastoma cell lines:

IMR-32, SK-N-BE(2)c (kindly provided from G. Della Valle, Department of Experimental Evolutionary Biology, University of Bologna, Italy); IMR-5 (from M. Schwab, Department of Tumor Genetics, Deutsches Krebsforschungszentrum, Heidelberg, Germany); Kelly (from Dr. R.A.F. MacLeod, DSMZ, Braunschweig, Germany) characterized by amplification and over-expression of MYCN [230] MYCN-unamplified/low-expressed SJ-N-KP (kindly provided from P. Rocchi, CIRC, University of Bologna, Italy); MYCN-unamplified/unexpressed GI-CA-N (from F. Pastorino, Gaslini Children's Hospital, Genova, Italy). The human NB cell lines IMR-32, Kelly, SJ-N-KP and GI-CA-N were obtained from different tumors at diagnosis and present p53 gene wild type, while SK-N-BE(2)c was obtained from a tumor relapsed after chemotherapeutic treatment and presents multi-drug related p53 mutations. NHO2A (from W. A.Weiss, Department of Neurology, University of California, San Francisco) is a cell line derived from homozygous TH-MYCN mouse tumor characterized by amplification and over-expression of cDNA human MYCN. Human cell cultures were maintained in RPMI-1640 (SIGMA-ALDRICH, Milwakee, WI) supplemented with 10% FBS (Euroclone, Pero, Milano,

Italy), 1% L-glutamine 2mM (GIBCO-Invitrogen, Carlsbad, CA), 1% non-essential amino acid solution 0.1 mM (SIGMA-ALDRICH, Milwakee, WI). For murine cell line RPMI-1640 was supplemented with 20% FBS, 1% sodium pyruvate 1mM (GIBCO-Invitrogen, Carlsbad, CA) and 0.07% β-mercaptoethanol 10nM (Merck, Darmstadt, Germany).

	Species	Loc.	Age	Sex	MYCN	INSS
IMR-32	Homo Sapiens	A[1]	12 month	M	Amplified/ over-expressed	4
IMR-5	Homo Sapiens			-	Amplified/ over-expressed	4
SK-N-BE(2)c	Homo Sapiens	A[1]	22 month	M	Amplified/ over-expressed	4
Kelly	Homo Sapiens	-	-	-	Amplified/ over-expressed	4
SJ-N-KP	Homo Sapiens	UNK[3]	5 year	-	Single copy/ *low*-expressed	-
GI-CA-N	Homo Sapiens	AG[2]	9 month	F	Single copy/ unexpressed	4
NHO2A	Mus Musculus	A[1]		-	Amplified/ over-expressed	-

Tab.1 Humn and murine NB cell lines. [1]Abdominal; [2]Adrenal Gland ,[3] Unknown

Cell lines were subcultured at 37°C / 5% CO_2 weekly, cells being detached from the monolayer with citric saline (135 mM potassium chloride (SIGMA-ALDRICH, Milwakee, WI), 15 mM sodium citrate (SIGMA-ALDRICH, Milwakee, WI)).

The generation of luciferase positive NB-cell lines required Phoenix cell line (Phoenix Retroviral Expression System, Orbigen). Cell culture was maintained in DMEM medium (SIGMA-ALDRICH, Milwakee, WI) supplemented with 10% FBS (Euroclone, Pero, Milano, Italy), 1% L-glutamine 2mM (GIBCO-Invitrogen, Carlsbad, CA), 1% streptomycin/penicillin antibiotics (GIBCO-Invitrogen, Carlsbad, CA).

The oligonucleotide-mediated gene modification was performed on 129/Ola- derived E14-IB10 Murine Embrional Staminal Cells (mESC) [231]. The cell line was cultured on Murine Embryonic Fibroblast (MEFs) feeders in Glasgow minimal essential medium (GIBCO-Invitrogen, Carlsbad, CA), supplemented with 10% FCS (Fisher Scientific, Thermo Scientific HyClone, Loughborough, Leicestershire), 1mM sodium pyruvate (GIBCO-Invitrogen, Carlsbad, CA), non-essential amino acids (GIBCO-Invitrogen, Carlsbad, CA), 1mM β-mercaptoethanol (Merck, Darmstadt, Germany) and 1000 U/ml of leukaemia inhibitory factor (LIF, GIBCO-Invitrogen, Carlsbad, CA). For transfections and puromycin selection, ES cells were cultured onto gelatin (SIGMA-ALDRICH, Milwakee, WI)-coated plates in Buffalo rat liver cells -conditioned medium [231]. The cell lines were cultured at 37°C / 5% CO_2, cells being detached from the monolayer of MEFs and from the BRL medium with 10x and 2x Trypsin (TVP), respectively. TVP was prepared with DPBS pH 7.4 (GIBCO-Invitrogen, Carlsbad, CA), EDTA 40 mM (GIBCO-Invitrogen, Carlsbad, CA), Chicken Serum 1% (GIBCO-Invitrogen, Carlsbad, CA), Trypsin 2.5% (GIBCO-Invitrogen, Carlsbad, CA).

2.3 Proliferation assay

To assess the cytotoxic and proliferative effects of PNAs and PNAmt at 24, 48 and 72 hours and chemotherapeutic drugs at 72 hours I used the Adenosine TriPhosphate monitoring system based on firefly (Photinus pyralis) luciferase (ATPlite^{TM} Perkin Elmer, Waltham, MA, USA). The experiments were performed on 96-well microplate adding 50 µl of mammalian cell lysis solution to a 100 µl cell suspension. After 5 min in an orbital shaker at 700 rpm, I added substrate solution containing luciferase and D-luciferin. After 5 min in an orbital shaker

and 10 min at dark the emitted light was measured with Infinite F200, TECAN. The measured luminescence is proportional to the ATP concentration. ATP is a marker for cell viability because it is present in all metabolically active cells and the concentration declines rapidly when the cells undergo necrosis or apoptosis. (ATPLT-0408 / REV. F). Each experiment was performed at least four times and the cell lines were seed 24 hours before the experiment to allow cell adhesion.

2.4 Generation of luciferase-positive neuroblastoma cell lines

The pMMP-LucNeo vector (Fig.16), a generous gift from Prof. A. Kung (Harvard University, Boston) was used to transform in XL1 E. coli competent cells (Agilent Technologies, Stratagene, La Jolla, CA).

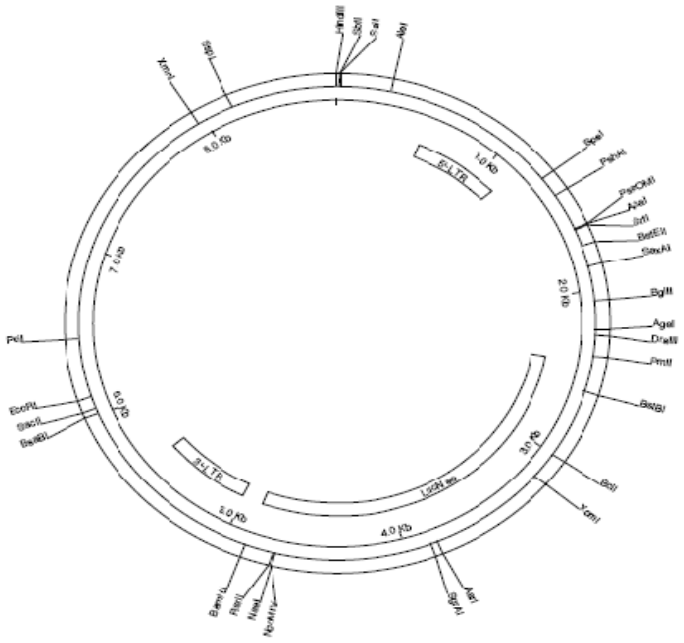

Fig.16 pMMP-LucNeo vector

One microgram of plasmid DNA was used to transform E. coli with heat shock at 42°C for 30 sec, bacteria were grown overnight at 37°C in LB medium composed of 5 g bacto-yeast extract, 10 g bacto-tryptone, 10 g NaCl, 1 ml ampiciline 1 mg/ml and 1 l water. The plasmid DNA was extracted and purified with QIAfilterPlasmid Maxi Kit (QIAGEN, Duesseldorf, Germany), the DNA was quantified using NanoDrop ND-1000 (NanoDrop Technologies, Wilmingon, DE).

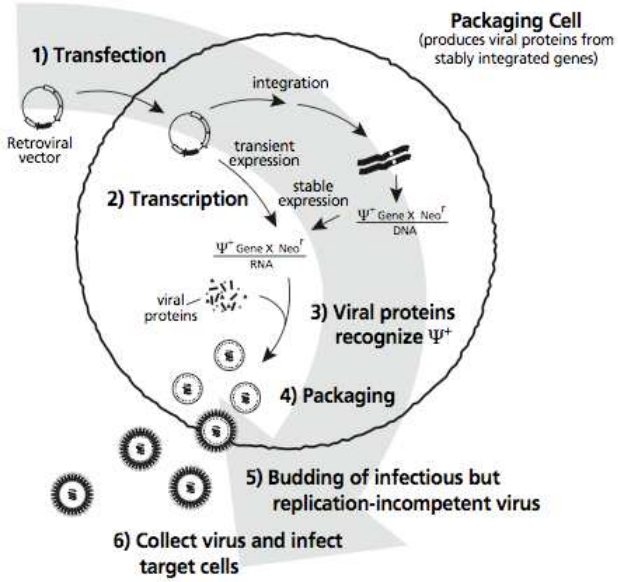

Fig.17 Transfection scheme

For each MA-NB cell lines, Phoenix packaging cells were seeded $2.8x10^5$ cell/well in a six wells plate, the day after the cells were transfected with 5 µg plasmid DNA and 10 µl Lipofectamine 2000 reagent (Invitrogen, Carlsbad, CA) in 1 ml of DMEM for 5 hours at 37°C. After the incubation 1 ml DMEM with 20% FBS was added and the day after the medium was changed. 1ml of medium contained retroviral vector particles, produced in the Phoenix packaging cell line, were filtered and introduced into MA-NB cell lines with Polybrene 8 µg/ml (Millipore, Billerica, MA) and 5 ml fresh medium. $2x10^5$ cells of IMR-5, SK-N-BE(2)c and Kelly were seeded 12 hours before the infection and 10^6 cells for IMR-32

cell line were seeded. After transduction, the NB cell lines were selected with 1 mg/ml G418 (GIBCO-Invitrogen, Carlsbad, CA) for 14 days, then stable transfectants Luciferase expression in 10^5 live intact cells was examined using Luciferase Assay Reagent (Promega, Madison, WI) and measured with a spectral scanning multimodal plate reader (Varioskan Flash, Thermo Scientific, Whaltham, MA) in the 560-670 nm range of absorbance. Six different dilution (10^6, 10^5, 10^4, 10^3, 10^2, 10) of luciferase positive NB live intact cells were analysed on the LB 981 (Berthold Technologies) after added of 100 µl of D-Luciferin Steady-Glo® Luciferase Assay System (Promega, Madison, WI).

2.5 Oligonucleotide-mediated gene modification in murine ES cells

The pSUPER-MLH1 plasmid and the two single-stranded OligoDeoxyriboNucleotides (ssODNs) were transfected following the TransFast-mediated transfection method [174]. $7x10^5$ ES cells were seeded onto a gelatin-coated 6-well in BRL-conditioned medium the day before transfection. For one well, 3 µg of pSUPER-MLH1 and 27 µl of TransFast transfection agent (Promega, Madison, WI) were diluted in 1.4 ml serum-free medium and incubated 15 min at room temperature. After 75 min of exposure to the transfection mixture at 37°C, 4ml of BRL-conditioned medium with serum was added to the cells. The cells were incubated over night and then each well was reseeded onto a new gelatin-coated well in 3 ml BRL-conditioned medium with 44.5 µl puromycin (1.8 µg/ml, SIGMA-ALDRICH, Milwakee, WI). After 48 hours of puromycin selection, cells were washed twice with PBS and one well was used for tranfection with sense ssODN (RD151, 1 µg/µl, SIGMA-ALDRICH, Milwakee, WI) and one with antisense ssODN (RD152, 1ug/µl, SIGMA-ALDRICH, Milwakee, WI). For one well, 3 µg of ssODN and 27 µl of TransFast transfection agent (Promega, Madison, WI) were diluted in 1.4 ml serum-free medium and incubated 15 min at room temperature. After 60 min of exposure to the transfection mixture at 37°C, 4 ml of BRL-conditioned medium with serum was added to the cells. ES cells were expanded and plated in pools of 5000 cells for well onto four 96-well feeder plates containing irradiated mouse embryonic fibroblasts (MEFs). In 3 subsequent screening rounds, cells were seeded onto 96-well MEF feeder plates in pools of 1000, 500 and 100 cells for well, respectively. From the most positive well 10^3

cells were seeded in 10 cm gelatin-coated dishes for colony picking. 300 colonies were picked and the best was reseeded in 10 cm gelatin-coated dish to be sure that a positive single-cell clone is truly clonal [176].

After establishment of a pure clonal cell line, I verify the presence of the target mutation by sequencing. The total RNA was isolated from $3x10^5$ positive clonal cells using RNAzol B (IsoTex Diagnostics, Inc): add 250 µl RNA-Bee to the cell pellet; pipet the lysate several time; add 50 µl chloroform; shake vigorously and incubate on ice for 5 min. Centrifuge at 12000 g for 15 min at 4°C; transfer the aqueous phase to a clean tube; add 125 µl isopropanol and incubate at room temperature for 15 min; centrifuge at 12000 g for 10 min at 4°C; remove the supernatant and wash the pellet twice with 250 µl 75% ethanol; centrifuge at 7500 g for 5 min at 4°C. Briefly air-dry the RNA pellet and dissolve RNA in 15 µl water. Total RNA was run in a 2% agarose gel and it was read at Nanodrop ND-1000 (NanoDrop Technologies, Wilmingon, DE). 1 µg of total RNA was reverse transcribed in cDNA using SuperscriptII RT enzyme (Invitrogen): add at the sample 1 µl dNTP 10 mM, 0,25 µl random examers (1 µg\ µl) and 11 µl of water, incubate the mix for 5 min at 65°C and for 1 min in ice. Add 4 µl 5x Buffer, 2 µl 0.1M DTT, 1 µl RNase OUT to the sample, incubate at 25°C for 2 min, add 1 µl of Superscript II RT Enzyme (200U), incubate at 25°C for 10 min, incubate at 50°C for 40 min and at 70°C for 15 min.

200-400 ng of cDNA were amplified in a PCR reaction with primers spanning the mutation. The reaction contained 2 µl Buffer II 10x (Applied Biosystem, Roche), 0,5 µl dNTPs 10 mM, 0,5 µl Taq DNA polymerase 1U (Euroclone), 0,8 µl forward primer 100 µM (ACCCCTTTGGCTCATTCTCT), 0,8 µl reverse primer 100 µM (CCTGAAGGATGACCGGATTA), 13,4 µl of water. I used PTC-200 Peltier Thermal Cycler (MJ Research) and PCR reaction conditions were 3 min at 94°C, for 40 cycles: 30 sec at 94°C, 30 sec at 60°C, 30 sec at 72°C and a final step of 2 min at 72°C. I analysed the PCR product on a 1,6% agarose gel in TAE 2.5x buffer.

I cut the 479 bp fragment from the gel under UV Transilluminator (UVP,Inc) and I used QIAquick Gel Extraction Kit (QIAGEN, Duesseldorf, Germany) to extract DNA: weigh gel slice, add 600 µl of Buffer QG; incubate at 50°C for 10 min with 14000 rpm shaking in Thermomixercompact (Eppendorf); add 200 µl isopropanol; apply the sample to the QIAquick column; centrifuge 1500 rpm for 2 min; discard flow-through; add 750 µl of Buffer PE; centrifuge 13000 rpm for 1 min; discard flow-through; centrifuge 13000 rpm for 1 min; add 30 µl of Elution Buffer; let for 1 min and centrifuge 11000 rpm for 1 min. The DNA was

quantified using NanoDrop ND-1000 (NanoDrop Technologies, Wilmingon, DE). I cloned the fragment in pGEM®-T Easy vector (Promega, A1360; Madison,WI): prepare one Standard Reaction with 5 µl 2x Rapid Ligation Buffer; 1 µl pGEM®-T Easy vector; 1 µl T4 DNA Ligase (3 Weiss units/µl); 3 µl PCR product (25 ng) and a Background Control Reaction with 5 µl 2x Rapid Ligation Buffer; 1 µl pGEM®-T Easy vector; 1 µl T4 DNA Ligase (3 Weiss units/µl); 3 µl water. Incubate both reactions for 60 min at room temperature. The ligated DNA was subcloning in DH5α™ Competent Cells (Invitrogen): thaw on ice DH5™ cells; add 2 µl DNA or 2 µl Background Control; incubate on ice for 30 min; heat shock cells for 20 sec in a 42°C water bath; incubate on ice for 2 min; add 950 µl pre-warmed LB medium; incubate at 37°C for 60 min at 225 rpm; spread 50 µl from each transformation on pre-warmed selective plates (1x); centrifuge eppendorf at 8000 rpm for 1 min; under bunsen burner remove 870 µl medium; resuspend and spread the cell suspension on pre-warmed selective plates (10x); incubate plates for 16 hours at 37°C. Count colonies on transformed plates; pick 23 colonies under bunsen burner; seed each colony in 2 ml of LB medium with 2 µl ampicillin; incubate tubes for 16 hours at 37°C and 150 rpm. Isolate the transformed DNAfrom minicolture with miniprep protocol: centrifuge 2 min at 8000 rpm; remove surnatant; add 100 µl solution I (5 ml 1M TrisHCl pH8.0, 9 ml 20% glucose, 4 ml 6.5 M EDTA, 182 ml demi water) and vortex; incubate for 5 min at room temperature; add 180 µl fresh solution II (0,4 ml 5N NaOH, 0,5 ml 20% SDS, 9,1 ml demi water) and vortex; incubate on ice for 5 min; add 150 µl cold solution III (60 ml 5M KAc, 11,5 ml acetic acid, 28,5 ml demi water) and vortex; incubate on ice for 5 min; centrifuge at 4°C at 14000 rpm for 5 min. Transfer supernatant in eppendorf containing 800 µl 100% ethanol; centrifuge at 14000 rpm for 15 min; remove supernatant; add 200 µl 70% ethanol; centrifuge at 14000 NanoDrop Technologies, Wilmingon, DE). 0,2 µl miniprep DNA samples were digested rpm for 2 min; remove supernatant; add 25 µl $T_{10}E_1$ and RNase (mix 5 ml $T_{10}E_1$ and 3 µl RNase). The 23 miniprep DNA were quantified using NanoDrop ND-1000 (with 1 µl Eco RI restriction enzyme in presence of 1 µl buffer H and water. To a final volume of 20 µl. The digestion product was analysed on a 0,6% agarose gel in TAE 2.5x buffer.

The positive samples presented a 500 bp fragment and a 3000 bp fragment (empty pGEM®-T vector). 16 clones were processed with BigDye®Terminator v3.1 Cycle Sequencing Kit (AppliedBiosystems) using T7 primer and they were sequenced.

2.6 *In vitro* treatment

PNAs-NLS was added at concentrations of 2.5, 5, 10 µM on Kelly and SK-N-BE(2)c and at the optimal concentration of 10 µM on IMR-32, IMR-5, NHO2A [229]. To evaluate the specificity of the effect of PNAs-NLS on MYCN, IMR-32, IMR-5, SK-N-BE(2)c, Kelly and NHO2A were treated at 10 µM with PNAmt-NLS. Cells were harvested and analysed at 24, 48 and 72 hours after treatment. Cell count was determined by the trypan blue dye exclusion method and cell viability was determined with ATPlite proliferation assay (see section 3.3). For each well, PNAs or PNAmt were diluted in serum-free medium and after 6 hours serum was added to the cells to avoid that the PNA molecules didn't precipitate in presence of serum (observed in laboratory experiments). Each experiment was repeated on at least three times.

To analyse the possible synergy of the PNAs-NLS with the conventional chemotherapeutic drugs used in clinical protocol against MYCN amplified neuroblastoma, the cell lines were treated at different concentration with Carboplatin (CBDCA), Cysplatin (CDDP), Vincristine (VCR) and Etoposide (VP-16) and analysed after 72 hours with ATPlite kit (see section 3.3). The concentration range used is shown in the table below (Tab.2). At the beginning we tested the concentration used in Fulda S., EJC 1995 and after several experiments we obtained our concentration ranges [232]. Each experiment was repeated on at least four times.

Log[drug] / Cell lines	CBDCA (µM)	CDDP (µM)	VCR (nM)	VP-16 (µM)
IMR-32	-1.22/2.78	-0.35/2.65	-3/1	-1.16/2.85
IMR-5	-0.22/2.78	-2.35/2.65	-1/3	-5.15/1.85
SK-N-BE(2)c	0.78/3	-0.35/1.65	-1/3	-1.15/3.1
Kelly	-2.34/1.77	-3/1.65	-4/0	-0.34/1.85

Tab. 2 Chemotherapeutic drugs concentrations.

2.7 TH-MYCN mice colony

All the experiments involving animals were reviewed and approved by the Bioethical Committee of Bologna University, Italy and by Italian Ministry of Health. Animals were kept under pathogen free conditions, with ad libitum access to food. TH-MYCN murine model was generated and kindly provided from W. A. Weiss, Department of Neurology, University of California, San Francisco [88]. To obtain a TH-MYCN mice colony we ordered also 8 129X1/Svj mice females of 8 week old to The Jackson Laboratory (Bar Harbor, ME). The strain 129 is a good breeder, at the beginning the mating system was between wild-type females and 3 hemizygous TH-MYCN males. Genomic DNA was isolated from mouse-tail tips harvested when animals were 17 days old. The lysis buffer used is constituted of Tris 1 M pH8.5, EDTA 0.5 M pH8, NaCl 5 M, SDS 10% and water. Each tail tip was incubated over-night in agitation in 500 µl lysis buffer and 2.25 µl proteinase K(Sigma). The suspension was put in 500 µl iso-propanol, gently mixed and DNA tail was picked and put in 100 µl Elution Buffer over-night at 37°C. Each DNA sample was quantified twice with the NanoDrop ND-1000 spectrophotometer (NanoDrop Technologies, Wilmington, DE). The genotypes of MYCN transgenic mice were determined by qualitative PCR analysis using primers RBBI2 (411) s (TGGAAAGCTTCTTATTGGTAGAAACAA), MYCN (26) as (AGGGATCCTTTCCGCCCCGTTCGTTTTAA) from http://mouse.ncifcrf.gov and as housekeeping mACTB (911) s (GCTCCTCCTGAGCGCAAG), mACTB (1106) as (ATGGAGGGGCCGGACTC). PCR reaction contained 100 ng gDNA, Buffer II 10x (Applied Biosystem, Roche), 0.8 mM dNTPs, 2 mM $MgCl_2$, 0.2 µM primer reverse and forward, 1U Taq DNA polymerase (Euroclone). We used PTC-225 Peltier Thermal Cycler (MJ Research) and PCR reaction conditions were 1 min at 95°C, for 40 cycles: 30 sec at 94°C, 30 sec at 68°C, 1 min at 72°C and a final step of 7 min at 72°C. We analysed the PCR product on a 1% Agarose gel with EtBr in TBE 0.5x.

Later, we started mate between hemizygous mice and we obtained also homozygous mice for the human MYCN transgene. Homozygous mice were identified analysing tail DNA not by southern blotting [88] but by real-time quantitative PCR with a new set of primers designed on the sequencing of an hemizygous PCR product. The primer sequences are: RBBI2 (533) s (CCTCTGCTAACCATGTTCA), MYCN (-128) as (ACAGCTCAAACACAGACAGAT) and as housekeeping mPOLR2DI1 (1151) s (CAGTTGCCAGGTGGATCTCTT), mPOLRD2DI1 (1287) as (TGCTCATGCCCACAATTAGTT).

qPCR analysis was performed to quantified human MYCN amplification using LightCycler® 480 Roche, according to the manufacture's instruction and SYBR Green I Master (Roche Applied Science, Mannheim, Germany). The real-time quantitative PCR was performed adding to 10 ng cDNA (4 µl final volume), 10 µl Fast Star SYBRGreen MasterMix 2x (Roche), 0.6 µl primers forward and reverse 10nM and water to final reaction volume of 20 µl. PCR reaction conditions were 2 min at 50°C, 10 min at 95°C, for 50 cycles: 15 sec at 95°C, 60 sec at 60°C. The dosage of transgene in the samples was determined using the ΔΔCt method, a comparative technique in which target gene dosage is normalized to the housekeeping gene control and relative to a calibrator (parents of each progenies and 476 hemizygous mouse).

In vivo experiments were performed using 22 hemizygous mice for microPET experiment, 40 homozygous mice to create the micro PET tumour progression curve and 9 homozygous mice to treatment.

2.8 Establishment orthotopic xenograft models

All experiments involving animals were reviewed and approved by the Bioethical Committee of Bologna University, Italy and by Italian Ministry of Health. Animals were kept under pathogen free conditions, with ad libitum access to food. After an ectotopic xenograft model experiment, orthotopic xenograft models were established by injection of $2x10^6$ IMR-32, SK-N-BE(2)c and IMR-5 cells in 20 µl NaCl solution. Four-week-old NOD-SCID mice (Charles River Laboratories, France) were anesthetized with 0.3 mg/kg body weight Zoletil 100 and Atropine Sulphate 1 mg/ml, subjected to laparotomy, and injected with neuroblastoma cells into the right adrenal gland. We confirmed the tumor presence with palpation, a microPET analysis and tumor histology. Luminescent p53 mutated orthotopic xenograft model was established by injection of $2x10^6$ Luciferase-positive SK-N-BE(2)c cells while Luminescent p53 wild type orthotopic xenograft models were established by injection of $2x10^6$ Luciferase-positive cell lines (IMR-32, Kelly, IMR-5) in 20 µl NaCl solution. Four-week-old NOD-SCID mice (Charles River Laboratories, France) were anesthetized with 0.3 mg/kg body weight Zoletil 100 and Atropine Sulphate 1 mg/ml, subjected to laparotomy, and injected with neuroblastoma cells into the right adrenal gland. No mice died as a result of this treatment. General physical status of the animals were recorded daily, and mice were killed by cervical dislocation after being anesthetized with 0.3 mg/kg body weight Zoletil 100 (Virbac S.r.l., Carros Cedex, France), when showing signs of poor health. The tumour presence was

confirmed in each models with Bioluminescence Imaging analysis and histology. All *in vivo* experiments were performed using 4 mice each cell line to set the model, 10 mice each luciferase-positive cell line to perform the luminescent progression curve, 8 mice were treated with chemotherapeutic compounds.

2.9 Molecular imaging

We used two different Imaging methods: microPET and Bioluminescence Imaging. All experiments involving animals were reviewed and approved by the Bioethical Committee of Bologna University, Italy and by Italian Ministry of Health.

Thanks to small animal micro PET imaging (Nuclear Medicine, S.Orsola-Malpighi Hospital, University of Bologna, Italy), we studied 37 hemizygous mice and 60 homozygous mice [233]. The animals' weight ranged from 14 to 26g.

Thirtyseven hemizygous animals underwent several small animal PET scans with ^{18}F-FDG, twice in a week, and ^{18}F-DOPA every week for two months from 20 to 50 days after birth. Sixty homozygous mice underwent several micro PET scans with ^{18}F-FDG, every three days for two months from 27th days of live until detection of positivity and from this initial point every week. We used hemizygous mice to compare ^{18}F-FDG and ^{18}F-DOPA, as radiolabelled compounds and evaluate their physiological and tumor uptake and a homozygous mice were analyzed to define a temporal window in which to detect the beginning of the tumor and to follow its progression.

The whole diagnostic procedure was carried out under a warm light to maintain the body temperature, especially during anaesthesia. The animal was anaesthetised with gas anaesthesia (Sevofluorane 3–5% and oxygen 1 l/min) and it was injected with 30 MBq of ^{18}F-FDG in a volume of 0.15 ml, or 30MBq of ^{18}F-DOPA in a volume of 0.25 ml, via tail vein with an insulin syringe. The animal was subsequently allowed to wake up for the uptake period (60 min), during which it was allowed to move freely. The residual dose was measured to verify the effective dose injected. Finally, a second anaesthesia was applied in the same way to perform the scan. Each anaesthetised animal was placed on the scanner bed in prone position. Images were acquired with a small animal PET tomograph (GE, eXplore Vista DR) for a total acquisition time of 20 min. As the axial field of view was 4 cm, one bed position was sufficient to cover the whole body. Once the scan had been completed, the gas anaesthesia was interrupted and the animal was placed in a warm recovery box until complete recovery.

^{18}F-DOPA and ^{18}F-FDG-PET images were reconstructed with iterative reconstruction OSEM

2D and read in three planes (axial, sagittal and coronal); the scan was considered positive if areas of increased uptake were present at sites consistent with the site of insurgence of the tumor. Necrosis was diagnosed when a cold central area appeared within the neoplastic mass. Semi-quantitative analysis was carried out for each identified tumour obtained from ^{18}F-FDG scan using the Target-to-Background-Ratio (TBR). TBR was calculated with the following formula (Max Count in the Target ROI)/(Mean Count in the Background ROI). The target region of interest (ROI) was placed on the most active area of the neoplastic mass (excluding necrotic areas) and as background ROI we chose a region of the skin surrounding the tumor. Mean TBR was calculated for each scan. Normal subcutaneous tissues had a TBR of 0.3. We also calculated tracer uptake in tumors with Standardized Uptake Value (SUV), correcting the value with the mean tumor volume that correspond at each positive micro PET point. The SUV is the ratio of the activity concentration measured in the microPET image and the injected dose divided by the animal's weight. All animals were sacrificed and histology was performed to verify PET results.

Thanks to Bioluminescence Imaging, we analysed luminescent orthotopic xenograft mice models. We performed an *in vivo* experiment to understand the kinetic and the body distribution of the substrate. A IMR-5 luciferase positive mouse received an intra peritoneal injection of 150 mg/kg D-luciferin (Gold Biotechnology, St.Louis, MO, USA), it was placed in the lith-tight chamber OD, a cooled CCD camera system LB981 (Berthold technologies, Wildbad, Germany) (Pharmaceutical Sciences, S.Orsola-Malpighi Hospital, University of Bologna, Italy) under Isoflurane anaesthesia (Isofluorane 3% and oxygen 1 l/min). Luminescent signals were acquired each 30 sec for 1 min for a total of 15 min. After this previous study, all mice received an intra peritoneal injection of 150 mg/kg D-Luciferin and placed in the lith-tight chamber OD, under Isoflurane anaesthesia. Pictures and luminescent images were acquired 8 min after D-luciferin injection in prone position for 3 min. The Winlight software version 2.9 of the low-light imager system LB981 (Berthold technologies, Wildbad, Germany) was used to analyze the BLI data. The luminescent signals were calculated as photon flux per second (ph/s) considering a ROI of 2246 mm^2.

2.10 *In vivo* treatment

PNAsense was administered by intra peritoneal injection at a dose of 50 mg/kg in microPET positive homozygous TH-MYCN mice of 35 days. Two schedules were performed: two mice were treated each two days for a total time of 20 days and one mouse was treated each days for a total time of 20 days. A group of 6 control animals were simultaneously treated with NaCl solution. All animals were monitored during the study, the weight and general behavior of each mouse were misured. Mice were sacrified at first sign of distress.

An initial dose-response study was performed using the p53 mutant model (SK-N-BE2c Luc mice) and a p53 wt (Kelly Luc mice) orthotopic xenograft model with two chemo therapeutical drugs, vincristine (0.06 mg/kg) and etoposide (14 mg/kg). Two animals for each model were treated and a group of 4 control animals were simultaneously treated with NaCl solution. These concentrations were obtained from the used concentrations in the treatment of high risk neuroblastoma patients.

2.11 Histology and immunohistochemistry

Each NB sample was divided into two parts. A NB piece was frozen in liquid nitrogen and it was kept at -80°C for molecular analysis and an other piece was fixed in formalin for histological analysis.

To assess the potential toxic effect of PNAwt, histological analysis was performed in all major organs in two wild-type 129X1/SvJ mice subjected to the same treatment schedule with PNAwt or saline. Together with Dr. Korinne Di Leo evaluated different organs: heart, lungs, liver, pancreas, parotid glands, esophagus, intestines, kidneys, adrenal glands, uterus, ovary, spleen, thymus, brain, bone marrow and peripheral blood.

Murine tissues were fixed in 4% formalin, dehydrated, embedded in paraffin, cut into 4 µm sections and stained with hematoxylin an eosin (H&E) methods. Bone marrow and peripheral blood were evalueted with May-Grunwald-Giemsa staining. For hematoxylin-eosin staining, tissue sections were subjected to subsequent incubations in toluene, 100% ethanol, 95% ethanol, 70% ethanol, distilled water, hematoxylin, distilled water, eosin, distilled water, 70% ethanol, 95% ethanol, 100% ethanol and toluene. After coverslip application, slides were observed by light microscopy. For May-Grunwald-Giemsa staining, the slides with blood smears were subjected to subsequent incubation with May-Grunwald for 3 min, washing in water, incubation with Giemsa for 7 min, washing in distilled water. After coverslip application samples were observed by light microscopy.

NB tissue sections were processed for immunohistochemistry. Sections were subjected to subsequent incubations in xilene, 100% ethanol, methanol and 0,3% hydrogen peroxide, 96% ethanol, 70% ethanol, distilled water and then incubation in citrate buffer in pressure cooker. The sections were washed with 1x PBS, incubated with goat serum for 15 min at room temperature, washed with 1x PBS and incubated with 1:75 anti-N-Myc primary antibody (Oncogene) over night. The day after the slides were washed in 1x PBS and they were incubated with anti-mouse secondary antibody (DAKO, Evision) for 20 min. After wash in 1xPBS, they were developed with a 5% Di-Amino-Benzidine chromogen in TAI Buffer pH 7.6 with 3% hydrogen peroxide. After wash in 1x PBS slides were subjected to subsequent incubations in distilled water, hematoxylin, distilled water, 70% ethanol, 95% ethanol, 100% ethanol and toluene. After coverslip application, slides were observed by light microscopy.

2.12 Fluorescence In Situ Hibridization (FISH)

FISH analysis was performed on fixed NB cells and on paraffin embedded tissue to confirm MYCN amplification. The tissue slides were treated with Paraffin Pre Treatment Kit from Abbott Molecular Inc (Des Plaines IL 60018 USA) and FISH analysis was performed according to the protocols recommended by the manufacturer (Vysis Inc., Downers Grove, IL, USA). Specific locus probe for MYCN (LSI-N-MYC(2p24), Vysis) and centromeric probe for chromosome 2 (CEP2(2p11.1-q11.1), Vysis) were used. Hybridization signals were analysed on a Olympus BX51 microscope coupled to a Cytovision Ultra system (Applied Imaging, Sunderland, UK).

2.13 DNA isolation and gene amplification analysis

Genomic DNA was isolated from NB cell lines and from frozen murine tissues using NucleoSpin® Tissue (Macherey-Nagel). According to the User Manual Genomic DNA from Tissue: collect ten millions cultured cells, resuspend in 200 µl lysis buffer T1, add 25 µl proteinase K solution and 200 µl Buffer B3, incubate the sample 15 min at 70°C. Collect 25 mg murine tissue (from tumour, liver and other organs), treated in a mechanical homogenizer, add 200 µl Buffer T1 and 25 µl proteinase K solution, vortex briefly the sample, incubate at 56°C over-night. Add 210 µl ethanol absolute to both sample types, place each sample into a Collection Tube of one NucleoSpin® Tissue Column, 1 min at 11000 x g, wash membrane

with 500 µl Buffer BW, 1 min at 11000 x g, add 600 µl Buffer B5, 1 min at 11000 x g, 1 min at 11000 x g. Place the NucleoSpin® Tissue Columnin a new microcentrifuge tube, add 100 µl prewarmed Elution Buffer (70°C), 1 min at 11000 x g. Each DNA sample was quantified twice with the NanoDrop ND-1000 spectrophotometer (NanoDrop Technologies, Wilmingon, DE).

qPCR analysis was performed to confirm MYCN amplification using LightCycler® 480 Roche, according to the manufacture's instruction and SYBR Green I Master (Roche Applied Science, Mannheim, Germany). The real-time quantitative PCR was performed added to 10 ng gDNA (4 µl final volume), 10 µl Fast Star SYBRGreen MasterMix 2x (Roche), 0.6 µl primers forward and reverse 10 nM and water to final reaction volume of 20 µl. PCR reaction conditions were 2 min at 50°C, 10 min at 95°C, 15 sec at 95°C, 60 sec at 60°C for 50 cycles. The dosage of target gene in the samples was determined using the ΔΔCt method, a comparative technique in which target gene dosage is normalized to the actin control and relative to a calibrator.

The primer sequences are: MYCN (49) s (CCAGACCTCGAGTTTGACTC), MYCN (161) as (TCAAACTTCTTCCAGATGTCC) and as housekeeping β-actin (991) s (GCTCCTCCTGAGCGCAAG), β-actin (1106) as (ATGGAGGGGCCGGACTC) for MYCN amplification analysis.

Genomic DNA was isolated from mES cells in 96-wells plate using a proper lysis buffer containing 100 mM Tris pH 8.0, 5 mM EDTA, 200 mM NaCl, 0.2% SDS and fresh 200 µg/ml Proteinase K. In each well add 50 µl lysis buffer, incubate the plate for 2 hours at 55°C, add 100 µl ethanol absolute, seal the plate and carefully invert it five times, 30 min at 3000 g at 4°C, remove supernatant, add 100 µl 70% ethanol, 15 min at 3000 g at 4°C, remove supernatant and add 60 µl Elution Buffer, incubate at 55°C over-night. qPCR analysis was performed to quantify the mutation title of each sample using LightCycler® 480 Roche, according to the manufacture's instruction and SYBR Green I Master (Roche Applied Science, Mannheim, Germany). The real-time quantitative PCR was performed added to 2 µl gDNA, 1.6 µl Fast Star SYBRGreen MasterMix 2x (Roche), 0.125 µl primers forward and reverse 10 pM and water to final reaction volume of 10 µl. PCR reaction conditions were 2 min at 50°C, 10 min at 95°C, for 50 cycles: 15 sec at 95°C, 60 sec at 66°C. The dosage of mutant allele was determined using the ΔCt method, a comparative technique in which mutant allele dosage is normalized to the wild type allele in each sample.

The primer sequences are: RD155 s (CTCTCCACGGGAAGGAAGCACTC), RD160

as (GTCTGGGTTCTTGCAGATCAA**C**) for wild-type mMYCN sequence, RD155 s (CTCTCCACGGGAAGGAAGCACTC) and RD156 as (GTCTGGGTTCTTGCAGATCAA**G**) for mutant mMYCN.

2.14 RNA isolation and gene expression analysis

Total RNA was extracted from $2x10^6$ NB cell lines and from 30 mg of frozen tissues according RNAspin Mini RNA Isolation Kit (GE Healthcare, UK): after homogenization, add 350 µl Buffer RA1 and 3.5 µl β-mercapto-ethanol to the samples. To clear the lysate filter it with a RNAspin Mini Filter unit. Centrifuge 1 min at 11000 x g, add 350 µl 70% ethanol, mix the samples and load them into a RNAspin Mini column. After 30 sec at 8000 x g, add 350 µl Membrane Desalting Buffer, centrifuge for 1 min at 11000 x g to dry the membrane. Centrifuge for 1 min at 11000 x g, digest DNA with 95 µl of DNase reaction mixture, incubate for 15 min at room temperature. Wash the membrane with 200 µl Buffer RA2, centrifuge 11000 x g for 1min, add 600 µl Buffer RA3, centrifuge 11000 x g for 1 min, add 250 µl Buffer RA3, centrifuge 11000 x g for 2 min. Elute the RNA in 40 µl H_2O RNase–free. Each RNA sample was quantified twice with the NanoDrop ND-1000 spectrophotometer (NanoDrop Technologies, Wilmingon, DE). The 2 µg RNA (final volume of 10 µl) was reverse transcribed using Superscript II RNAseH (Invitrogen): add 1 µl dNTP 10 mM and 1 µl oligo dT to 10 µl of sample, incubate the mix for 5 min at 65°C and for 1 min in ice. Add 4 µl Buffer 5x, 2 µl DTT 0.1M, 1 µl RNase OUT to thesample, incubate at 42°C for 2 min, add 1 µl of Superscript II (50U), incubate at 42°C for 50 min and at 70°C for 15 min. Quantitative PCR analysis was performed to confirm MYCN over expression and to analyse the efficacy of the PNA treatments. We used LightCycler® 480 Roche, according to the manufacture's instruction and SYBR Green I Master (Roche Applied Science, Mannheim, Germany). The real-time quantitative PCR was performed added to 10 ng cDNA (4 µl final volume), 10 µl Fast Star SYBRGreen MasterMix 2x (Roche), 0.6 µl primers forward and reverse 10 nM and water to final reaction volume of 20 µl. PCR reaction conditions were 2 min at 50°C, 10 min at 95°C, for 50 cycles: 15 sec at 95°C, 60 sec at 60°C. Each sample was amplified in triplicate. ΔΔCt calculations were used to determine the level of expression of target genes relative to reference control and to a calibrator (untreated samples or normal tissue).

The primer sequences for analyse MYCN over expression in NB tumors, NB cell lines and to test the efficacy of PNA treatment are:

Name	Sequence	Type
MYCN (741) s	CGACCACAAGGCCCTCAGT	Target gene
MYCN (841) as	TGACCACGTCGATTTCTTCCT	Target gene
β-actin (700) s	TCCTCCCTGGAGAAGAGCTACGAG	Reference gene
β-actin (1018) as	ACACGGAGTACTTGCGCTCAGG	Reference gene
MYC (794) s	GCGACTCTGAGGAGGAACAAGA	Target gene
MYC (929) as	GAGCCTGCCTCTTTTCCACA	Target gene
BIRC4 (839) s	ACAAGGAGCAGCTTGCAAGA	Reference gene
BIRC4 (963) as	AGCATGTTGTTCCCAAGGGT	Reference gene

2.15 Protein extraction and western blot analysis

The N-myc protein was assessed in total protein extracts. The total proteins were extracted resuspending the pellet of cells or homogenized tissues in a lysing solution consisting 0.1 M KH_2PO_4 pH 7.5, Igepal 1%, 0.1 mM β-glicerolfosphate and a Complete Protease Inhibitors (Roche). After 10 min of incubation on ice, the sample was centrifuged at 15000 x g for 3 min at 4°C and the supernatant was collected containing total cellular proteins.

Protein were quantified with Lowry method [234] and the standard curve was constructed using known amounts of BSA protein (Bovine Serum albumin), by reading in a spectrophotometer at 660 nm (Beckman).

Proteins were separated by one-dimensional gel electrophoresis in denaturing conditions (SDS-PAGE: Sodium Dodecyl Sulphate - Polyacrylamide Gel Electrophore). The samples, containing 100 micrograms of proteins were solubilized by incubation at 95°C for 5 min after the addition of 2X Laemmli sample buffer (125 mM Tris pH 7, 4% SDS, 20% glycerol, 10% β-mercaptoethanol and bromophenol blue 0.004%) and water to a volume of about 20 ml. Following the preparation of Separating gel 7-10% (7-10% acrylamide, 375 mM Tris pH 8.8, 0.1% SDS, 0.1% APS, TEMED 0.1%) and 4% stacking gel (4% acrylamide, 125 mM Tris pH 6.8, 0.1% SDS, 0.1% APS, TEMED 0.1%), the samples were loaded in gel electrophoresis and run at 160 V for about 60-90 min in electrophoresis buffer (125 mM Tris, 0.96 M glycine and 0.5% SDS) with a molecular weight marker, SeeBlue Plus2 Pre-Stained

Standard (Invitrogen).

Proteins were separated by SDS-PAGE and they were transferred to PVDF membrane (polyvinylidene fluoride, Hybond-P, Amersham Biosciences) by western blot using the Bio-Rad wet system (Mini Trans-Blot Cell). The membrane was activated in methanol for 10 sec and then re-balanced in water for 5 min. Sponges and filters, before use, were soaked in transfer buffer (25 mM Tris, 192 mM glycine, methanol 10%), and then were assembled filter sponge-gel-membrane-filter-sponge and the transfer is was performed in transfer buffer at 250 mA for 2 hours. The membrane was subjected to successive incubation of 1 hour at room temperature with blocking solution (PBS, Tween 0.2% and 5% milk), with the primary antibody: mouse monoclonal N-myc IgG (NCM II 100, Calbiochem) or mouse monoclonal ß-actin (Calbiochem) and, after 3 washes in PBS and Tween 0.2%, with corresponding secondary antibody Sheep anti-mouse IgG-HRP (horseradish peroxidase) (Amersham Biosciences). All antibodies were diluted in PBS, Tween 0.2% and 3.5% BSA. The membrane was washed 3 times in PBS and 0.2% Tween for 5 min and was incubated for 1-2 min in the dark with the ECL detection solution (Amersham Biosciences). The survey was carried out to ChemiDoc (Biorad), using the program QuantityOne.

2.16 Mutant MYCN mice

The pure clone obtained with oligotargeting tecnique was injected in blastocysts to obtain a mutant mouse with the single point mutation in murine MYCN gene.

Blastocysts, a pre-implantation embryos, are isolated from 24 wild type donor females 3.5 days after mating and microinjected with 12 genetically modified mouse embryonic stem cells. 15-12 injected blastocysts are transplanted to the uterus of pseudopregnant recipient females that have been mated with sterile males. Offspring developed from successfully injected blastocysts will be a mixture of wild type cells and genetically modified cells, so called chimeric mice. The IB10 ES cells originate from the mouse strain 129/Ola that has

agouti (brownish-grey) coat colour and the blastocysts come from a strain with black coat colour (Black6). Some of the offspring born will be wild type mice (black) and others will be chimeras (patchy black/brown), the latter will be mated to investigate if the genetic modification can be inherited, i.e. transmitted through the germ line.

The chimeras are mated to 129/ola wild type mice and if the germ cells of the chimera originate from the genetically modified cells, the modification (-) can be inherited by the offspring. The wild type allele is denoted +. The chimeras are mated to bejge wild type mice, and the offspring can have either black or bejge coat colour. All bejge pups originate from germ cells in the chimera that are of 129 origin will be genotyping for the mutation. When the heterozygous (+/-) mice are mated, 25% of the offspring in the F2 generation will be homozygous for the mutation and we will have the homozigous mutation on mouse MYCN gene.

2.17 Statistical analysis

Both *in vitro* and *in vivo* data were presented as mean □ Standard Error Mean (SEM). *In vitro* data were obtained from at least three independent experiments. For the Xenograft murine models the bioluminescence intensity relative to the tumour progression was reported as mean □ SEM considering the photon flux (ph/s) as the sum of prone signals for each mouse after background subtraction. The BLI curves for each xenograft model were computed for each time point by the average of ten mice signals.

3

Results

3.1 *MYCN*-amplified neuroblastoma transgenic murine model

3.1.1 TH-MYCN transgenic mice

For the realization of the colony of TH-MYCN human Neuroblastoma mice we used the strain 129X1/SvJ, because the penetrance of the tumor increases, compared with the use of the C57BL/6J strain [88] [184]. Mice were mating between transgenic hemizygous 129X1/SvJ-Tg (TH-MYCN) 41Waw male inbred mice and 129X1/SvJ female inbred mice. It was chosen to mate in harem transgenic male with wild-type females because it was shown that transmission of the transgene is better if it occurs through the male germ line, because of the imprinting (as also confirmed in the Mouse Repository site, Mouse Models for Human Cancers Consortium http://mouse.ncifcrf.gov) [235] [236] Later we started mating between hemizygous mice to obtain homozigous mice. In four years the colony has reached the number of 719 animals, of which 60.4% were transgenic mice, shown by PCR analysis. We obtained 285 wild-type animals, 339 hemizygous mice (47.2%) and 95 homozygous mice (13.2%).

Genetic screening to distinguish homozygous and hemizygous mice was performed by quantitative Real-Time PCR analysis. I obtained genomic DNA of each mouse from a small piece of tail and in each sample it is measured the level of human MYCN cDNA amplification compared with brothers, parents and a hemizygous control mouse (476). Each progeny was obtained from mating an hemizygous male with an hemyzigous female mice. It followed that the RATIO (index which correlates the MYCN gene level with its housekeeping control gene level) of a homozygous sample is twice parents', brother's and hemizygous control level. In Figure 18, it is shown an example of genotyping analysis.

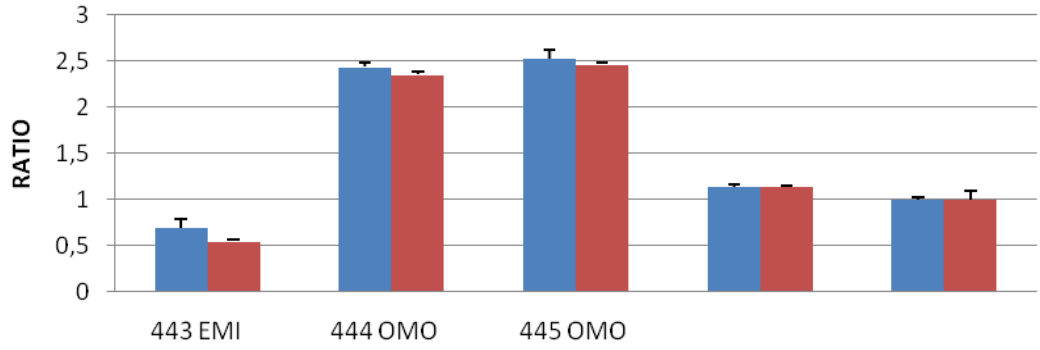

Fig. 18. Genotyping of a family of TH-MYCN mice. The ratio is obtained between MYCN gene level and the housekeeping gene level of all the progeny comprise the parents, the analysis was normalized for MYCN level of an hemizigous control mouse (476 HEMI). The progeny included two homozygous specimens for that gene with a ratio around 2.0, one hemizygous mouse with a ratio of 1 and one wild-type specimen, that its ratio is closer to zero. Analyses carried out in duplicate. WT = wild-type mouse, **HEMI** = hemizygous mouse for the human MYCN gene, **HOMO** = homozygous mice for the human MYCN gene.

After genotyping, hemizygous and homozygous mice were palpated weekly to identify the time and the mode of dissemination of the tumor mass, which usually appears in abdominal or thoracic position [88]. We observed a tumor in 96 hemizygous mice and in all 95 homozygous mice: these data confirmed the literature data, in which hemizygous mice had a tumor incidence of 25-30%, in our case 28.3%. The observed latency was from 7 to 36 weeks in hemizygous, while homozygous mice showed an early occurring around four weeks and only in few cases around six weeks. They had a tumor incidence of 100% (Fig.19)[185] [186] [187].

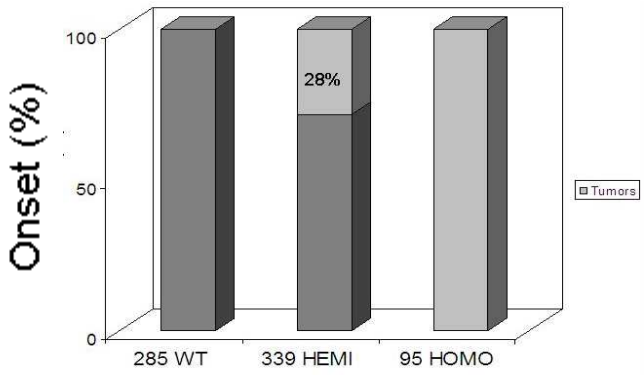

Fig. 19. Number of homozygous and hemizygous mice developed tumors. In the graph I show the total number of mice obtained (719) and in particular how many wild-type mice (285), hemizygous mice (339) and homozygous mice (95) there were. All homozygous mice developed tumors (100%) and only 28% of hemizygous mice developed tumors.

The mass evolved rapidly in two-three weeks in homozygous mice and in four-five weeks in hemizygous mice during which there was an increase in weight of 2-3 grams and mouse looked motionless, ataxic and curved. From the autopsy it was observed that at an early stage the tumor was present predominantly in the right part of the abdomen near kidney and in an advanced stage it was spread throughout the abdominal cavity incorporating kidneys, adrenal glands and a large part of the intestine. In advanced stage, cancer was composed of multiple hemorrhagic and necrosis masses and it was firmly attached to the spine. The adherence to the spine may suspect a bone marrow infiltration, which would explain the reduced mobility that we have seen, also observed in the literature [88]. Histological analysis of all tumors has confirmed that this is neuroblastoma (Fig. 20).

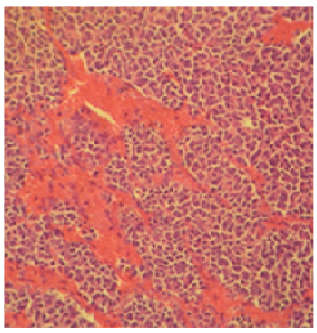

Fig 20. H&E staining illustrates the presence of small round blue cells in the tissue and it confirms the presence of a neuroblastoma tumor.

It was observed that the tumor progression in homozygous mice reflected clinical setting. The short latency and the absolute incidence made this homozygous TH-MYCN mice model easier to monitor and useful to study possible pharmacological treatments.

3.1.2 microPET analysis

Four hemizygous mice were subjected periodically to Micro-PET analysis with ^{18}F-FDG from day 20 after birth, every three days for 6 weeks. All mice were subjected to Micro-PET analysis with also another radiotracer, ^{18}F-DOPA, each week. The scans with ^{18}F-DOPA are less than those with ^{18}F-FDG, because the production of this radiotracer came only one time each week. It was chosen to start the scans so early to detect the exact time of appearance of the tumor. In fact, even referring to literature on this transgenic model, many factors like the environment, the strain, create variability.

In Micro-PET ^{18}F-FDG images, the areas of high uptake of the radiotracer are located in the heart, which is an organ of high metabolic activity and bladder because here the tracer accumulates rapidly before elimination. These are the physiological areas of the ^{18}F-FDG uptake. Since the early ^{18}F-FDG scans, they highlighted elongated uptake areas in the abdomen and in a capturing area close to the dorsal spine, at the same level of the liver. From the Micro-PET images obtained with ^{18}F-DOPA, the physiological areas of high uptake are spine, cerebral hemispheres, because of its uptake is related to the production of dopamine, and bladder. ^{18}F-DOPA scans showed also two symmetrical absorber areas near kidneys, our interest area. Moreover it was often highlighted a dorsal area in the same position also with ^{18}F-FDG tracer (Fig.21).

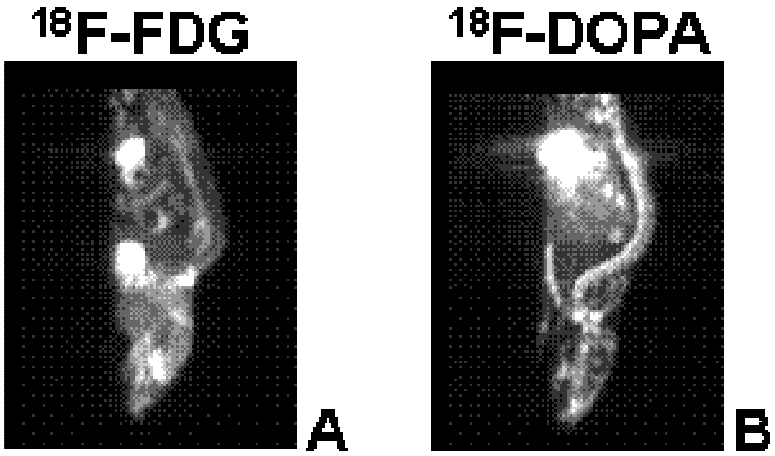

Fig. 21. microPet analysis is made on the same mouse using two different radiotracers. 4.A ^{18}F-FDG scan shows an abdominal uptake in addition to the areas of physiological uptake (heart and bladder) 4.B ^{18}F-DOPA scan shows an abdominal uptake and the physiologic areas of uptake (SNC, SNP and bladder)

Following these results mice were sacrificed to confirm if the abdominal areas uptake corresponded to a tumor. Necropsy has not identified the presence of a tumor in these four animals.

A second group of ten hemizygous mice were subjected periodically to Micro-PET analysis with ^{18}F-FDG and ^{18}F-DOPA from 40 days after birth for 4 weeks each four days. The scan starting date was determined by the fact that no hemizygous mice had developed cancer before this age. Three of these mice developed tumor during scan monitoring (Fig.22).

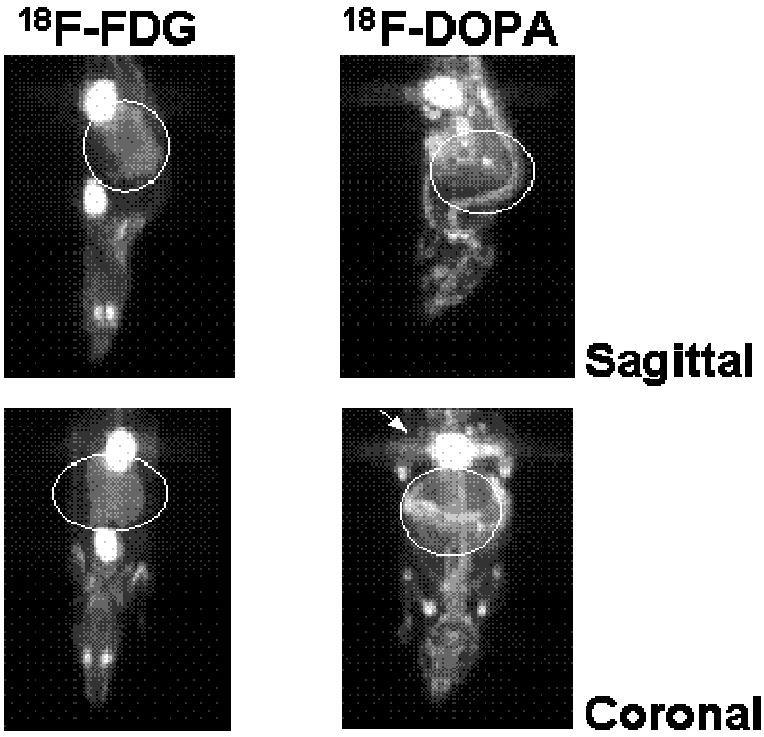

Fig. 22. Tumor signal with both radiotracers in one mouse with advanced stage of Neuroblastoma. The figure shows sagital and coronal cuts. The images show abdominal areas more or less extensive composed of different uptake areas, moreover the level of uptake in some areas is comparable to the physiological uptake of heart and bladder.The tumor (white circle) is clearly more evident in ^{18}F-FDG scan (left side), ^{18}F-DOPA scan (right side) is less informing and the great urinary bladder radioactivity saturates the image reducing the diagnostic power in the interested area (thick arrow).

In this case the necropsy confirmed the presence of a tumor and histology showed that it was neuroblastoma. These were the first data that allowed correlate the Micro-PET analysis with histology, thanks to these data we decided to use the ^{18}F-FDG radiotracer and not ^{18}F-DOPA for the next studies.

Twenty three hemizygous mice were subjected periodically to Micro-PET analysis with ^{18}F-FDG from 40 days after birth for 6 weeks each four days. Only one mouse was positive at 64 days after birth, three were positives after the last scan, around 80-100 days after birth and other mice didn't develop tumor. For money and time that each experiment required, next experiments were performed only on homozygous mice because the onset is 100% and the time of insurgence is more closer between animals.

Sixty homozygous mice were analyzed with ^{18}F-FDG radiotracer. In the study twenty five homozygous mice have been included to define the temporal window for the appearance of the tumor and its progression. The examination was performed every three days starting from the twenty seventh day of life of the animal to the identification of the earliest tumor

mass (defined first positivity) and then every week (defined second, third, forth or fifth positivity, in accordance to mice's life). Two examples of microPET analysis performed on two homozygous TH-MYCN mice are showed in figure 23 and 24.

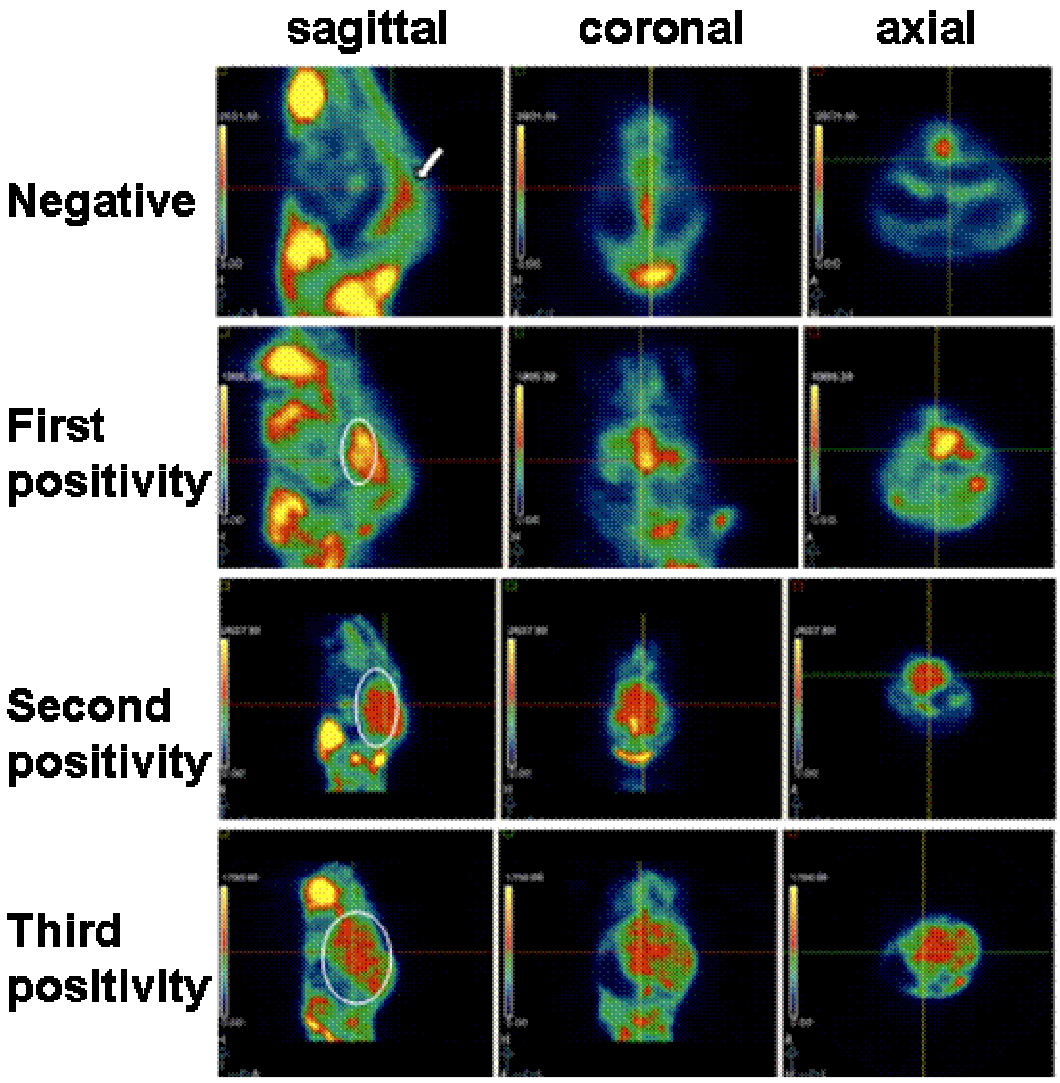

Fig. 23. MicroPET analysis of tumor progression and evolution on an homozygous mouse in three different sections. This animal survived until the third positivity. These scans show formation and evolution of the tumor mass on the right side of the animal. The color scale on the left of each image is the index of the presence of radiotracer and it is directly proportional to the concentration of glucose in the tissues of the animal, except for the bladder where the radiopharmaceutical compound is accumulated to be excreted. Negative scan shows areas of high glucose metabolism (yellow signal) but, for their location there are no areas of overlap with a possible tumoral signal. In particular, in the sagittal section yellow areas show the heart and bladder, respectively, an organ with high metabolic activity and the site of collection of the drug metabolized by the animal. In the first positivity the white circle indicates the presence of neuroblastoma localized adjacent to the spinal uptake. The spinal uptake is present also in the negative scan (thick arrow). Second and third positivity show the evolution of tumor; in third positivity the tumoral area presents a dishomogeneous uptake this fact is due to different metabolism of cancer cells as a consequence of vascularisation. Sagittal (sagittal section); Coronal (coronal section); Axial (axial section),

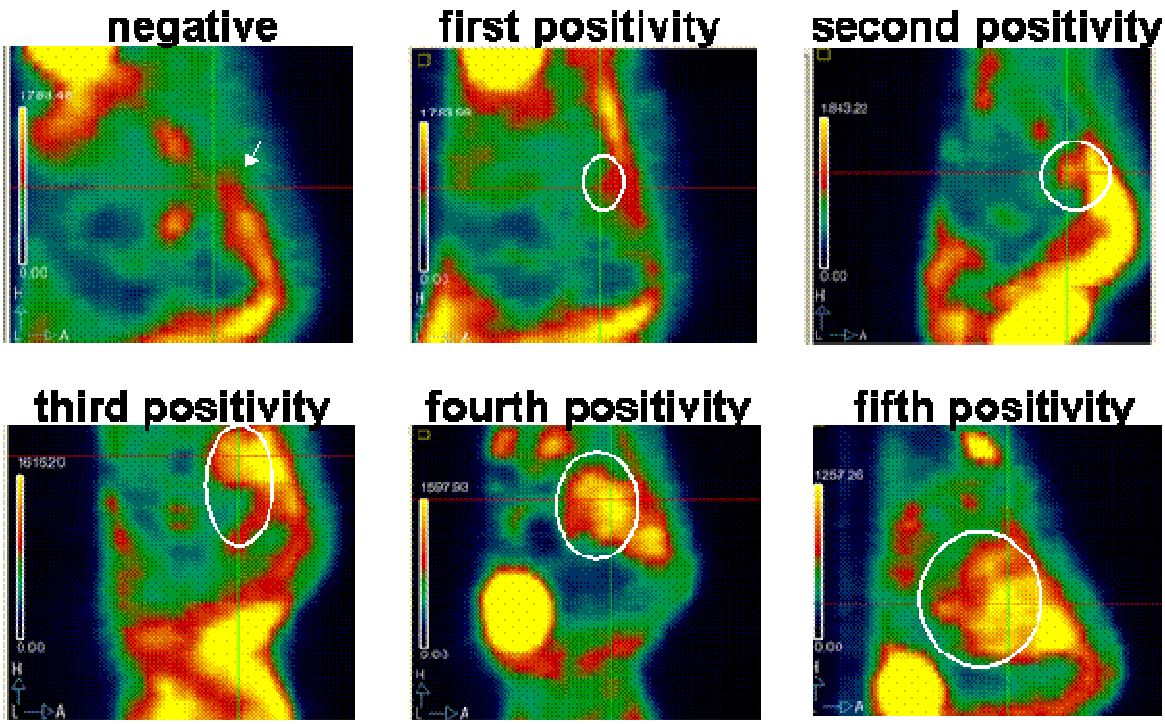

Figure 24. MicroPET analysis of tumor progression on an homozygous mouse in sagital section. This animal survived until the fifth positivity. The color scale on the left of each image is the index of the presence of radiotracer and it is directly proportional to the concentration of glucose in the tissues of the animal, Yellow areas show organ with high metabolic activity, like the heart, and the site of collection of the drug metabolized by the animal, the bladder. The white circle indicates the presence of neuroblastoma localized adjacent to the spinal uptake. The spinal uptake is present also in the negative scan (thick arrow).

TBR (Tumor-to-Background-Ratio) was calculated for each positive scan of each animal. The background uptake is the uptake of a healthy part of the skin because this type of murine model develops metastasis in several organs [Weiss]. All tumors diagnosed with microPET were confirmed by histology. (Figure 25).

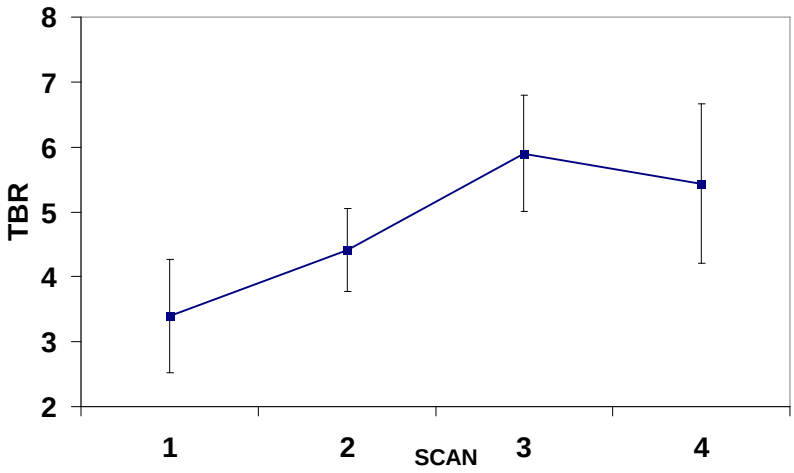

Fig. 25. Mean TBR from 25 homozygous mice for each positivity. Mean TBR values correlate with progression of the tumoral mass. Each point corresponds to a microPET positivity and it was calculated as the mean from 25 scans on different animals. The graph shows the exponential increase of the tumor mass during the first three microPET positivity and it shows a slight decline in the fourth positivity, probably this is due to the strong presence of necrotic tissue in the tumor in the last stage.

After this analysis, we decided to normalize the uptake index to the real volume of the tumor. We did not have the possibility to analyze the tumor with a TAQ scan and for estimate the tumor size, thirty five homozygous mice were analyzed with ^{18}F-FDG radiotracer and then they were sacrificed to confirm the presence of the tumor and to calculate the tumor volume. We divided the progression in five positive points and for each point 7 animals were sacrificed. In figure 26 it is possible visualize the tumor growth.

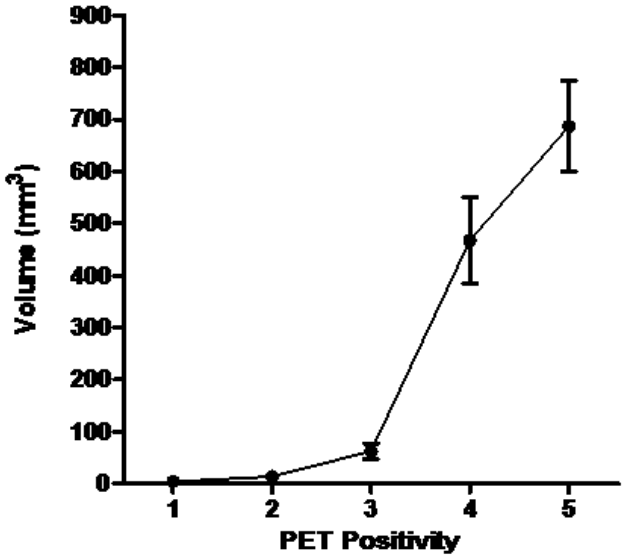

Fig. 26: Mean volume from 7 homozygous mice for each positivity. Each point corresponds to mean value obtained from seven tumor samples collected at the same microPET positivity. First positivity corresponds at 3.8 mm^{2}of volume.

After the calculation of mean tumor volume, mean SUV (Standardized Uptake Value) was calculated. This semi-quantitative parameter was corrected with the mean tumor volume of each positive point and it showed the increase in tumor malignancy with a negative flexion at the fourth and fifth scans probably related to necrosis processes (fig. 27).

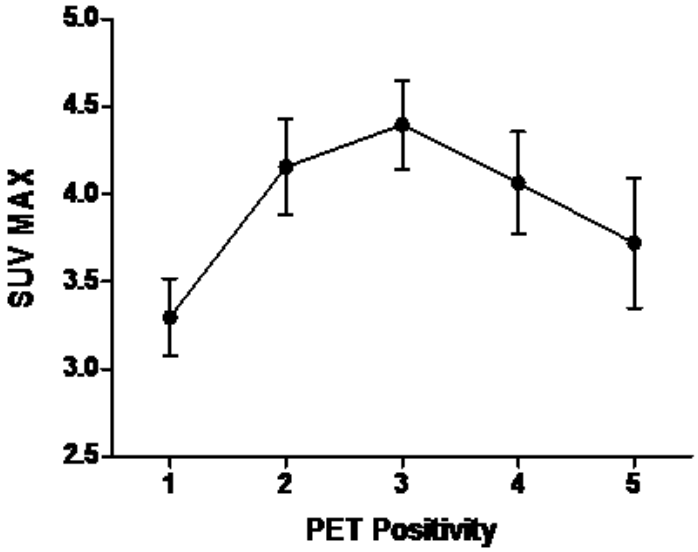

Fig. 27. Progression of the tumoral mass accorded to SUV values.

3.1.3 Transgenic tumor characterization

The autopsy allowed collection tumor samples useful for the histological and molecular evaluation. From the post-mortem examination, all positive animals to the evaluation by micro-PET have a tumor mass located predominantly in the abdominal region. In the advanced stage of tumor progression, the tumor mass alters the structure of the surrounding organs, for example it is possible find adhesion part. Both homozygous and hemizygous mice tumors don't present clear difference. The hemizygous tumor is bigger in size respect to homozygous tumor. The tumor masses occur heterogeneous in the samples in which it's possible to distinguish necrotic regions. It has not yet been found the presence of metastases. The tumor presence was confirmed with histological analysis and the presence of human MYCN cDNA was seen with immunohistochemistry, molecular and proteomic analysis.

Histological data confirm that all samples were neuroblastoma. From the analysis of the tumor masses of TH-MYCN homozygous transgenic mice in the four different stages of

Micro-PET analysis we observed clear difference between the earlier and the last stage of develop. In the earliest stage of tumor development it was detected the presence of a small tumor mass that sometimes it originated from adrenal gland and we did not see blood vessel. In the last stage of development, the tumor mass showed a maturity and progression of the angiogenic processes, it was not possible to observe the adrenal gland. In all stage the kidney compartments are not infiltrated and they are healthy.

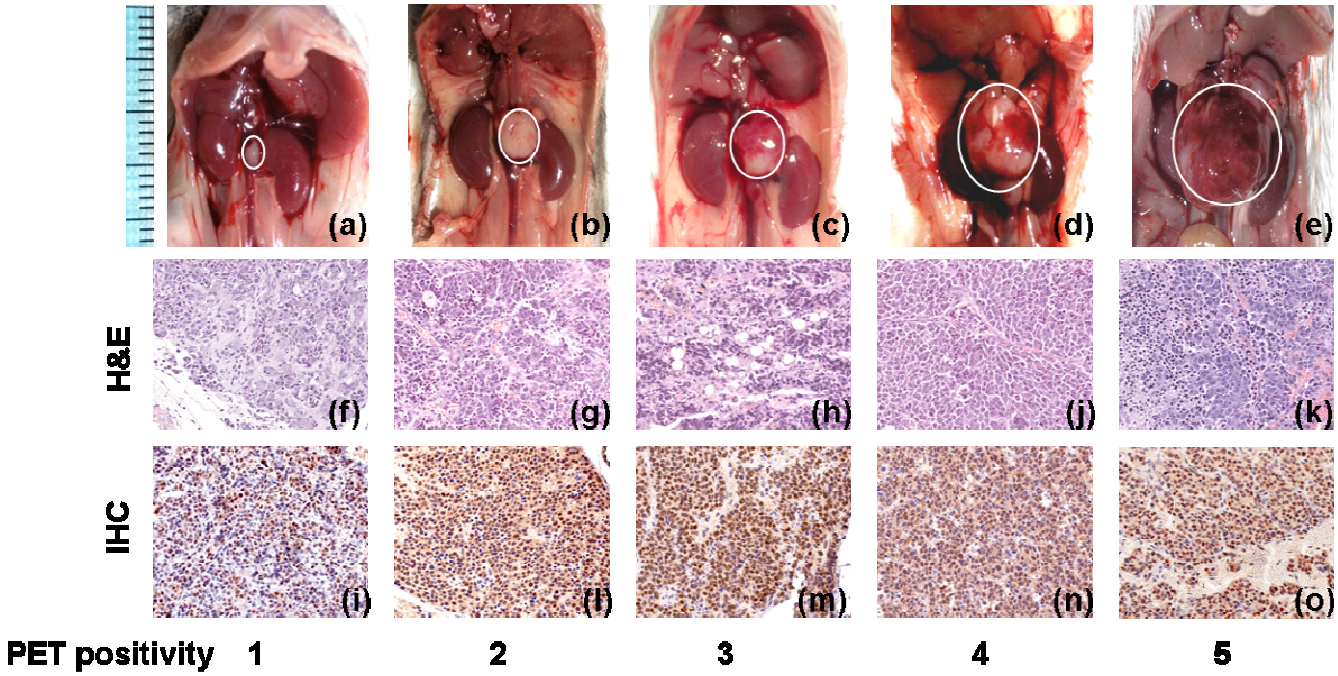

Fig 28. Samples from TH-MYCN mice at different stage of progression form autoptic exam (a-d), H&E staining (e-h) and immunohistochemistry with monoclonal anti-MYCN Antibody (j-l). Positive cells are evident in brown.

As evident in the Fig.28 on an immunohistochemical assay with the monoclonal antibody N-MYC on tumor tissue of homozygous transgenic mice, the majority of cells in the samples resulted positive for the presence of N-Myc to the detection with the chromogenic DAB that gives brown signal.

MYCN gene amplification was evaluated in the tumor masses of hemizygous and homozygous mice. In both homozygous and hemizygous tumors the MYCN gene amplification level was greater than the average gene dosage reported at the time of the genotyping. The levels of MYCN oncogene expression in both models were estimated by Real Time PCR on reverse transcribed. The expression of MYCN in each model is quite high (Fig. 29).

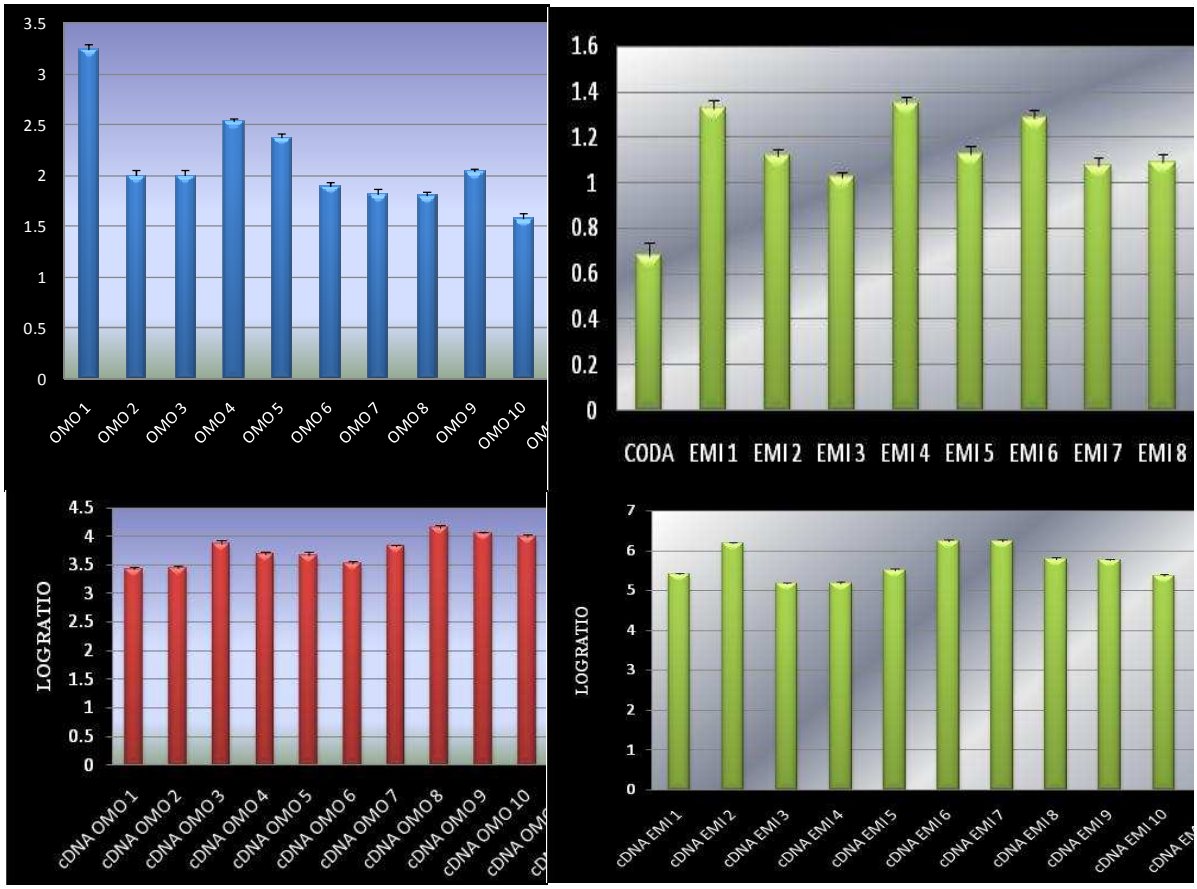

Fig. 29. Human MYCN cDNA amplification and overexpression level saw in hemizygous and homozygous tumors.

3.2 *MYCN*-amplified neuroblastoma xenograft orthotopic mice models

3.2.1 *In vitro* validation of bioluminescent signal

Stably transfected p53wt (Kelly, IMR-32, IMR-5) or p53mut (BE2(c)) MA-NB cells subsequently used for in vivo experiments were analyzed to identify the specific luciferase emission peak (attended on 560 nm) and to identify a correlation between luciferase expression and cells number.

The results showed that all the cell lines presented a relative luciferase emission peak (560 nm) (Fig. 30A) highlighting a perfect linear correlation between number of cells used and photons detected (Fig. 30B)

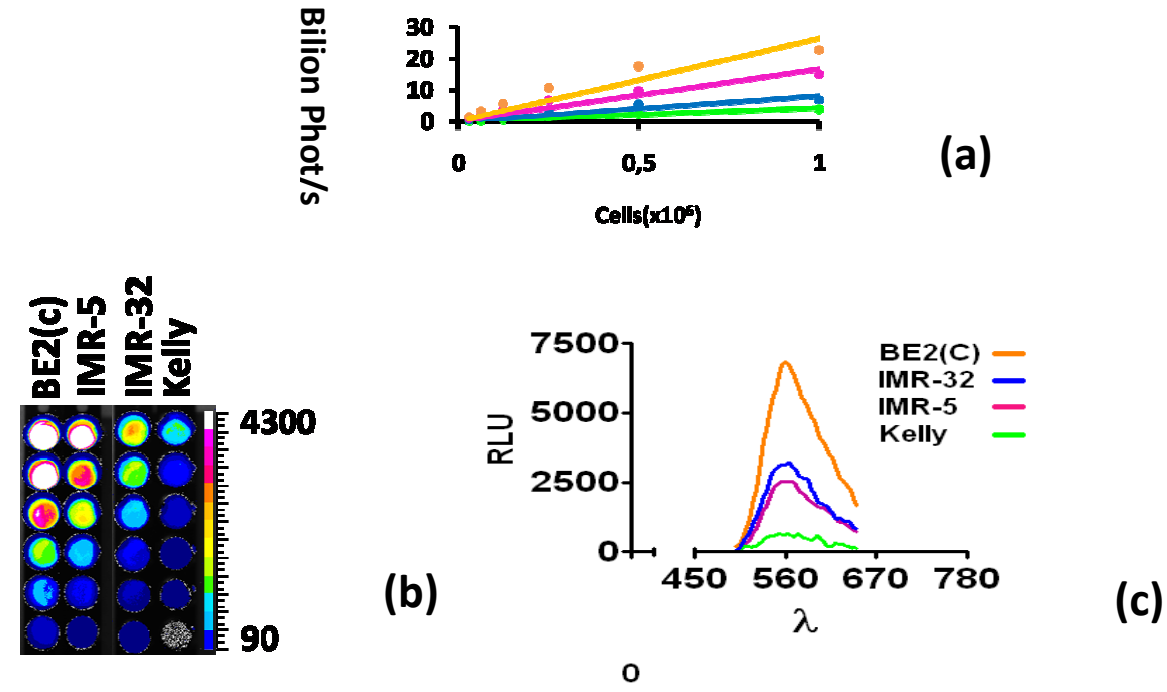

Fig. 30 Quantification oh Photons emitted related to number of cell line (A); overlay of cell signals (B); *in vitro* evaluation of luciferase emission peak (C).

3.2.2 *Ex vivo* analysis of xenograft orthotopic tumor

The analysis was performed ex vivo on the tumoral mass removed from specimen at the late stage of the disease (Fig. 31).

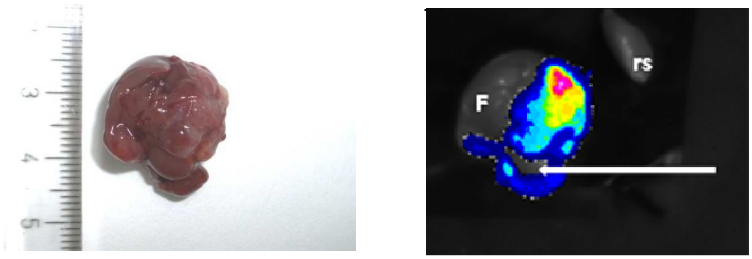

Fig. 31. Tumoral mass of a mouse inoculated with line IMR5-Luc1. F = liver; rs = healthy kidney, kidney involved in inoculation (white arrow)

Figure shows important changes in the distribution of healthy organs because of the high dimensions of the mass. The adrenal gland inoculated is indistinguishable from the tumor and the kidney below is clearly incorporated by the tumoral tissue but not infiltrated at an initial macroscopic examination (arrow), adhesions are also present in liver tissue. The luminescence signal *ex vivo* is much sharper, the layers of skin that in fact define an attenuation of the intensity distribution and of the photons detected. This analysis has allowed an assessment of the organ specific tumoral mass, the data shown in Figure 38 highlight that there are a lack of infiltration in the liver and kidney.

3.2.3 *In vivo* bioluminescent imaging

We have generated four new BLI MA-NB xenograft orthotopic murine models, three of them carrying p53wt (Kelly, IMR-32 and IMR-5), while one is the first reported carrying p53mut (BE2(c)). All the four tumor mouse models presented a 100% of tumor incidence.

The MA-NB xenograft orthotopic model harboring p53 mutations (SK-N-BE(2)c) showed a tumor characterized by a shorter latency (two weeks) and a higher BLI signal respect the p53wt MA-NB xenograft orthotopic mouse models obtained after Kelly and IMR-32 cells inoculum (Fig. 32). The IMR-5 model, obtained from a sub clone cell line of IMR-32, showed a strong aggressiveness respect the IMR-32 model (Fig. 33).

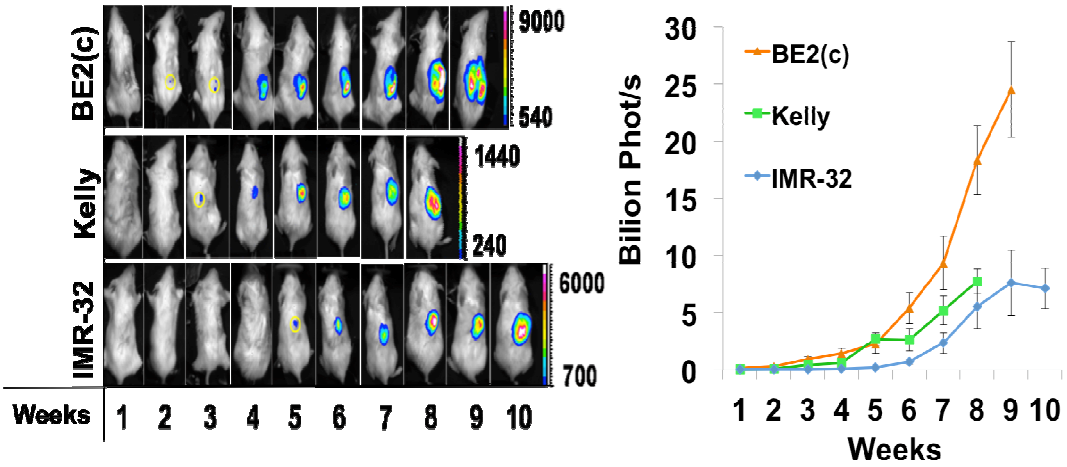

Fig.32 *In vivo* monitoring of three different NB Xenograft Orthotopic mice models. Graphic rappresentation of tumor burden onset and progression at different timepoints (left side); signal detected from Berthold luminograph once a week starting one week after day of cells injection (right side).

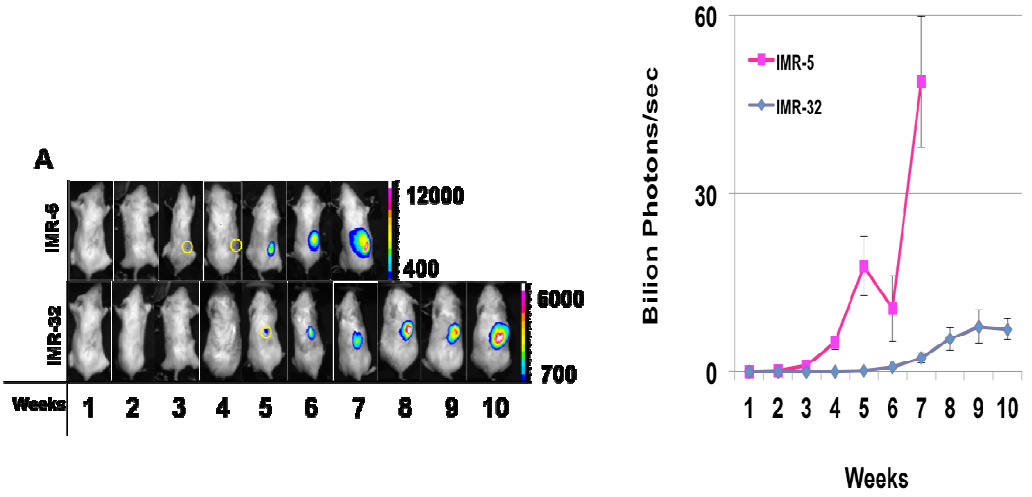

Fig. 33 *In vivo* monitoring of two different NB Xenograft Orthotopic mice models: the model obtained from the original cell line and the model obtained with a sub clone of the same cell line. Graphic rappresentation of tumor burden onset and progression at different timepoints (left side); signal detected from Berthold luminograph once a week starting one week after day of cells injection (right side).

3.2.4 Molecular and histological orthotopic tumor characterization

All animals were sacrificed after first illness symptoms, and showed abdominal tumor mass. The adrenal gland where tumor cells have been injected was not visible and, in some cases, the tumor included the other adrenal gland.

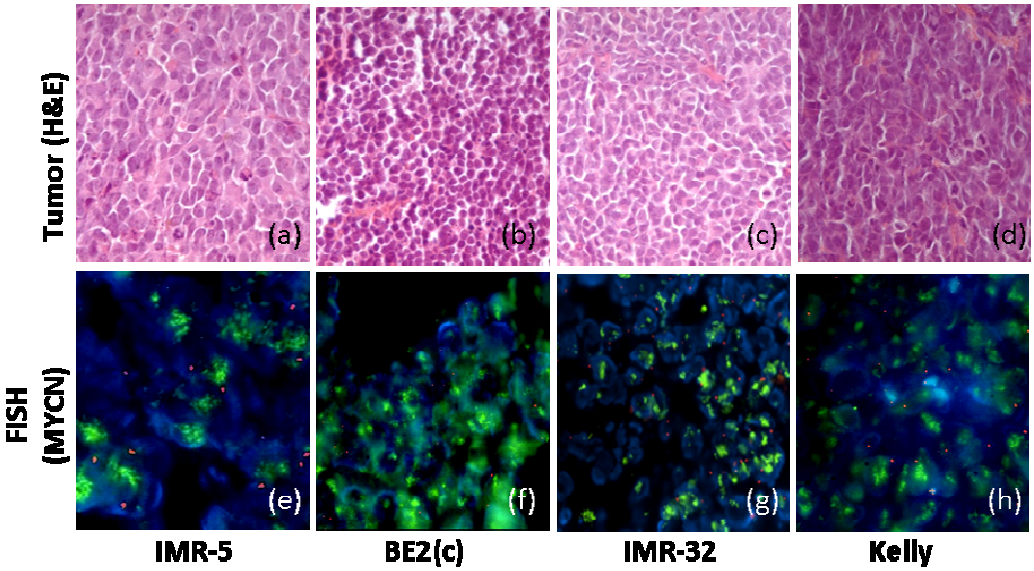

Fig.34 H&E staining of Orthotopic MA-NB models confirms the presence of small ruond blue cells. Sample at endpoint for IMR-5 (a), BE2(c) (b), IMR-32 (c), and Kelly (d) cell lines. FISH analysis confirms the presence of MYCN oncogene for IMR-5 (e), BE2(c) (f), IMR-32 and adrenal gland (g) and Kelly (h) cell lines.

Histopathology analysis highlights the presence of the characteristic “small round blue cells” in every p53wt or p53mut MA-NB sample (Fig. 34 a-d).

The presence of *MYCN* amplification and overexpression was confirmed by FISH and real time quantitative RT-PCR respectively from all the four p53wt or p53mut MA-NB tumors (Fig. 35). The levels of expression of MYCN appear to be on average about four times those analyzed on the cell line low-Expressed SJ-N-KP. The datum is further corroborated by comparison with the non-amplified and non-expressed GI-CA-N cell line.

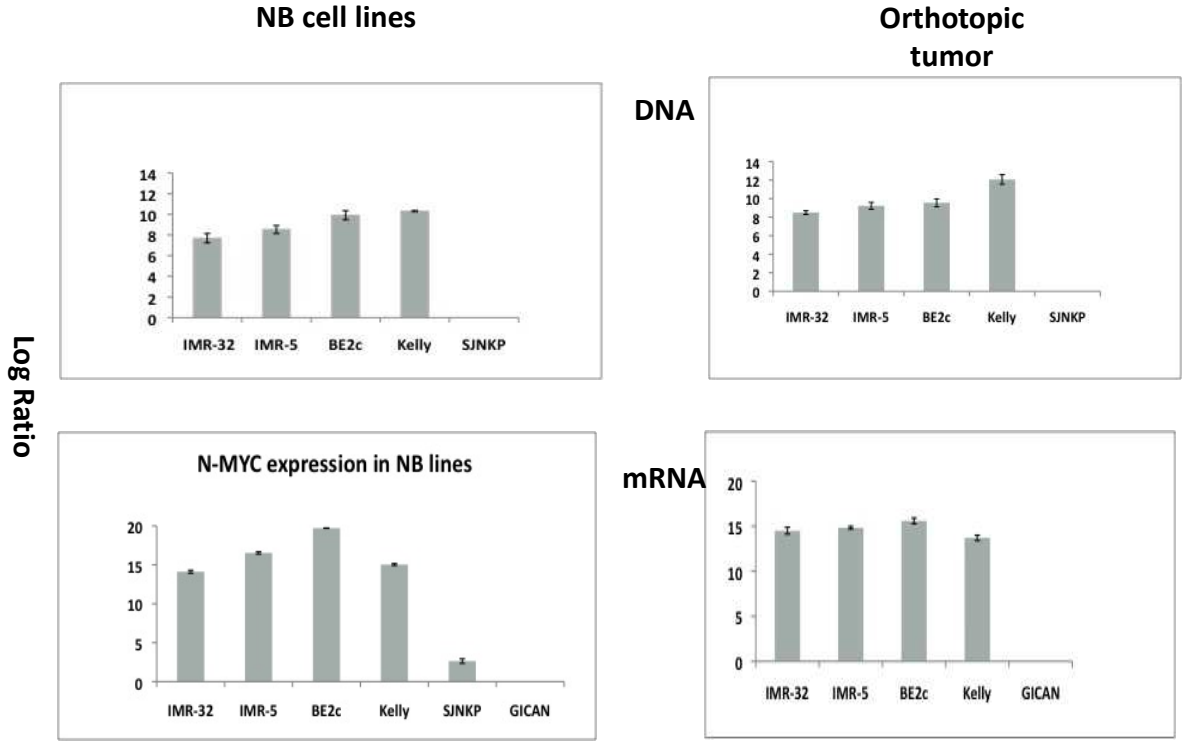

Fig. 35 Molecular analysis from both cell lines and tumor sample showing the presence of MYCN oncogene and MYCN mRNA.

3.3 PNA anti-MYCN treatments

3.3.1 Cell lines MYCN characterization

It's confirmed that the cell lines used in this experiment have the amplification of MYCN oncogene.

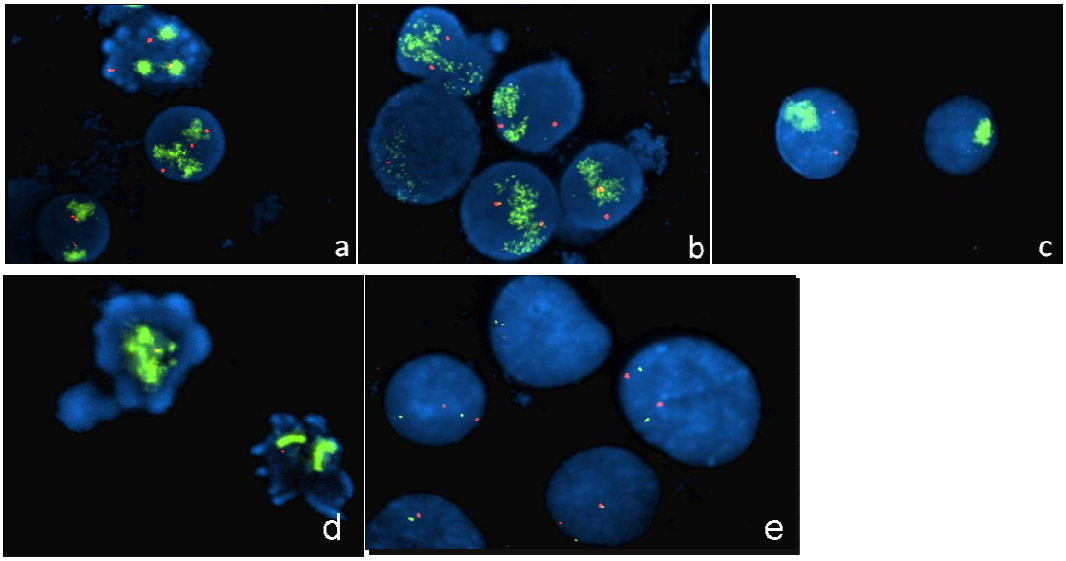

Fig 36. FISH analysis of the amplification of the MYCN gene in neuroblastoma cell lines (a) IMR-32, (b) IMR-5 (c) SK-N-BE (2)c and of the amplification (d) Kelly (e) SJ-N-KP; Probe "gene specific"= green signal; centromeric probe chromosome 2 = red signal.

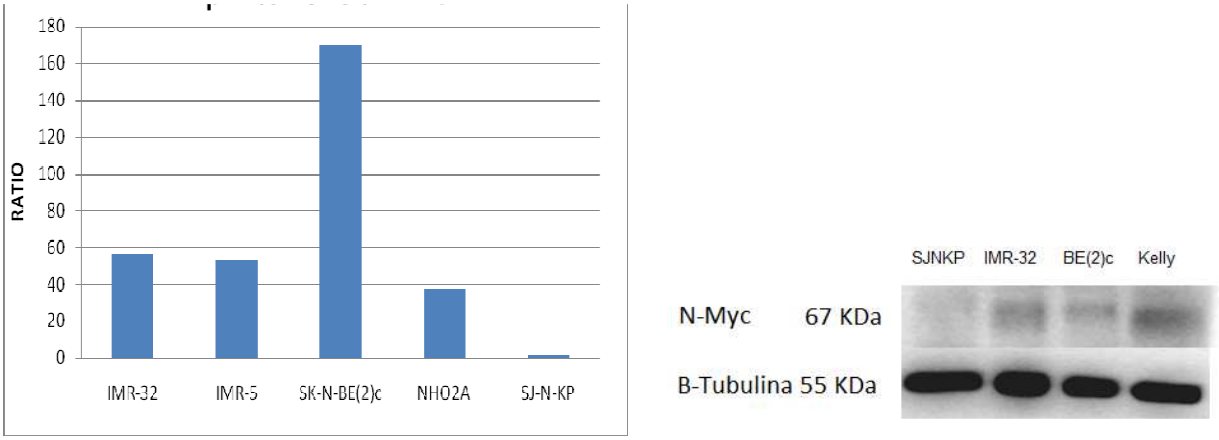

Fig 37. Amplification (qPCR analysis) and expression (western blot analysis) of MYCN oncogene in NB cell lines.

3.3.2 *In vitro* PNA treatment

At the beginning it was chosen to test the anti-gene PNA s-NLS on the cell line NHO2A for the study of the homozygous model.The cells were treated with PNA anti- gene s-NLS (PNA anti-gene wild-type, WT) anti-MYCN and PNA anti-gene (PNA anti-gene mut) 10 mM, for 24, 48, 72, 96 hours. The duration of treatment was derived from analysis of the growth curve previously made as up to 96 hours the cells have grown exponentially. Cells treated with PNA anti-gene WT at the light microscopy show altered morphology already after 8 and 24 hours after treatment, the effect is accentuated after 48 hours, it is very evident at 72 hours and still present after 96 hours (Fig. 38). Compared with the control cell K (untreated), they tend to move away from the plate and form clusters, have a globular shape, very dark and most of the cells die. To test the specificity and the possible toxicity of the PNA anti-gene anti-MYCN PNA was used in anti-gene mut, whose sequence has been altered by three point mutations. In terms of morphological appearance of the cells treated with the anti-gene PNA mut is halfway between the control cells and those treated with the anti-gene PNA wt. From observations with light microscopy it reveals that some cells tend to detach from the plate, but most grow normally, indicating that the PNA anti-gene WT is specific for the inhibition of MYCN, and non-toxic to cells.

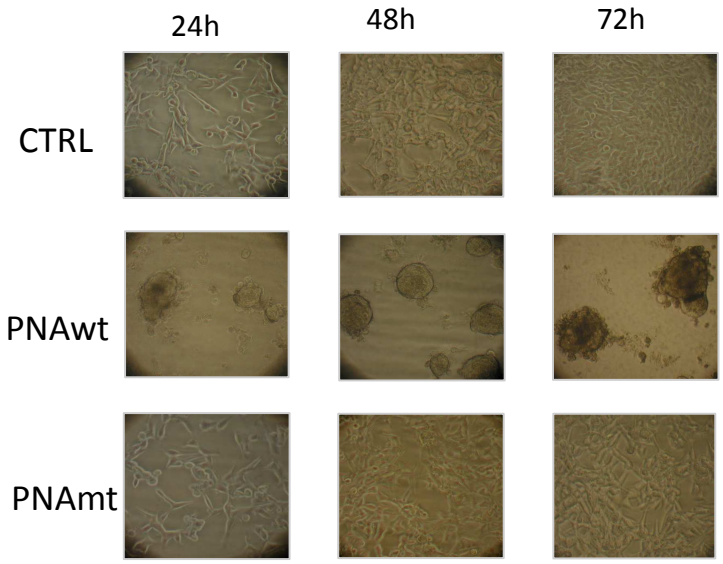

Fig.38 Cell growth inhibition by anti-*MYCN* PNA-NLS in NHO2A murine NB cells:morphological analysis.

It was also evaluated cell proliferation following treatment with PNA anti-gene and PNA anti-gene WT mut 10 μM for 24, 48, 72 hours, by the wise ATPlite (Fig. 39).

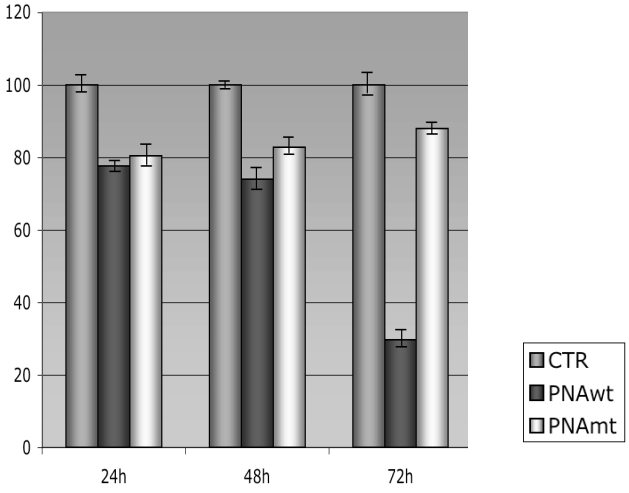

Fig.39 Cell growth inhibition by anti-*MYCN* PNA-NLS in NHO2A murine NB cells: proliferation assay.

The inhibition of proliferation by 36% at 48 hours and 61% at 72 hours with the PNA anti-gene WT, while remaining constant at around 16-19% with the anti-gene PNA mut. The performance of cells treated with the PNA anti-gene mut is similar to K, while in cells treated with the PNA anti-gene WT growth crashes to 72 hours.

The production of MYCN transgene transcript was evaluated in NHO2A cells, after treatment with PNA anti-gene and PNA anti-gene WT and mut 10 μM for 6, 12, 24 and 48 hours. It was built a Real-Time PCR semi-quantitative, normalizing the values on the housekeeping gene β-actin. PNA anti-gene WT significantly inhibits the transcription of MYCN transgene 12 hours after treatment. The PNA anti-gene mut showed instead no significant effects on cells (Fig. 40).

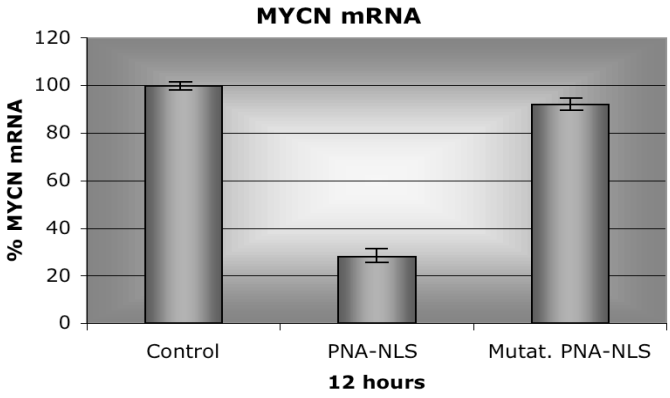

Fig. 40 Anti-*MYCN* anti-gene PNA-NLS specifically inhibits the *MYCN* transcription in NHO2A cells.

The analysis was extend to human NB cell lines. The treatment with anti-gene PNA at 24, 48 and 72 hours shows that the action of the drug is dependent on the cell line considered. The Fig.41 shows such Kelly lines and IMR-32 are more susceptible than lines IMR-5 and SK-N-BE (2)c above 72 hours. The incomplete inhibition of the remaining two lines is also more evident always 3 days after treatment. Lines such as IMR-5 and SK-N-BE (2) c are less responsive not only to the peptide-nucleic acids..

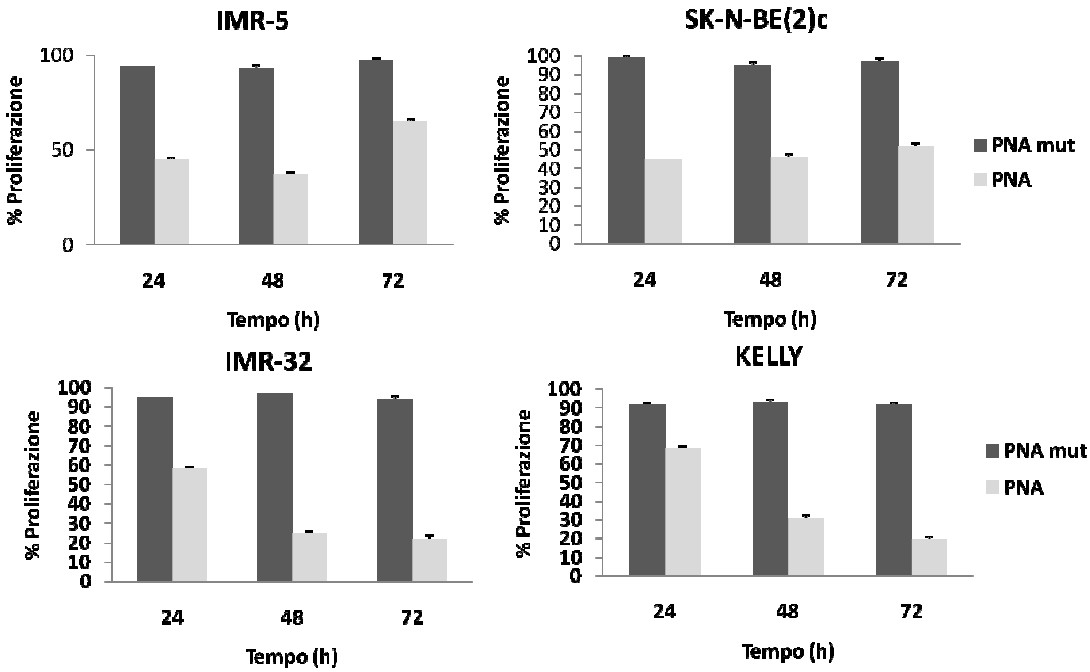

Fig.41 Cell growth inhibition by anti-*MYCN* PNA-NLS in human NB cells: proliferation assay.

3.3.3 *In vivo* PNA treatment

To test the effect of PNAwt tumor *in vivo*, TH-MYCN homozigous mice were treated intraperitoneally with doses of PNAwt (50 mg / kg) or saline, for 20 days from 35 days after birth. Tumor growth was assessed by micro-PET with ^{18}F-FDG tracer. The tumor metabolic signal was quantified by the TBR value (Target to Background Ratio).The TBR doesn't show a clear decrease in mice treated with PNAwt but thetreated miceshowed a prolongation of the life time.

3.4 *In vitro* and *in vivo* chemotherapeutical treatments

In order to improve the therapeutic effect to such cellular histotypes we wanted to study the PNA in combination with chemotherapy protocol COJEC. Here then defined dose-response curves for five chemotherapy drugs is on the lines that have proved resistant to peptidonucleic acids, rather than those found to be sensitive. Chemotherapy is currently used in the treatment of neuroblastoma is in fact characterized by high toxicity due to the incomplete specificity of these drugs to cancer cells. The use of a molecule that does not show toxicity as the PNA in combination with these drugs could then work around this problem by allowing the same therapeutic effect at reduced doses.

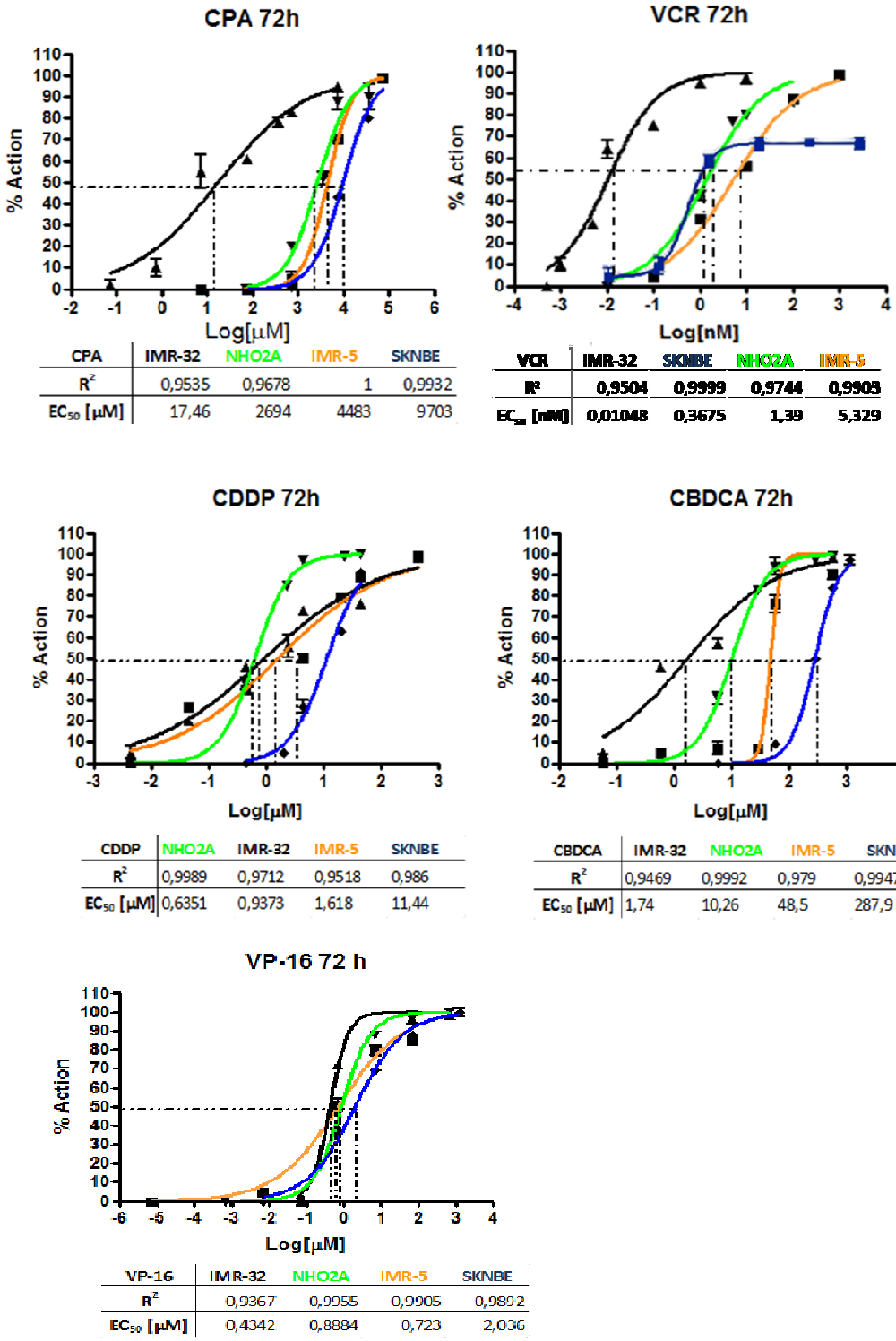

Fig 44. Dose-response curves for five chemotherapy drugs in four neuroblastoma cell lines with amplification of MYCN. CDDP = cisplatin, CBDCA = carboplatin; CPA = cyclophosphamide, VCR = Vincristine, Etoposide VP-16 = EC50 = concentration of drug that defines the 50% inhibition of cell

Once you have these mouse models of orthotopic nuroblastoma, it was possible to test in vivo effect of chemotherapeutic pi `u used in the clinic, particularly vincristine and etoposide.

Therefore, it is chosen to treat orthotopic xenograft model as a model Kelly Luc p53 as wild-type and mutated p53 is orthotopic xenograft model was used SKNBE (2) c Luc. It is decided to use the model inoculated with Kelly instead of the wild-type p53 model inoculated with the line IMR-32 Luc is because it has a latency period of five weeks 3 weeks compared to the model line inoculated with Luc Kelly.

For this study are used as the drug vincristine and Etoposide. The choice of these drugs is established by in vitro laboratory data by focusing on the use of inhibitors the spindle and the topoisomerase to the detriment of alkylating agents such as cisplatin and carboplatin.

This pilot study involving 8 murine specimens of 7 weeks, 4 Model Kelly SKNBE and 4 for model (2) c. Both models were treated at the beginning of the seventh weeks post-inoculation to try to simulate it 'or that happens in the clinic where the neuroblastoma

Agnostic is the market later tively. It should be re corded that they nee Kell y Luc and Luc The IMR-32 are derived from a patient at the fourth stage of disease, while the line SKNBE (2) c Luc comes one patient relapsed after chemotherapy.The models were monitored by "Imaging bioluminescent" by luminometer LB981 Berthold Nightowl to detect the presence of tumor initiation, during and end of treatment.

Underwent chemotherapy 4 xenograft models. The samples were treated with vincristine (0.06 mg/Kg concentration) for 2 times a week in combinationwith Etoposide (concentration 14mg/Kg) every 7 days. Both are chemotherapy were administered intraperitoneally for 4 weeks total.

The drugs were diluted in saline. For each model were used with 2 controls inoculated Kelly and Luc SKNBE line (2) c respectively Luc and treated with saline 3 times week for 4 weeks total. The graph in Figure 45 represents the line of survival of orthotopic specimens xengraft Kelly Luc undergoing chemotherapy with vincristine and etoposide in 4 weeks (from 45 to 73 days post-inoculation). Is evident from the graph that the specimens undergoing chemotherapy treatment have a higher survival curve compared with controls that have a survival rate in accord with data reported by laboratory in

the development of orthotopic model Kelly.

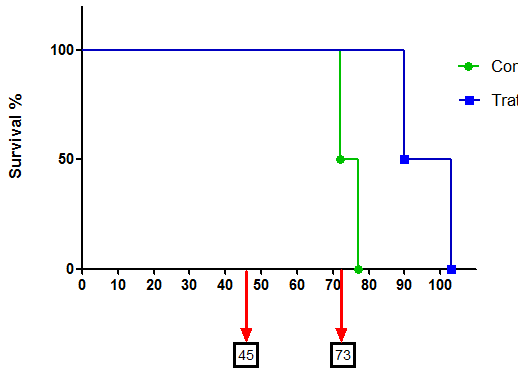

Fig 45: Survival curve of Xenograft orthotopic Kelly Luc model

The specimens tested in the study were sacrificed at the first sign of distress. Controls receiving saline were sacrificed at 72 and 77 days post-inoculation while the treated with chemotherapy drugs were sacrificed at 90 and 103 days post-inoculation. Samples Control survive an average of 74.5 days while the samples treated with chemotherapy survive 96.5 days. From this pilot study data show that specimens treated survive for 20 days pi `u` compared with controls and can be regarded as a meaningful or compared to the average life of a murine model.

Fig 46 represents the survival curve of the orthotopic xenograft model SKNBE (2) C and treated with chemotherapy with vincristine and etoposide. Treatment 'and ran for four weeks from 45 to 73 days after inoculation days post-inoculation. The specimens are subjected to the study sati killed during the treatment period because it is showed signs of suffering. While the controls receiving saline were sacrificed days to 45 days and 50respectively, were treated with chemotherapy drugs sacrificed both at 59 days. The average survival is 47.5 for controls and 59 models treated with chemotherapy.

Comparing the survival curve of the two mouse models one may observe that inoculated with cells SKNBE (2) c Luc show more aggression `a, as already confirmed in from in vitro data from our laboratory.

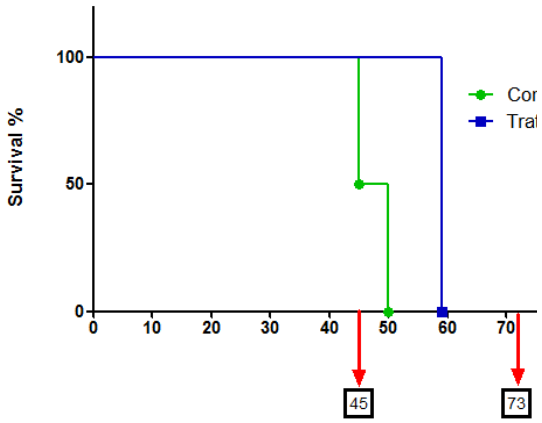

Fig 45: Survival curve of Xenograft orthotopic SKNBE2c Luc model

The models were monitored during treatment and after treatment by Nightowl Berthold LB981 luminometer to detect any decrease in the signal in the treated specimens compared with controls.
For this pilot study is not detected a significant reduction of signal in specimens treated with chemotherapy compared with controls treated with saline, in both models (Kelly and Luc SKNBE (2) c Luc).
Also according to the statistical analysis with Log rank test (Mantel-Cox), we obtained a value P-value of 0.08. The P-value obtained is> 0.05, then the value of survival is not significant due to a small number of animals used.

3.5 Toxicological study

3.5.1 General toxicological study

To assess the potential toxic effect of PNAwt, histological analysis was performed in all major organs, in mice treated with placebo or PNAwt. The analysis showed no significant pathological changes in tissues of treated mice compared to those of control mice (Figure 46), indicating that the PNAwt does not alter the cell morphology of major organs, after 20 days of treatment.

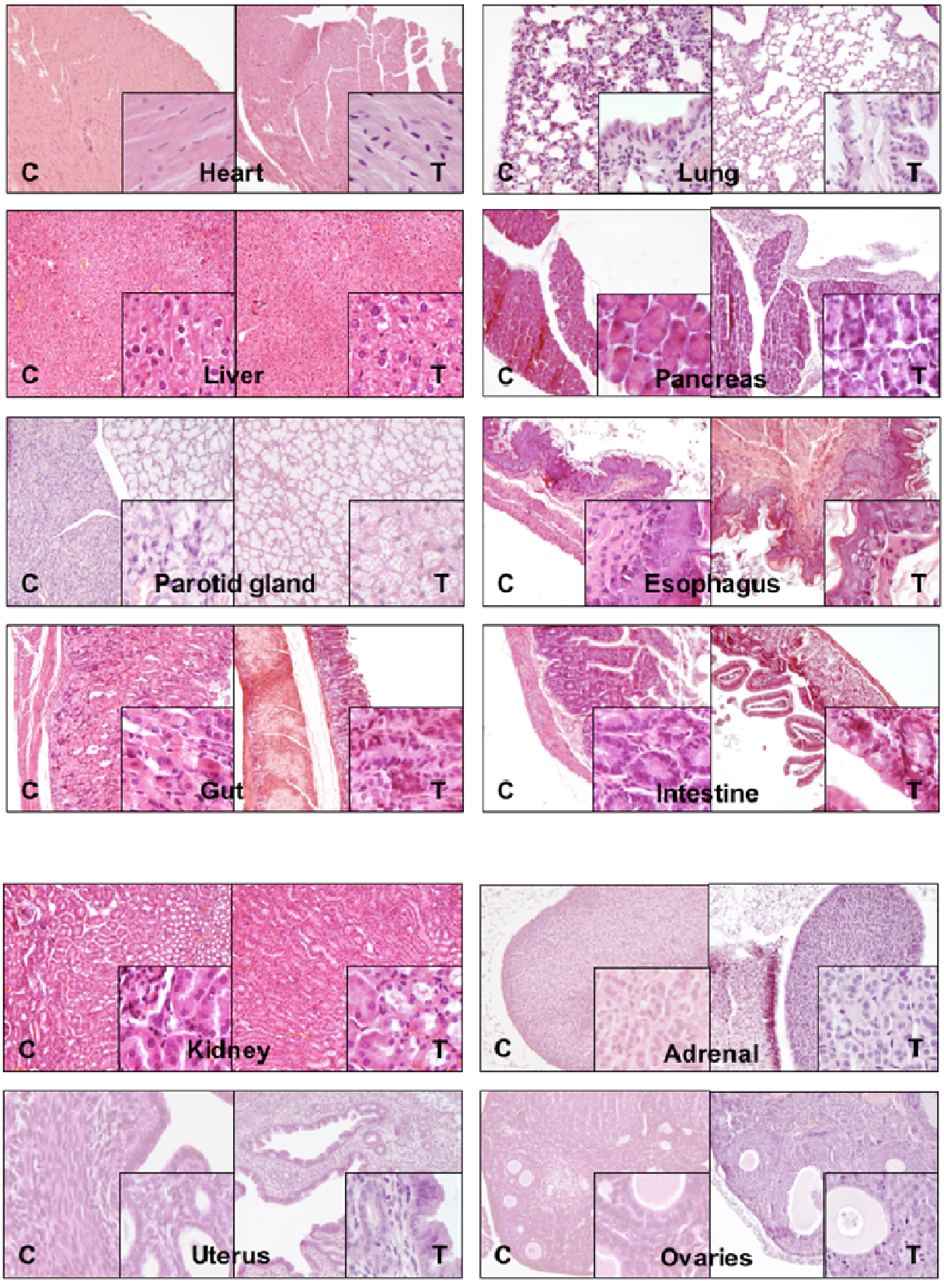
C
Heart
T
C
Lung
T
C
Liver
T
C
Pancreas
T
C
Parotid gland
T
C
Esophagus
T
C
Gut
T
C
Intestine
T
C
Kidney
T
C
Adrenal
T
C
Uterus
T
C
Ovaries
T

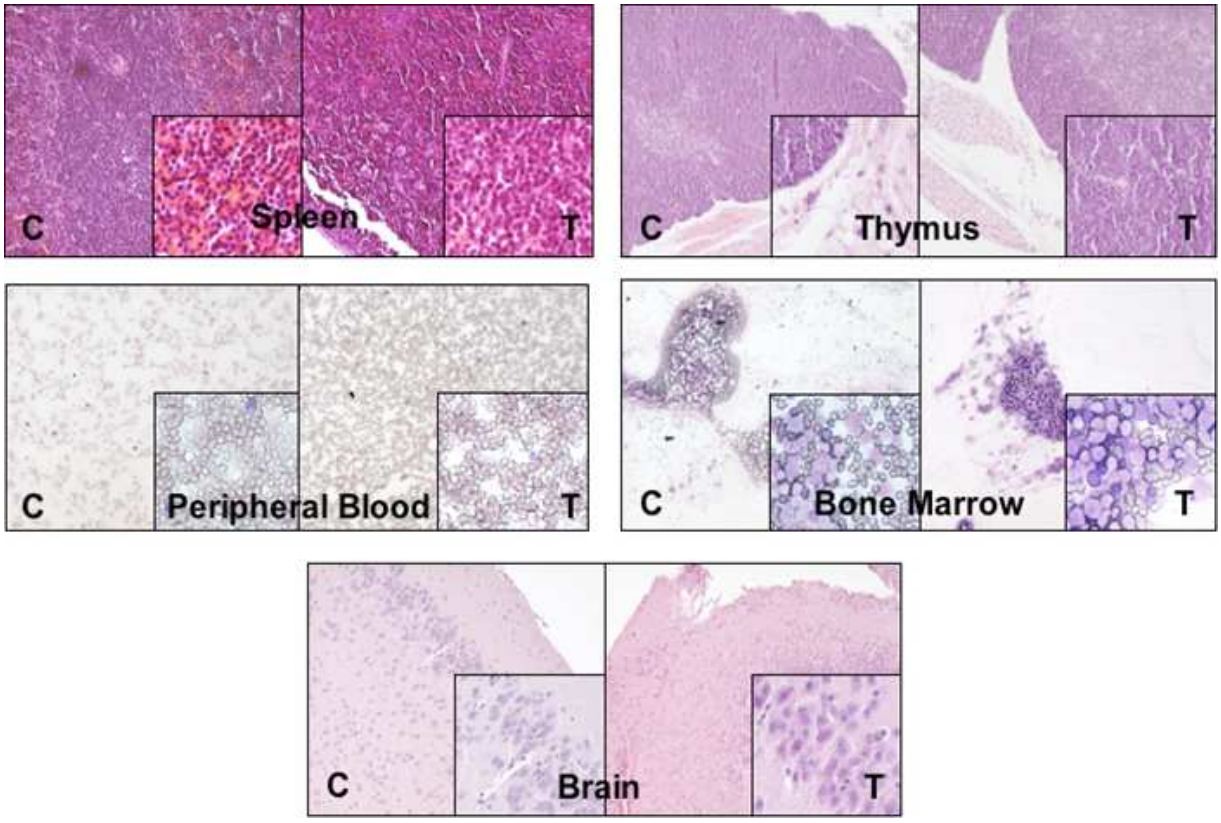

Fig 46: Toxicology study.

3.5.2 Creation mutant MYCN mice

Use quantitative genomic PCR to monitor enrichment for the mutant during subcloning.

To detect a single base mismatch add an additional mismatch on the penultimate base for both wild type and mutant targets. During subcloning, the wild type-to-mutant ratio of the seeded pools is monitored using qPCR to select the strongest pool and assist in deciding thye density at which the next pool is seeded.

Enrichment of the seeded pools during subcloning

4

Discussion

Neuroblastoma remains today the most common and deadly pediatric solid tumor. About 25% of Neuroblastoma cases present amplification of *MYCN* oncogene, which is associated with therapy resistance and frequent relapse, with long term survival probabilities less than 15%.

Moreover, high grade of tumor resistance in relapsed cases is often characterized by both *MYCN*-amplification and multitherapy-related p53 gene mutations. Considering this last particular aggressive clinical entity, even if accurate preclinical murine models that recapitulate MA-NB p53mut are highly needed, they are not described until now.

MYCN proto-oncogene plays a fundamental role. Its activity contribute to the deregulation of a consistent number of genes, including genes related to apoptosis, cell cycle,

metastasis, resistance to chemotherapy.

Recent studies highlight how MYCN amplification can regulate the expression of a specific pattern of genes leading to a more aggressive phenotype (Westermann F., 2008). In particular molecular studies on relapsed Neuroblastoma point out the N-MYC activation of other genes responsible of molecular therapies resistance (Keshelava N., 2007; Fontana L., 2008; Pajic M., 2005). Although surgery, chemotherapy and radiotherapy are still today capable to guarantee an extension of the half-life of patients, the biggest obstacle lies in the powerlessness to obtain a complete remission. The low therapeutic efficacy obtained until today is caused to a non complete use of the molecular mechanism already emerged that are at the base both of the pathology and of a high chemotherapic resistance.

In our previous studies at the Laboratory of Pediatric Oncology of the University of Bologna, we characterized the anti-tumor activity in MYCN-amplified NB cells of a specific anti-MYCN PNA inhibiting the human MYCN gene expression (Tonelli R. et al, 2005), demonstrating a potent and specific anti-tumor activity and apoptosis. The MYCN silencing also reduced the MDM2 protein level, rescuing p53 levels and inducing apoptosis in MNA-NB cells (Slack A. et al, 2005). In a preliminary previous study, PNA anti-MYCN gene did not show toxicity in no-expressing MYCN cells (Tonelli R. et al, 2005).

The first part of the project has been dedicated to the set up of appropriate preclinical in vitro and in vivo model to evaluate the potential therapeutic role of the targeting of MYCN in neuroblastoma.

In particular, we characterized for the first time, the real time tumorigenic evolution of the TH-MYCN transgenic homozygous neuroblastoma mouse model, by using Small-animal Positron Emission Tomography (PET). This transgenic mouse model in which the expression of *MYCN* is targeted to neural crest cells using the rat tyrosine hydroxylase promoter, closely recapitulates human neuroblastoma for molecular, biologic and cytogenetic features, and is an optimal immunocompetent model to evaluate new therapies (TH-*MYCN*-Weiss, EMBO 1997, Chesler, Cancer Res, 2007).

In this model, we tested for the first time, the accuracy of ^{18}F-fluorodeoxyglucose (^{18}F-FDG) and ^{18}F-DOPA PET to detect early neuroblastoma and to evaluate the metabolic behavior of

the tumor progression in mice transgenic for TH-*MYCN*.

The results showed that ^{18}F-FDG was more sensitive that ^{18}F-DOPA for early detection and for serial evaluation of malignant progression. Furthermore, the urinary excretion of ^{18}F-DOPA was very high and urinary bladder radioactivity saturated the images, reducing the diagnostic power of the technique.

Small-animal PET with ^{18}F-FDG in TH-*MYCN* mice permitted the identification of neuroblastoma at an early stage, and offers a sensitive method to follow metabolic progression of these tumors. Thus, these results could have potential indication not only for the tumor monitoring in this mouse model, but also have some potential implications in a clinical diagnostic view. MicroPET with ^{18}F-FDG was able to visualize the presence of tumor in early stage approximately five weeks from birth.

The use of molecular imaging by small-animal PET in the TH-*MYCN* mouse model can be used to improve the accuracy of *in vivo* preclinical testing of new therapies for neuroblastoma, by ensuring that homogeneous conditions are applied in all the animals under study.

Moreover, we created three new bioluminescent xenograft orthotopic MA-NB mouse models. Two of them carried p53wt, and consistently enrich the only MA-NB p53wt bioluminescent mouse model reported until now [28].

Moreover, we have reported for the first time a BLI xenograft orthotopic murine model carring MA-NB and multitherapy-related p53 mutations in which this unique allelic variant presents a missense mutation that affects its role as guardian of the genome.

The BLI xenograft orthotopic mice models generated from implanted human MA-NB cell lines, characterized by normal or mutated p53, clearly showed tumorigenesis with different p53-related progression trends when implanted orthotopically in SCID mice (Fig. 2).

The mouse model generated from implanted human p53mut MA-NB cells (BE2(c) cells deriving from stage 4 p53mut MA-NB after chemotherapic treatment) showed a more aggressive tumor evolution that consistently differed from those observed in the other two p53wt MA-NB mouse models for a shorter latency and higher BLI signal (Fig. 2).

Human neuroblastoma is characterized by a normal p53 status in the majority of the cases at the onset [34]. Unfortunately mutations of p53 related to chemotherapy and radiotherapy treatments often occur [34].

The therapy-related mutations in p53 found in NB are generally mutations of a single nucleotide resulting in variation of p53 DNA binding domain and therefore affecting its normal functions [34]. Tumors harboring these acquired p53 alterations become therefore highly resistant to treatment.

In some cases, according to the 2 hit model proposed by knudson, mutation of one allele is followed by the loss of the second one [33]. This hypotesis seems fit exactly with the p53mut MA-NB BE2(c) cell line in which only a p53 allelic variant harboring a missense mutation in the codon 135 [33].

The needs to study a possible cytotoxic compound acting in a p53mut independent way creates the basis for the creation of preclinical models useful for this kind of studies.

The transgenic p53wt and p53-haploinsufficient TH-*MYCN* MA-NB murine model together with the bioluminescent orthotopic p53wt MA-NB [19, 28] represent preclinical models in which the p53 gene is not mutated but, only in the case of the haploinsufficient model, altered in the number of allelic variants.

The BLI orthotopic xenograft models generated in this work represent therefore two essential and still challenging clinical subset of Neuroblastoma patients: the p53wt MA-NB tumors at diagnosis before any chemotherapic treatment (IMR-32 and Kelly) but, more relevant, the resistant p53mut MA-NB obtained from a stage 4 patient after classic chemotherapic treatment (BE2(c)).

These models offer the possibility to understand what are the molecular events at the basis of different MA-NB tumor progressions allowing targeted preclinical studies in a totally human derived tumor in which specific drugs in specific preclinical phases could be tested.

The p53mut MA-NB BLI xenograft ortothopic model, in particular, offers the possibility to test whether or not therapies acting in a p53 independent way could be effective against relapsed MA-NB in which the absence of an intact p53 protein does not allow any p53

dependent therapy defining a strong chemoresistance.

Moreover, the ability to follow human tumors growing in vivo represent a model that should result more predictive of the behavior of human disease.

In the second part of the project, the preclinical in vitro and in vivo models has been used to evaluate the potential therapeutic role of the targeting of MYCN in neuroblastoma.

I*n vitro* studies performed in neuroblastoma cel lines carring MYCN amplification confirmed the Remarkably, the silencing of MYCN by anti-MYCN PNA showed cell growth inibition activity also in the multidrug-resistant SK-N-BE cell line, carrying MYCN amplification.

This result is particularly relevant because showed the potentiality of the pharmacological efficacy of a p53-independent MYCN-based therapy.

Finally we evaluated for the first time, the *in vivo* anti-tumor activity of an antigene PNA-*MYCN* in the TH-MYCN murine model of Neuroblastoma by real-time molecular imaging using microPET (36)

Very remarkably, the treatment of mice with PNA-*MYCN* led to the tumor metabolic signal in the TH-MYCN mice, and significantly prolonged their survival. These *in vivo* results were obtained without the need for continuous treatment, but systemic administration (intraperitoneal (IP), 50 mg/kg) every two days for 20 days. Toxicological analysis of PNA-*MYCN* in immunocompetent mice after the same treatment schedule did not reveal any signs of toxicity.

Overall, our results indicate that the targeting of N-Myc has potential critical therapeutic role in MYCN-amplified Neuroblastoma and supports development of systemic oligonucleotide anti-*MYCN*-gene therapy for the treatment of Neuroblstoma, the most deadly and devastating form of childhood cancer. We have demonstrated potential clinical suitability of an antigene strategy through its cellular and molecular activity, ability to specifically inhibit transcription and *in vivo* efficacy with no evidence for toxicity.

In the present study regarding the in vitro studies, the construction of dose-response curves to drugs currently used clinically, has fully reflected our expectations.

It has enabled not only to classify the drugs according to their effectiveness `ı but also to distinguish the different cell lines according to their sensibility to the following used drugs: vincristine, Cispolatino, Carboplatin, Etoposide. Among the four compounds the one with the most cytotoxic effect is Vincristine. This efficiency could be `ad'azione due to the high specificity of the drug vincristine is in fact an inhibitor of cell specific cycle. It causes cell death only when target M not allowing the cell cycle, unlike other drugs, the trigger mechanisms shelter. The cell stops at M until the microtubules connecting the kinetochore, where this does not happen to be in the cell apoptosis.
This in vitro study attempts to reflect the treatment being used in the clinic according to the protocol
European COJEC NB-AR-01. In addition to drugs used in our study provides the COJEC the use of cyclophosphamide. To date it has not been possible to use this medication Because in bioactivation needs a liver to become ciclofosfoamide 4-hydroxy (4-OH CP) to complete its cytotoxic effects of mustard Phosphoramides [151] through the enzymes P450.

in this regard, to test the models and their response to drugs, in this study is The effect of anticancer drugs in one of two models of wild-type p53 neuroblastoma, Kelly Luc, and the model with mutated p53, SKNBE (2) c Luc.
Although only a preliminary pilot study on a small court of specimens, is significantly given the survival of both models treated. The results confirmed in vitro and clinical data and validate the increased aggressiveness of the tumor-derived `a
SKNBE line (2) c neuroblastoma tumor in relapsed stage 4. The results reveal that the specimens p53 wild-type treated with chemotherapy have an extension of survival of 25 days compared to the life of an animal is a mouse given significant.
However, this study as a "pilot"needs more data to confirm the result obtained.

Even if MMR raises a strong barrier to succeful oligonucleotide mediated gene targeting in ES cell, the transient down regulation of MMR activity thanks to transient suppression of MLH1 by RNA interference [174]. I have succesfully applied the oligotargeting method to change a single base in murine MYCN gene of murine embryonic stem cell and used this cells

to generate the first mutant mouse line that was created via single base oligonucleotide-mediated gene targeting. Generation of mutant mice by 1 nt modification in ES cell, which are germ line competent.The basal mechanism of ssODN-mediated gene targeting is not yet fully understood but the proposed model sees ssODN annealing to its chromosomal complement within the context of a replication fork. The single stranded DNA regions present during DNA synthesis may enhance ssODN annealing. This best accessibility may explain why also in my experiment ssODNs in the sense orientation performed better than ssODNs in the anti-sense orientation. I have successfully applied this strategy to generate the first mutant mouse that presents a single base mutation in its genome. Oligonucleotide-modified MYCN allele can be transmitted through the germ line of mice.

5

Bibliography

1. Gurney, J.G., et al., *Trends in cancer incidence among children in the U.S.* Cancer, 1996. 78(3): p. 532-41.

2. Pizzo, P.A., et al., *Principle and practice of pediatric oncology,* Fifth edition, 2006.

3. Dembowska-Bagińska, B., et al., *Cancer among adolescents 15-19 years of age. Own experience.* Med Wieku Rozwoj. 2006 Jul-Sep;10(3 Pt 1):725-35.

4. Castleberry, R.P., *Neuroblastoma.* Eur J Cancer, 1997. 33(9): p. 1430- 7; discussion 1437-8.

5. Johnson KJ, et al., *Perinatal characteristics and risk of neuroblastoma*. Int J Cancer. 2008 Sep 1;123(5):1166-72.

6. Maris, J.M., et al., *Molecular genetic analysis of familial neuroblastoma.* Eur J Cancer, 1997, 33(12): p. 1923-8.

7. Knudson, A.G., et al., *Mutation and cancer: neuroblastoma and pheochromocytoma.* Am J Hum Genet, 1972. 24(5): p. 514-32.

8. Knudson, A.G., Jr. Et al., *Mutation and childhood cancer: a probabilistic model for the incidence of retinoblastoma.* Proc Natl Acad Sci U S A, 1975. Dec;72(12): 5116-20.

9. Mosse YP, et al., *Identification of ALK as a major familial neuroblastoma predisposition gene*. Nature. 2008 Oct 16;455:930–935.

10. Bourdeaut, F., et al., *Germline mutations of the paired-like homeobox 2B (PHOX2B) gene in neuroblastoma.* Cancer Lett. 2005 Oct 18;228(1-2):51-8. Review.

11. Schramm, A., et al., *Biological effects of TrkA and TrkB receptor signaling in neuroblastoma.* Cancer Lett. 2005 Oct 18;228(1-2):143-53. Review.

12. O'Connor, D.T., et al., *Secretion of chromogranin A by peptide-producing endocrine neoplasms.* N Engl J Med. 1986 May 1;314(18):1145-51.

13. Helman, L.J., et al., *Chromogranin A expression in normal and malignant human tissues.* J Clin Invest, 1988. 82(2)

14. Cooper, M.J., et al., *Human neuroblastoma tumor cell lines correspond to the arrested differentiation of chromaffin adrenal medullary neuroblasts.* Cell Growth Differ. 1990 Apr;1(4):149-59.

15. Hsiao, R.J., et al., *Chromogranin A in children with neuroblastoma. Serum concentration parallels disease stage and predicts survival.* J Clin Invest. 1990 May;85(5):1555-9.

16. Eder, U., et al., *Levels and molecular forms of chromogranins in human childhood neuroblastomas and ganglioneuromas.* Neurosci Lett. 1998 Aug 28;253(1):17-20.

17. O'Hare, M.M., et al., *Expression and precursor processing of neuropeptide Y*

in human and murine neuroblastoma and pheochromocytoma cell lines. Cancer Res. 1989 Dec 15;49(24 Pt 1):7015-9.

18. Cohen, P.S., et al., *Neuropeptide Y expression in the developing adrenal gland and in childhood neuroblastoma tumors.* Cancer Res. 1990 Sep 15;50(18): 6055-61.

19. Kogner, P., et al., *Neuropeptide Y in neuroblastoma: increased concentration in metastasis, release during surgery, and characterization of plasma and tumor extracts.* Med Pediatr Oncol. 1993;21(5):317-22.

20. Rascher, W., et al., *Serial measurements of neuropeptide Y in plasma for monitoring neuroblastoma in children.* J Pediatr, 1993. 122(6): p. 914-6.

21. Dötsch, J., et al., *Plasma neuropeptide Y of children with neuroblastoma in relation to stage, age and prognosis, and tissue neuropeptide Y.* Regul Pept. 1998 Sep 25;75-76:185-90

22. Qualman, S.J., et al., *Neuroblastoma. Correlation of neuropeptide expression in tumor tissue with other prognostic factors.* Cancer, 1992. 70(7): p. 2005-12.

23. Sestini, R., et al., *Quantitation of somatostatin receptor type 2 gene expression in neuroblastoma cell lines and primary tumors using competitive reverse transcription-polymerase chain reaction.* Clin Cancer Res, 1996. Oct;2(10):1757-65.

24. Kogner, P., et al., *Somatostatin in neuroblastoma and ganglioneuroma.* Eur J Cancer, 1997. 33(12): p. 2084-9.

25. Pence, J.C., et al., *In vitro differentiation of human neuroblastoma cells caused by vasoactive intestinal peptide.* Cancer Res, 1990. Aug 15;50(16):5177-83.

26. Pence, J.C., et al., *The autocrine function of vasoactive intestinal peptide on human neuroblastoma cell growth and differentiation.* Arch Surg, 1993. May;128(5):591-5.

27. Evans, A.E., et al., *A proposed staging for children with neuroblastoma. Children's cancer study group A.* Cancer, 1971. Feb;27(2):374-8.

28. Hayes, F.A., et al., *Surgicopathologic staging of neuroblastoma: prognostic significance of regional lymph node metastases.* J Pediatr, 1983. Jan;102(1):59-62.

29. Nitschke, R., et al., *Localized neuroblastoma treated by surgery: a Pediatric Oncology Group Study.* J Clin Oncol, 1988. Aug;6(8):1271-9.

30. Bernardi, B., et al., *Localized neuroblastoma. Surgical and pathologic staging.* Cancer, 1987. 60(5): p. 1066-72.

31. Nakagawara, A., et al., *Proposal and assessment of Japanese tumor node metastasis postsurgical histopathological staging system for neuroblastoma based on an analysis of 495 cases.* Jpn J Clin Oncol, 1991. Feb;21(1):1-7.

32. Brodeur GM, et al., *Revisions of the international criteria for neuroblastoma diagnosis, staging, and response to treatment. Journal of Clinical Oncology* 11(8): 1466-1477, 1993.

33. Brodeur GM, et al., *International criteria for diagnosis, staging, and response to treatment in patients with neuroblastoma. Journal of Clinical Oncology* 6(12): 1874-1881, 1988.

34. Castleberry RP, et al., *The Pediatric Oncology Group experience with the international staging system criteria for neuroblastoma.* Journal of Clinical Oncology 12(11): 2378-2381, 1994.

35. Look, A.T., et al., *Clinical relevance of tumor cell ploidy and N-myc gene amplification in childhood neuroblastoma: a Pediatric Oncology Group study*. J Clin Oncol, 1991. Apr;9(4):581-91.

36. Look, A.T., et al., *Cellular DNA content as a predictor of response to chemotherapy in infants with unresectable neuroblastoma.* N Engl J Med, 1984. Jul 26;311(4):231-5.

37. Carén, H., et al., *High-resolution array copy number analyses for detection of deletion, gain, amplification and copy-neutral LOH in primary neuroblastoma tumors: Four cases of homozygous deletions of the CDKN2A gene BMC Genomics.* 2008 Jul 29;9:353.

38. Bilke, S., et al., *Inferring a Tumor Progression Model for Neuroblastoma From Genomic Data* J Clin Oncol. 2005 Oct 10;23(29):7322-31. Epub 2005 Sep 6.

39. Pezzolo, A., et al., *Presence of 1q gain and absence of 7p gain are new predictors of local or metatastic relapse in localized resectable neuroblastoma.* Neuro Oncol. 2008 Oct 15.

40. Brodeur, G.M., et al., *Amplification of N-myc in untreated human neuroblastomas correlates with advanced disease stage.* Science. 1984 Jun 8;224(4653):1121-4.

41. Seeger, R.C., et al., *Association of multiple copies of the N-myc oncogene with rapid progression of neuroblastomas.* N Engl J Med, 1985. Oct 31;313(18):1111-6.

42. Brodeur, G.M., et al., *Gene amplification in human neuroblastomas: basic mechanisms and clinical implications.* Cancer Genet Cytogenet, 1986. Jan 1;19(1-2):101-11.

43. Schwab, M., et al., *Chromosome localization in normal human cells and neuroblastomas of a gene related to c-myc.* Nature, 1984. Mar 15-21;308(5956):288-91.

44. 41. Corvi , R., et al., *MYCN is retained in single copy at chromosome 2 band p23-24 during amplification in human neuroblastoma cells.* Proc Natl Acad Sci U S A, 1994. Jun 7;91(12):5523-7.

45. Fong, C.T., et al., *Loss of heterozygosity for the short arm of chromosome 1 in human neuroblastomas: correlation with N-myc amplification.* Proc Natl Acad

Sci U S A, 1989. 1989 May;86(10):3753-7.

46. Takeda, O., et al., *There may be two tumor suppressor genes on chromosome arm 1p closely associated with biologically distinct subtypes of neuroblastoma.* Genes Chromosomes Cancer, 1994. May;10(1):30-9.

47. Lastowska, M., et al., *Gain of chromosome arm 17q predicts unfavourable outcome in neuroblastoma patients.* U.K. Children's Cancer Study Group and the U.K. Cancer Cytogenetics Group. Eur J Cancer, 1997. Sep;33(10):1627-33.

48. Bown, N., et al., *17q gain in neuroblastoma predicts adverse clinical outcome. U.K. Cancer Cytogenetics Group and the U.K.* Children's Cancer Study Group. Med Pediatr Oncol, 2001. Jan;36(1):14-9.

49. Bown, N.P., et al., *High incidence of constitutional balanced translocations in neuroblastoma.* Cancer Genet Cytogenet, 1993. Sep;69(2):166-7.

50. Guo, C., et al., *Deletion of 11q23 is a frequent event in the evolution of MYCN single-copy high-risk neuroblastomas.* Med Pediatr Oncol, 2000. Dec;35(6):544-6.

51. Maris, J.M., et al., *Allelic deletion at chromosome bands 11q14-23 is common in neuroblastoma.* Med Pediatr Oncol, 2001. Jan;36(1):24-7.

52. Islam, A., et al., *High expression of Survivin, mapped to 17q25, is significantly associated with poor prognostic factors and promotes cell survival in human neuroblastoma.* Oncogene. 2000 Feb 3;19(5):617-23.

53. Islam, A., et al., *Role of survivin, whose gene is mapped to 17q25, in human neuroblastoma and identification of a novel dominant-negative isoform, survivin-beta/2B.* Med Pediatr Oncol. 2000 Dec;35(6):550-3.

54. Plantaz, D., et al., *Gain of chromosome 17 is the most frequent abnormality detected in neuroblastoma by comparative genomic hybridization.* 1997 Am J Pathol. 1997 Jan;150(1):81-9.

55. Henrich, K.O., et al., *Reduced expression of CAMTA1 correlates with adverse outcome in neuroblastoma patients.* Clin Cancer Res. 2006 Jan 1;12(1):131-8.

56. Bilke, S., et al., *Inferring a tumor progression model for neuroblastoma from genomic data.* J Clin Oncol. 2005 Oct 10;23(29):7322-31.Epub 2005 Sep 6.

57. Ladenstein R., et al., *Randomized Trial of prophylactic granulocyte colony-stimulating factor during rapid COJEC induction in pediatric patients with high-risk neuroblastoma: the European HR-NBL1/SIOPEN study*, J Clin Oncol 2010; 28(21): 3516-3524.

58. Eilers, M., et al., *The MYC protein activates transcription of the alpha-prothymosin gene.* Embo J, 1991. 10(1): p. 133-41.

59. Grandori, C., et al., *The Myc/Max/Mad network and the transcriptional control of cell behavior.* Annu Rev Cell Dev Biol, 2000. 16: p. 653-99.

60. Nesbit, C.E., et al., *MYC oncogenes and human neoplastic disease.* Oncogene, 1999. 18(19): p. 3004-16.

61. Ingvarsson, S., *The myc gene family proteins and their role in transformation and differentiation.* Semin Cancer Biol, 1990. 1(6): p. 359-69.

62. Vennstrom, B., et al., *Isolation and characterization of c-myc, a cellular homolog of the oncogene (v-myc) of avian myelocytomatosis virus strain 29.* J Virol, 1982. 42(3): p. 773-9.

63. Schwab, M., et al., *Amplified DNA with limited homology to myc cellular oncogene is shared by human neuroblastoma cell lines and a neuroblastoma tumour.* Nature, 1983. 305(5931): p. 245-8.

64. Nau, M.M., et al., *L-myc, a new myc-related gene amplified and expressed in human small cell lung cancer.* Nature, 1985. 318(6041): p. 69-73.

65. Sugiyama, A., et al., *Isolation and characterization of s-myc, a member of the rat myc gene family*.Proc Natl Acad Sci U S A, 1989. 86(23): p. 9144-8.

66. Asai, A., et al., *The s-Myc protein having the ability to induce apoptosis is selectively expressed in rat embryo chondrocytes.* Oncogene, 1994. 9(8): p. 2345-52.

67. Resar, L.M., et al., *B-myc inhibits neoplastic transformation and transcriptional activation by c-myc.* Mol Cell Biol, 1993. 13(2): p. 1130-6.

68. DePinho, R.A., et al., *Myc family oncogenes in the development of normal and neoplastic cells.* Adv Cancer Res, 1991. 57: p. 1-46.

69. Dalla-Favera, R., et al., *Oncogene amplification in promyelocytic leukaemia cell line HL-60 and primary leukaemic cells of the same patient*. Nature, 1982. 299(5878): p. 61-3.

70. Magrath, I., et al.,*The pathogenesis of Burkitt's lymphoma.* Adv Cancer Res, 1990. 55: p. 133-270.

71. Payne, G.S.,et al., *Multiple arrangements of viral DNA and an activated host oncogene in bursal lymphomas.* Nature, 1982. 295(5846): p. 209-14.

72. Neil, J.C., et al., *The role of feline leukaemia virus in naturally occurring leukaemias.* Cancer Surv, 1987. 6(1): p. 117-37.

73. Landschulz, W.H., et al., *The leucine zipper: a hypothetical structure common to a new class of DNA binding proteins.* Science, 1988. 240(4860): p. 1759-64.

74. Luscher, B., et al., *New light on Myc and Myb. Part I. Myc.* Genes Dev, 1990. 4(12A): p. 2025-35.

75. Murre, C., et al., *Interactions between heterologous helix-loop-helix proteins generate complexes that bind specifically to a common DNA sequence.* Cell, 1989. 58(3): p. 537-44.

76. Davis, R.L., et al., *The MyoD DNA binding domain contains a recognition code for muscle-specific gene activation.* Cell, 1990. 60(5): p. 733-46.

77. Pession, A., et al., *The MYCN oncogene as a specific and selective drug target for peripheral and central nervous system tumors.* Curr Cancer Drug Targets. 2005 Jun;5(4):273-83.

78. Kohl, N.E., et al., *Transposition and amplification of oncogene-related sequences in human neuroblastomas.* Cell, 1983. 35(2 Pt 1): p. 359-67.

79. Schwab, M., et al., *Chromosome localization in normal human cells and neuroblastomas of a gene related to c-myc.* Nature, 1984. 308(5956): p. 288-91.

80. Jopling, C.L., et al., *N-myc translation is initiated via an internal ribosome entry segment that displays enhanced activity in neuronal cells*. Oncogene, 2001. 20(21): p. 2664-70.

81. Bonvini, P., et al., *In vivo degradation of N-myc in neuroblastoma cells is mediated by the 26S proteasome.* Oncogene, 1998. 16(9): p. 1131-9.

82. Yancopoulos, G.D., et al., *N-myc can cooperate with ras to transform normal cells in culture.* Proc Natl Acad Sci U S A, 1985. 82(16): p. 5455-9.

83. Schwab, M., et al., *Human N-myc gene contributes to neoplastic transformation of mammalian cells in culture.* Nature, 1985. 316(6024): p. 160-2.

84. Small, M.B., et al., *Neoplastic transformation by the human gene N-myc*. Mol Cell Biol, 1987. 7(5): p. 1638-45.

85. Schwab, M., et al., *Sustained expression of the human protooncogene MYCN rescues rat embryo cells from senescence.* Proc Natl Acad Sci U S A, 1988. 85(24): p. 9585-9.

86. Negroni, A., et al., *Decrease of proliferation rate and induction of differentiation by a MYCN antisense DNA oligomer in a human neuroblastoma cell line.* Cell Growth Differ, 1991. 2(10): p. 511-8.

87. Schmidt, M.L., et al., *The biological effects of antisense N-myc expression in human neuroblastoma.* Cell Growth Differ, 1994. 5(2): p. 171-8.

88. Weiss, W.A., et al., *Targeted expression of MYCN causes neuroblastoma in transgenic mice.* Embo J, 1997. 16(11): p. 2985-95.

89. Ramsay, G., et al., *Human proto-oncogene N-myc encodes nuclear proteins that bind DNA.* Mol Cell Biol, 1986. 6(12): p. 4450-7.

90. Slamon, D.J., et al., *Identification and characterization of the protein encoded by the human N-myc oncogene.* Science, 1986. 232(4751): p. 768-72.

91. Pession, A., et al., *The MYCN oncogene as a specific and selective drug target for peripheral and central nervous system tumors.* Curr Cancer Drug Targets, 2005. 5(4): p. 273-83.

92. Chang, D.W., et al., *The c-Myc transactivation domain is a direct modulator of apoptotic versus proliferative signals.* Mol Cell Biol, 2000. 20(12): p. 4309-19.

93. Nakajima, H., et al., *Inactivation of the N-myc gene product by single amino acid substitution of leucine residues located in the leucine-zipper region.*Oncogene, 1989. 4(8): p. 999-1002.

94. Dang, C.V., et al., *Involvement of the 'leucine zipper' region in the oligomerization and transforming activity of human c-myc protein.* Nature, 1989. 337(6208): p. 664-6.

95. Blackwood, E.M., et al., *Max: a helix-loop-helix zipper protein that forms a sequence-specific DNA-binding complex with Myc*. Science, 1991. 251(4998): p. 1211-7.

96. Solomon, D.L., et al., *Distinct DNA binding preferences for the c-Myc/Max and Max/Max dimers.* Nucleic Acids Res, 1993. 21(23): p. 5372-6.

97. Grandori, C., et al., *Myc target genes.* Trends Biochem Sci, 1997. 22(5): p.

177-81.

98. Brenner, C., et al., *Myc represses transcription through recruitment of DNA methyltransferase corepressor*. Embo J, 2005. 24(2): p. 336-46.

99. Kohl, N.E., et al., *Human N-myc is closely related in organization and nucleotide sequence to c-myc.* Nature, 1986. 319(6048): p. 73-7

100. Strieder, V., et al., *Regulation of N-myc expression in development and disease.* Cancer Lett, 2002. 180(2): p. 107-19.

101. Wakamatsu, Y., et al., *Regulation of the neural crest cell fate by N-myc: promotion of ventral migration and neuronal differentiation.* Development, 1997. 124(10): p. 1953-62.

102. Stanton, L.W., et al., *Alternative processing of RNA transcribed from NMYC*. Mol Cell Biol, 1987. 7(12): p. 4266-72

103. Hamann, U., et al., *The MYCN protein of human neuroblastoma cells is phosphorylated by casein kinase II in the central region and at serine 367.* Oncogene, 1991. 6(10): p. 1745-51.

104. Sansone, R., et al., *Age-dependent prognostic significance of N-myc amplification in neuroblastoma. The Italian experience.* Cancer Genet Cytogenet, 1991. 54(2): p. 253-7

105. Berthold, F., et al., *The current contribution of molecular factors to risk estimation in neuroblastoma patients.* Eur J Cancer, 1997. 33(12): p. 2092-7.

106. Corvi, R., et al., *MYCN is retained in single copy at chromosome 2 band p23-24 during amplification in human neuroblastoma cells.*Proc Natl Acad Sci U S A, 1994. 91(12): p. 5523-7.

107. Brodeur, G.M., et al., *Consistent N-myc copy number in simultaneous or consecutive neuroblastoma samples from sixty individual patients.* Cancer Res, 1987. 47(16): p. 4248-53.

108. Amler, L.C., et al., *The DDX1 gene maps within 400 kbp 5' to MYCN and is frequently*

coamplified in human neuroblastoma. Genes Chromosomes Cancer, 1996. 15(2): p. 134-7.

109. Amler, L.C., et la., *Amplified N-myc in human neuroblastoma cells is often arranged as clustered tandem repeats of differently recombined DNA.* Mol Cell Biol, 1989. 9(11): p. 4903-13.

110. Norris, M.D., et al., *Expression of N-myc and MRP genes and their relationship to N-myc gene dosage and tumor formation in a murine neuroblastoma model.* Med Pediatr Oncol.2000

111. Amler, L.C., et al., *The DDX1 gene maps within 400 kbp 5' to MYCN and is frequently coamplified in human neuroblastoma*. Genes Chromosomes Cancer, 1996. 15(2): p. 134-7.

112. Squire, J.A., et al., *Co-amplification of MYCN and a DEAD box gene (DDX1) in primary neuroblastoma.* Oncogene, 1995. 10 (7): p. 1417-22.

113. Wimmer, K., et al., *Co-amplification of a novel gene, NAG, with the N-myc gene in neuroblastoma.* Oncogene, 1999. 18(1): p. 233-8.

114. Fisher DE. *The p53 tumor suppressor : Critical regulatory of life & death in cancer.*

Apoptosis 2001; 6(1-2): 7-15.

115. Levine AJ. *p53,the cellular gatekeeper for growth and division,*Cell 1997; 88: 323-331.

116. Oren M. *Decision making by p53: life, death and cancer.* Cell Death and Differentiation 2003; 10: 431-442.

117. Birch JM, et al., *Relative frequency and morphology of cancers in carriers of germline*

TP53 mutations. Oncogene 2001; 20(34): 4621-4628.

118. Rossbach HC, et al., *Composite adrenal anaplastic neuroblastoma and virilizing adrenocortical tumor with germline TP53 R248W mutation.* Pediatr Blood Cancer 2008;

50(3): 681-683.

119. Levine AJ, et al., *The p53 tumor suppressor gene.* Nature 1991; 351; 453-456.

120. Szymanska K, et al., *TP53 and mutations in human cancer*. Acta Biochimica Polonica 2003; 50: 231-238.

121. Tweddle DA, et al., *The p53 pathway and its inactivation in neuroblastoma.* Cancer Lett 2003; 197: 93-98.

122. Moll UM, et al., *Wild-type p53 protein undergoes cytoplasmic sequestration in undifferentiated neuroblastomas but not in differentiated tumors.* Proc Natl Acad Sci U S A 1995; 92(10): 4407-4411.

123. Moll UM, et al., *Cytoplasmic sequestration of wild-type p53 protein impairs the G1 checkpoint after DNA damage.* Mol Cell Biol 1996; 16(3): 1126-1137.

124. Wolter J, et al., *p53 family: Therapeutic targets in neuroblastoma*. Future Oncol 2010; 6(3): 429-444.

125. Keshelava N, et al., *Drug resistance patterns of human neuroblastoma cell lines derived from patients at different phases of therapy.* Cancer Res 1998; 58(23): 5396-5405.

126. Keshelava N, et al., Loss of p53 function confers high-level multidrug resistance in neuroblastoma cell lines. Cancer Res 2001; 61(16): 6185-6193.

127. Chesler L, et al., *Chemotherapy-induced apoptosis in a transgenic model of neuroblastoma proceeds through p53 induction.* Neoplasia 2008; 10(11): 1268-1274.

128. Nielsen, P.E., et al., Sequence-selective recognition of DNA by strand displacement with a thymine-substituted polyamide. Science, 1991. 254(5037): p. 1497-500.

129. Egholm, M., et al., PNA hybridizes to complementary oligonucleotides obeying the Watson-Crick hydrogen-bonding rules. Nature, 1993. 365(6446): p. 566-8.

130. Brown, S.C., et al., *NMR solution structure of a peptide nucleic acid complexed with*

RNA. Science, 1994. 265(5173): p. 777-80.

131. Wittung, P., et al., *DNA-like double helix formed by peptide nucleic acid.* Nature, 1994. 368(6471): p. 561-3.

132. Nielsen, P.E., et al., *Evidence for (PNA)2/DNA triplex structure upon binding of PNA to dsDNA by strand displacement*. J Mol Recognit, 1994. 7(3): p. 165-70.

133. Demidov, V.V., et al., *Stability of peptide nucleic acids in human serum and cellular extracts.* Biochem Pharmacol,1994. 48(6): p.1310-3.

134. Hyrup, B., et al., *Peptide nucleic acids (PNA): synthesis, properties and potential applications*. Bioorg Med Chem, 1996. 4(1): p. 5-23.

135. Kuhn, H., et al., *Kinetic sequence discrimination of cationic bis-PNAs upon targeting of double-stranded DNA.* Nucleic Acids Res, 1998. 26(2): p. 582-7.

136. Kurg, R., et al., Inhibition of the bovine papillomavirus E2 protein activity by peptide nucleic acid. Virus Res, 2000. 66(1): p. 39-50.

137. Nielsen, P.E., et al., *Peptide nucleic acids (PNAs): potential antisense and anti-gene agents.* Anticancer Drug Des, 1993. 8(1): p. 53-63.

138. Hanvey, J.C., et al., *Antisense and antigene properties of peptide nucleic acids.* Science, 1992. 258(5087): p. 1481-5.

139. Tyler, B.M., et al., *Peptide nucleic acids targeted to the neurotensin receptor and administered i.p. cross the blood-brain barrier and specifically reduce gene expression.* Proc Natl Acad Sci U S A, 1999. 96(12): p. 7053-8.

140. Boffa, L.C., et al., *Invasion of the CAG triplet repeats by a complementary peptide nucleic acid inhibits transcription of the androgen receptor and TATA-binding protein genes and correlates with refolding of an active nucleosome containing a unique AR gene sequence.* J Biol Chem, 1996. 271(22): p. 13228-33.

141. Vickers, T.A., et al., *Inhibition of NF-kappa B specific transcriptional activation by PNA strand invasion.* Nucleic Acids Res, 1995. 23(15): p. 3003-8.

142. Ray, A., et al., *Peptide nucleic acid (PNA): its medical and biotechnical applications and promise for the future.* Faseb J, 2000. 14(9): p. 1041-60.

143. Bentin, T., et al., *Enhanced peptide nucleic acid binding to supercoiled DNA: possible implications for DNA "breathing" dynamics.* Biochemistry, 1996. 35(27): p. 8863-9.

144. Wittung, P., et al., *Phospholipid membrane permeability of peptide nucleic acid.* FEBS Lett, 1995. 375(3): p. 27-9.

145. Aldrian-Herrada, G., et al., *A peptide nucleic acid (PNA) is more rapidly internalized in cultured neurons when coupled to a retro-inverso delivery peptide. The antisense activity depresses the target mRNA and protein in magnocellular oxytocin neurons.* Nucleic Acids Res, 1998. 26(21): p. 4910-6.

146. Tyler, B.M., et al., *Specific gene blockade shows that peptide nucleic acids readily enter neuronal cells in vivo.* FEBS Lett, 1998. 421(3): p. 280-4.

147. Sei, S., et al., *Identification of a key target sequence to block human immunodeficiency virus type 1 replication within the gag-pol transframe domain.* J Virol, 2000. 74(10): p. 4621-3

148. Norton, J.C., et al., *Inhibition of human telomerase activity by peptide nucleic acids.* Nat Biotechnol, 1996. 14(5): p. 615-9.

149. Faruqi, A.F., et al., *Peptide nucleic acid-targeted mutagenesis of a chromosomal gene in mouse cells.* Proc Natl Acad Sci U S A, 1998. 95(4): p. 1398-403.

150. Branden, L.J., et al., *A peptide nucleic acid-nuclear localization signal fusion that mediates nuclear transport of DNA.* Nat Biotechnol, 1999. 17(8): p. 784-7.

151. Basu, S., et al., *Synthesis and characterization of a peptide nucleic acid conjugated to a D-peptide analog of insulin-like growth factor 1 for increased cellular uptake.* Bioconjug Chem, 1997. 8(4): p. 481-8.

152. Pooga, M., et al., *Cell penetration by transportan.* Faseb J, 1998. 12(1): p. 67-77.

153. Cutrona, G., et al., *Effects in live cells of a c-myc anti-gene PNA linked to a nuclear*

localization signal. Nat Biotechnol, 2000. 18(3): p. 300-3.

154. Derossi, D., et al., *The third helix of the Antennapedia homeodomain translocates through biological membranes.* J Biol Chem, 1994. 269(14): p. 10444-50.

155. Pession, A., et al., *Targeted inhibition of NMYC by peptide nucleic acid in N-myc amplified human neuroblastoma cells: cell-cycle inhibition with induction of neuronal cell differentiation and apoptosis.* Int J Oncol, 2004. 24(2): p. 265-72.

156. Hamilton, S.E., et al., *Cellular delivery of peptide nucleic acids and inhibition of human telomerase.* Chem Biol, 1999. 6(6): p. 343-51.

157. Braun, K., et al.,*HPV18 E6 and E7 genes affect cell cycle, pRB and p53 of cervical tumor cells and represent prominent candidates for intervention by use peptide nucleic acids (PNAs).*Cancer Lett. 2004 Jun 8;209(1):37-49.

158. Boffa, L.C., et al., *Dihydrotestosterone as a selective cellular/nuclear localization vector for anti-gene peptide nucleic acid in prostatic carcinoma cells.*Cancer Res. 2000 Apr 15;60(8):2258-62.

159. Cutrona. G., et al., *Inhibition of the translocated c-myc in Burkitt's lymphoma by a PNA complementary to the E mu enhancer.*Cancer Res. 2003 Oct 1;63(19):6144-8.

160. Sun, L., et al., *Antisense peptide nucleic acids conjugated to somatostatin analogs and targeted at the n-myc oncogene display enhanced cytotoxity to human neuroblastoma IMR32 cells expressing somatostatin receptors.*Peptides. 2002 Sep;23(9):1557-65.

161. Boffa. L.C., et al., *Therapeutically promising PNA complementary to a regulatory sequence for c-myc: pharmacokinetics in an animal model of human Burkitt's lymphoma.* Oligonucleotides. 2005 Summer;15(2):85-93.

162. Paffhausen. T., et al., *Targeted MYCN expression affects cytotoxic potential of chemotherapeutic drugs in neuroblastoma cells.* Cancer Lett. 2007 May 18;250(1):17-24. Epub 2006 Dec 4.

163. Fulda. S., et al., *MycN sensitizes neuroblastoma cells for drug-induced apoptosis.*

Oncogene. 1999 Feb 18;18(7):1479-86.

164. Mary, J., et al.,*"Farmacologia"*, Zanichelli, 2004, Seconda edzione

165. Clementi, F., et al., *"Farmacologia Generale e Molecolare"* UTET, 1999,

166. Zhang, J., et al., *Clinical Pharmacology of Cyclophosphamide and Ifosfamide* Current Drug Therapy ,2006, 1, 55.84

167. Wang, D., et al., *Cellular processing of platinum anticancer drugs.* Nat Rev Drug Discov. 2005 Apr;4(4):307-20. Review.

168. Gonzalez, V.M., et al., *Is cisplatin-induced cell death always produced by apoptosis?* Mol Pharmacol. 2001 Apr;59(4):657-63.

169. Sancar, A., et al., *Molecular mechanisms of mammalian DNA repair and the DNA damage checkpoints.* Annu Rev Biochem. 2004;73:39-85. Review.

170. Yamada, H.Y., et al., *Spindle checkpoint function and cellular sensitivity to antimitotic drugs.* Mol Cancer Ther. 2006 Dec;5(12):2963-9. Review.

171. Li, T.K., et al., *Tumor cell death induced by topoisomerase-targeting drugs.*Annu Rev Pharmacol Toxicol. 2001;41:53-77. Review.

172. Sordet. O., et al. *Apoptotic topoisomerase I-DNA complexes induced by oxygen radicals and mitochondrial dysfunction.*Cell Cycle. 2004 Sep;3(9):1095-7. Epub 2004 Sep 12. Review.

173. Beck, W.T., et al., *Cytotoxic signalling by inhibitors of DNA topoisomerase II.*Biochem Soc Trans. 2001 Nov;29(Pt 6):702-3.

174. Aarts M, et al., *Generation of a mouse mutant by oligonucleotide –mediated gene modification in ES cells.* Nucleic Acids Res. 2006; 34, No.21: e147

175. Aarts M., et al., *Gene modification in embryonic stem cells by single-stranded DNA oligonucleotides.* Methods Mol Biol. 2009, 530, 79-99.

176. Aarts M., et al., *Parameters of oligonucleotide-mediated gene modification in mouse ES*

cells. J cell Mol Med, 2010 Jun;14(6B):1657-67.

177. Killion. J.J., et al., *Orthotopic models are necessary to predict therapy of transplantable tumors in mice.* Cancer Metastasis Rev. 1998-1999;17(3):279-84. Review.

178. Gordon, J.W., et al., *Integration and stable germ line transmission of genes injected into mouse pronuclei.* Science, 1981. 214(4526): p. 1244-6.

179. Dunn, DA., et al., *Foundation review: transgenic animals and their impact on the drug discovery industry.* Drug Discov Today, 2005. 10(11):p.757-67.

180. Kerbel, R.S., et al., *What is the optimal rodent model for anti-tumor drug testing?* Cancer Metastasis Rev, 1998. 17(3): p. 301-4.

181. Dildrop, R., et al., *IgH enhancer-mediated deregulation of N-myc gene expression in transgenic mice: generation of lymphoid neoplasias that lack c-myc expression.* Embo J, 1989. 8(4): p. 1121-8.

182. Rosenbaum, H., et al., *N-myc transgene promotes B lymphoid proliferation, elicits lymphomas and reveals cross-regulation with c-myc.* Embo J, 1989. 8(3): p. 749-55.

183. Banerjee, S.A., et al., *5' flanking sequences of the rat tyrosine hydroxylase gene target accurate tissue-specific, developmental, and transsynaptic expression in transgenic mice.* J Neurosci, 1992. 12(11): p. 4460-7.

184. Weiss, W.A., et al., *Genome-wide screen for allelic imbalance in a mouse model for neuroblastoma.* Cancer Res, 2000. 60(9): p. 2483-7.

185. Norris, M.D., et al., *Expression of N-myc and MRP genes and their relationship to N-myc gene dosage and tumor formation in a murine neuroblastoma model.* Med Pediatr Oncol, 2000. 35(6): p. 585-9.

186. Burkhart, C.A., et al., *Effects of MYCN antisense oligonucleotide administration on tumorigenesis in a murine model of neuroblastoma.* J Natl Cancer Inst, 2003. 95(18): p. 1394-403.

187. Hansford, L.M., et al., *Mechanisms of embryonal tumor initiation: distinct roles for*

MycN expression and MYCN amplification. Proc Natl Acad Sci U S A, 2004. 101(34): p. 12664-9.

188. Hackett, C.S., et al., *Genome-wide array CGH analysis of murine neuroblastoma reveals distinct genomic aberrations which parallel those in human tumors.* Cancer Res, 2003. 63(17): p. 5266-73.

189. Kerbel, R.S., *Human tumor xenografts as predictive preclinical models for anticancer drug activity in humans: better than commonly perceived-but they can be improved.* Cancer Biol Ther. 2003 Jul-Aug;2(4 Suppl 1):S134-9. Review.

190. Henriksson, K.C., et al., *A fluorescent orthotopic mouse model for reliable measurement and genetic modulation of human neuroblastoma metastasis.* Clin Exp Metastasis. 2004;21(6):563-70.

191. Campostrini. N., et al., *Proteomic analysis of an orthotopic neuroblastoma xenograft animal model.*J Chromatogr B Analyt Technol Biomed Life Sci. 2004 Sep 5;808(2):279-86.

192. Marimpietri. D., et al., *Combined therapeutic effects of vinblastine and rapamycin on human neuroblastoma growth, apoptosis, and angiogenesis.* Clin Cancer Res. 2007 Jul 1;13(13):3977-88.

193. McCarville, M.B., et al., *Angiogenesis inhibitors in a murine neuroblastoma model: quantitative assessment of intratumoral blood flow with contrast-enhanced gray-scale US.* Radiology. 2006 Jul;240(1):73-81.

194. Pastorino, F., et al., *Vascular damage and anti-angiogenic effects of tumor vessel-targeted liposomal chemotherapy.* Cancer Res. 2003 Nov 1;63(21):7400-9.

195. Dickson. P.V., et al., *Bevacizumab-induced transient remodeling of the vasculature in neuroblastoma xenografts results in improved delivery and efficacy of systemically administered chemotherapy.* Clin Cancer Res. 2007 Jul 1;13(13):3942-50.

196. Hamner, J.B., et al., *Bortezomib inhibits angiogenesis and reduces tumor burden in a murine model of neuroblastoma.* Surgery. 2007 Aug;142(2):185-91.

197. Sharpless, N.E., et al., *The mighty mouse: genetically engineered mouse models in cancer drug development*. Nat Rev Drug Discov. 2006 Sep;5(9):741-54. Epub 2006 Aug 18. Review.

198. Phelps, M.E., *Inaugural article: positron emission tomography provides molecular imaging of biological processes.* Proc Natl Acad Sci U S A, 2000. 97(16): p. 9226-

199. Phelps, M.E., et al., *Application of annihilation coincidence detection to transaxial reconstruction tomography.* J Nucl Med, 1975. 16(3): p. 210-24.

200. Tai, Y.C., et al., *Instrumentation aspects of animal PET.* Ann Rev Biomed Eng, 2005. 7: p. 255-85.

201. Sossi, V., et al., *Micropet imaging: in vivo biochemistry in small animals.* J Neural Transm, 2005. 112(3): p. 319-30.

202. Hume, S.P., et al., *Pharmacological constraints associated with positron emission tomographic scanning of small laboratory animals.* Eur J Nucl Med, 1998. 25(2): p. 173-6.

203. Gjedde, A., et al., *Pentobarbital anesthesia reduces blood-brain glucose transfer in the rat.* J Neurochem, 1980. 35(6): p. 1382-7.

204. Chatziioannou, A.F., *Molecular imaging of small animals with dedicated PET tomographs.* Eur J Nucl Med Mol Imaging, 2002. 29(1): p. 98-114.

205. Saija, A., et al., *Modifications of the permeability of the blood-brain barrier and local cerebral metabolism in pentobarbital- and ketamine-anaesthetized rats.* Neuropharmacology, 1989. 28(9): p. 997-1002.

206. Dhandayuthapani, S., et al., *Green fluorescent protein as a marker for gene expression and cell biology of mycobacterial interactions with macrophages*. Mol Microbiol, 1995. 17(5): p. 901-12.

207. Gambhir, S.S., et al., *Assays for noninvasive imaging of reporter gene expression.* Nucl Med Biol, 1999. 26(5): p. 481-90.

208. Shields, A.F., et al., *Imaging proliferation in vivo with [F-18]FLT and positron emission tomography.* Nat Med, 1998. 4(11): p. 1334-6.

209. Wu, A.M., et al., *High-resolution microPET imaging of carcinoembryonic antigen-positive xenografts by using a copper-64-labeled engineered antibody fragment.* Proc Natl Acad Sci U S A, 2000. 97(15): p. 8495-500.

210. Kornblum, H.I., et al., *In vivo imaging of neuronal activation and plasticity in the rat brain by high resolution positron emission tomography (microPET).* Nat Biotechnol, 2000. 18(6): p. 655-60.

211. Lewis, J.S., et al., *Small animal imaging. current technology and perspectives for oncological imaging.* Eur J Cancer, 2002. 38(16): p. 2173-88.

212. Kornblum, H.I., et al., *The use of microPET for the development of neural repair therapeutics: studies in epilepsy and lesion models.* J Clin Pharmacol, 2001. Suppl: p. 55S-63S.

213. Wipke, B.T., et al., *Dynamic visualization of a joint-specific autoimmune response through positron emission tomography.* Nat Immunol, 2002. 3(4): p. 366-72.

214. Smith, I.C., et al., *Positron emission tomography using [(18)F]-fluorodeoxy-D-glucose to predict the pathologic response of breast cancer to primary chemotherapy.* J Clin Oncol, 2000. 18(8): p. 1676-88.

215. Di Chiro, G., *Positron emission tomography using [18F] fluorodeoxyglucose in brain tumors. A powerful diagnostic and prognostic tool.* Invest Radiol, 1987. 22(5): p. 360-71.

216. Kubota, K., et al., *Differential diagnosis of lung tumor with positron emission tomography: a prospective study.* J Nucl Med, 1990. 31(12): p. 1927-32.

217. Hoh, C.K., et al., *Cancer detection with whole-body PET using 2-[18F]fluoro-2-deoxy-D-glucose.* J Comput Assist Tomogr, 1993. 17(4): p. 582-9.

218. Gambhir, S.S., et al., *A tabulated summary of the FDG PET literature.* J Nucl Med,

2001. 42(5 Suppl): p. 1S-93S.

219. Sokoloff, L., et al., *The [14C]deoxyglucose method for the measurement of local cerebral glucose utilization: theory, procedure, and normal values in the conscious and anesthetized albino rat.* J Neurochem, 1977. 28(5): p. 897-916.

220. Franzius C. *FDG-PET/CT in pediatric solid tumors.* Q J Nucl Med Mol Imaging. 2010 Aug;54(4):401-10.

221. Rufini V, et al., *Comparison of 123I-MIBG SPECT-CT and 18F-DOPA PET-CT in the evaluation of patients with known or suspected recurrent paraganglioma.* Nucl Med Commun. 2011 Apr 4

222. Sadikot R., et al., *Bioluminescence Imaging.* Proc Am Thorac Soc 2005;2:537-540

223. Rehemtulla, A., et al., *Rapid and quantitative assessment of cancer treatment response using in vivo bioluminescence imaging.* Neoplasia. 2000 Nov-Dec;2(6):491-5.

224. Doholen G., et al., *Antioxidant Activity in the Newborn Brain: A Luciferase Mouse Model.* Neonatology 2008;93:125-131

225. Blesch A., *Lentiviral and MLV based retroviral vectors ex vivo and in vivo gene transfer*. Methods 2003;33:164-172

226. Sadikot RT., et al., *Bioluminescence imaging*, Proc Am Thorac Soc. 2005; 2(6):537-40,511-2

227. Contag C.H., Contag P.R., Mullins J.I., Spilman S.D., Stevenson D.K.,Benaron D.A *Photonic detection of bacterial pathogens in living hosts. Mol. Microbiol .2005 18:593–603.*

228. Wu J.C., et al., *Noninvasive optical imaging of firefly luciferase reporter gene expression in skeletal muscles of living mice.* Mol. Ther (2001). 4:297–306.

229. Tonelli, R. et al., *Antigene peptide nucleic acid specifically inhibits MYCN expression in human neuroblastoma cells leading to cell growth inhibition and apoptosis.* Molecular Cancer Therapy. 2005;4(5)

230. Pession A., et al., *N-myc amplification and cell proliferation rate in human neuroblastoma.* J Path 1997 ; 183 : 339-44

231. Hooper M, et al., *HPRT-deficient (Lesch-Nyhan) mouse embryos derived from germline colonization by cultured cells.* Nature. 1987; 326: 292–5.).

232. Fulda S, et al., *Antiproliferative potential of cytostatic drugs on neuroblastoma cells in vitro*. European J of Cancer 1995; 31: 616-621.

233. Nanni C, et al., *FDG small animal PET permits early detection of malignant cells in a xenograft murine model* . Eur J Nucl Med Mol Imaging (2007) 34:755

234. Lowry, O.H., et al., *Protein measurement with the Folin phenol reagent.* J Biol Chem, 1951. **193**(1): p. 265-75.

235. Allen, N.D., et al., *Epigenetic control of transgene expression and imprinting by genotype-specific modifiers.* Cell, 1990. **61**(5): p. 853-61.

236. Sasaki, H., et al., *Inherited type of allelic methylation variations in a mouse chromosome region where an integrated transgene shows methylation imprinting.* Development, 1991. 111(2): p. 573-81.

237.